ENGINEERING PROTEIN ANTIGENS TO REFOCUS THE IMMUNE RESPONSE

A Dissertation
Presented to
The Academic Faculty

by

Ammar Arsiwala

In Partial Fulfillment
of the Requirements for the Degree
Doctor of Philosophy in the
School of Chemical and Biomolecular Engineering

Georgia Institute of Technology
August 2019

ENGINEERING PROTEIN ANTIGENS TO REFOCUS THE IMMUNE RESPONSE

Approved by:

Dr. Ravi Kane, Advisor
School of Chemical and Biomolecular Engineering
Georgia Institute of Technology

Dr. Manu Platt
School of Biomedical Engineering
Georgia Institute of Technology

Dr. Mark Prausnitz
School of Chemical and Biomolecular Engineering
Georgia Institute of Technology

Dr. Todd Sulchek
School of Mechanical Engineering
Georgia Institute of Technology

Dr. Julie Champion
School of Chemical and Biomolecular Engineering
Georgia Institute of Technology

Date Approved: July 18, 2019

Dedicated to my mother, Farida Arsiwala

ACKNOWLEDGEMENTS

The work discussed in this thesis is a combined result of help and support from a lot of people, and I am immensely grateful to each one of them. It would have been impossible to achieve what I have, without contributions – both scientific and personal, from my mentors, colleagues and friends and family.

Firstly, I would like to thank my advisor Dr. Ravi Kane for supporting my research and guiding me both professionally and personally over the past five years. He has been extremely prompt in responding whether in person or over email. He has encouraged me to work on several areas of research and to juggle multiple projects at the same time – something I have always liked doing. His support and his passion for the work we do was contagious and helped me stay positive throughout. He has taught me skills related to effective data presentation and public speaking which will be very valuable to me in my future professional career. He has also been extremely understanding and supportive during the several personal struggles I went through in the past few years. I would like to sincerely thank him for being a *big part* of this successful journey of completing my doctorate degree.

I would like to thank my committee members, Dr. Prausnitz, Dr. Champion, Dr. Sulchek, and Dr. Platt, for their time and valuable feedback over the course of my PhD. They have helped me see things differently in my research and their suggestions have had a meaningful impact in the overall quality of my research.

My work would have not been possible without the help from all my collaborators. I am extremely grateful to - Jessica McCaffery and Dr. Alberto Moreno, for helping us the

with Malaria work; Dr. Jim Duehr, Juan Manuel and Dr. Florian Krammer, for helping with the Zika work; and Dr. Susi Lindermann and Dr. Rafi Ahmed, for helping with the Influenza work. The expertise of each of these groups in their field was tremendously helpful in shaping my work and making it possible. I feel fortunate to have gotten the opportunity to work with and learn from all of them.

Having spent my first year of PhD at Rensselaer Polytechnic Institute (RPI), I feel fortunate to have gained the best of both Institutes. I would like to specially thank Manish Arha for being my grand-mentor when I started research work in lab. He was at the time, and has been since then an emotional support system for me. Most of the molecular biology I know is because of Manish. I would also like to thank other post-docs from RPI - Marc Douaisi and Jake Martin who similarly trained me on several other aspects of my work.

A bulk of my growth as a researcher happened under the mentorship of senior graduate students Chad Varner and Tania Rosen. I had the opportunity to work with them on their projects and learn significantly in the process. Together they set-up and established several protocols in our lab, that I gained from later in the course of my PhD work. It was a joy working with Chad and Tania, and I am truly grateful to the both of them. Tania, one of my closest friends whom I have known for more than a decade now has been a great emotional support system for me personally and professionally. She has taught me how to be eternally happy, to laugh more, and to be grateful for so much that we all already have. I am *truly, truly fortunate* to have her in my life. Both Chad and Tania have also been very helpful in guiding me for my search for employment post-graduation, as

were other lab alumni – Chakradhar Padala, Mohan Boggara, Ronak Maheshwari, Krunal Mehta, and Ravi Pangule.

I am thankful for the highly collaborative nature of our lab which gave me the opportunity to mentor and receive *tremendous* help from graduate students Steven Frey (for the Influenza work) and Ana Castro (for the Zika work). I was able to execute my experiments seamlessly as planned because of their continued support for my work. I got to collaborate with post-docs Jihun Park and Neha Dhar and contribute to their projects and learn from them in the process. I am thankful to the both of them for being extremely comfortable to work with and being kind to me. I also got an opportunity to mentor graduate students Geetanjali Pendyala and Nicole Hu in my final year to get them started with their projects. I would like to thank other graduate students in the group – Abhirup Mukherjee, Troy Batugal and Mark Stathos, as well as all their undergrads to make the lab environment extremely fun to work in and contributing to making the lab so closely-knit.

I would like to extend a very heartfelt and special thanks to my army of undergrads that have helped me in the last three years of my PhD, without whose efforts, minds and extra hands this work would have been *impossible* to achieve in the time that it did. I am greatly indebted to every single one of them – Jaeyoon Yi, Andrew Kell, Alexandra Holderied, Victoria Okudoh, Timothy Rogers, Vivek Hariharan, Shruthi Murali, Puneeth Guruprasad, Joaquin Ramas, and Jackson Dean. I cannot emphasize enough on how meaningful their contributions have been in propelling my research work forward and making my graduation a reality.

Last but equally importantly, I would like to thank my family and friends for their limitless love and support. I am immensely grateful to my parents, Farida and Mazhar Arsiwala and my additional set of parents, Zaiboon and Ashfaque Arsiwala - for supporting and loving me unconditionally. Their upbringing has made me able to achieve what I have so far in life. I would like to thank my brother and sister-in law, Yusuf and Nafisa – for being *the constants* in my life. Thank you for making me feel more secure and confident and making me believe that I can do *anything* - I am immensely thankful to the both of them. A big thank you to one of my closest friends, Youthika Chauhan without whom I would not have made it this far in life – thanks for taking care of me like a parent would, and for picking me up *every single time*. I would like to thank my friend Prajakatta Mulay for being there for me, for being my travel-buddy, and for teaching me the real meaning of *innocence*. A full-of-love thank you to my buddy Akshat Mullerpatan for *so much* that he has done for me. Akshat is the reason that my struggles to transition my life in the United States were emotionally manageable. He has made me stronger, more humble, sillier and funnier, and has taught me how one truly *cares*. My extended family has been extremely loving and caring, and seeing them feel immensely proud of my accomplishments makes me thankful for having them in my life. Lots of love to all the Arsiwalas, Bayadwalas, Cutlerywalas, Diwans, Masawis, Rampurwalas, Dhuliawalas, Petiwalas and Lunawadawalas, and all other well-wishers back home in India who have helped me turn this dream to reality.

TABLE OF CONTENTS

LIST OF FIGURES

SUMMARY

Infectious diseases continue to be a threat to millions globally – largely because of highly effective immune evasion mechanisms evolved in pathogens. Our work focuses on engineering proteins to shield selected epitopes thereby refocusing the immune response to other regions on the protein antigen. In the context of vaccine design, nanopatterning can help preferentially elicit broadly neutralizing antibodies while suppressing the response to epitopes that serve as immunological decoys. We have developed two approaches to achieve this shielding and refocusing – one referred to as "Nanopatterning" that uses site-specifically conjugated polymeric shields and a second approach that uses engineered antibody fragments (Fabs) as shielding agents. For the nanopatterning approach we have demonstrated preferential immunosuppression of a defined epitope on green-fluorescent protein (GFP) as a model antigen. We then extended this nanopatterning idea to engineer a promising malarial antigen – Merozoite surface protein-1 (MSP1) that is unusual in eliciting so-called "blocking antibodies" that interfere with the neutralizing "inhibitory antibodies" and that even promote infection. We have nanopatterned MSP-1 to elicit antibodies that recognize MSP-1 from heterologous strains, differing in sequence at as many as 21 of 96 residues. The second approach explores the use of Fabs as shielding agents. Here, we have demonstrated the ability to refocus the immune response to broadly neutralizing epitopes of two antigens – Hemagglutinin (HA) of the Influenza virus and Domain III (DIII) of the Zika Virus (ZIKV) Envelope protein. We have shown that by either tethering the Fab to the antigen (for HA and DIII) or by using bivalent soluble Fab shields (for HA), the immune response can be focused on their broadly protective epitopes. In summary, this work explores two new approaches to achieve immunofocusing –

allowing refocusing of the immune response to protein antigens. These tools should be broadly applicable for the design of broadly protective vaccines against pathogens such as malarial parasites, influenza, flaviviruses and HIV.

CHAPTER 1. INTRODUCTION

Our bodies combat infections from pathogens using a variety of effector cells and molecules that together make up the immune system. Broadly, immune responses are classified as: (i) innate immune responses – which are always immediately available to combat a wide range of pathogens, and are non-specific in nature; and (ii) adaptive immune responses – which are developed during the lifetime of an individual, generate an immunological memory, and can sometimes confer lifelong protective immunity to reinfection against the same pathogen [1]. The first step in this process of developing immunological memory is immune recognition – wherein certain immune cells, called as B lymphocytes (B cells), recognize and interact with the antigen (the foreign pathogen or their components) to develop an immune response against the pathogen [2]. B cells present B-cell receptors (BCRs) on their surface which bind to a region on the antigen. Once a B cell binds to an antigen, a series of downstream events occur, triggering the B cells to proliferate and differentiate into plasma cells, which ultimately produce antibodies specific to the antigen [3]. Immunity mediated by macromolecules such as antibodies is referred to as antibody-mediated or humoral immunity. The focus of the current thesis is on immunity developed via the B cell arm of the immune system, producing antibodies specific to certain defined regions of the antigen. Another class of immune cells called T lymphocytes (T cells) complement the B cells in combating the pathogen. A class of T cells called as Helper T cells provide signals to the antigen-stimulated B cells influencing the production of antibodies [4]. During the course of this immune response, some B cells activated by the antigen differentiate into memory B cells, providing long lasting immunity following exposure to infection with that pathogen later in life [1].

Vaccination is the deliberate stimulation of the immune response towards a pathogen known to cause disease. Early vaccination attempts involved using attenuated organisms with reduced pathogenicity (called as live-attenuated vaccines), which could still stimulate an immune response and protective immunity but not disease [5]. A second class of vaccines is based on killed organisms (called as inactivated vaccines), which addressed some of the safety concerns associated with live vaccines such as lethal systemic infections [6]. Evolving from this approach, is a class of vaccines called subunit vaccines – which use specific pieces or fragments of the pathogen known to be immunogenic. Subunit vaccines are based on purified whole surface proteins, peptide fragments, polysaccharides or capsids [7].

A drawback of vaccines based on purified recombinant proteins or peptides is that they do not activate the immune system in the same way that a natural infection does [8]. These subunit vaccines, thus usually require the coadministration of additional components, referred to as adjuvants, which enhance the immunogenicity of antigens [9]. Adjuvants activate a class of immune cells called antigen-presenting cells (APCs) by providing ligands for Toll-like receptors (TLRs) and other receptors on APCs – which are the innate viral and bacterial sensor pathways[10]. For example, Freund's complete adjuvant (FCA) is an oil-in-water emulsion of killed mycobacteria comprising immunostimulatory components such as the complex glycolipid and other bacterial cell wall components.

Vaccines constitute one of the most effective tools to prevent infectious diseases [11, 12]. However, for numerous important diseases, currently available vaccines do not provide broad, durable, and effective protection – largely because of highly effective immune evasion mechanisms in pathogens [13-16]. For instance, in several cases, immunodominant regions of protein antigens are highly variable in sequence and elicit narrow or even strain-specific

immune responses. Consequently, there is a growing need to refocus the immune response on the conserved and broadly neutralizing epitopes.

The current work explores novel tools to achieve immunofocusing to engineer antigens from three medically highly relevant infectious diseases – Malaria, Influenza, and Zika. Malaria is a vector-borne parasitic tropical disease caused by *Plasmodium,* found in 91 countries [17]. *Plasmodium falciparum* and *P. vivax* are the predominant species that infect humans, with an estimated incidence of 219 million cases worldwide in 2017 – of which 99.7% of the cases were caused by *P. falciparum* [17]. There were an estimated 435,000 deaths from malaria globally in 2017-2018, with children under 5 years of age being the most vulnerable group [17]. The development of an effective vaccine is important to control malaria transmission, in addition to the existing control measures. RTS,S/A01, based on the pre-erythrocytic subunit of the parasite, is the only malaria vaccine that has reached phase 3 clinical trials. However, this vaccine induces short-lived responses [18, 19] with only modest efficacy of ~40% [17]. It has been suggested that next generation vaccines must build on the success of the current pre-erythrocytic subunit vaccines, as well as explore blood-stage or transmission blocking immunity [20].

Influenza viruses cause mild to severe respiratory infections and constitute a major public health problem. While seasonal influenza epidemics cause an estimated 250,000 to 500,000 deaths annually worldwide [21], the "Spanish" influenza pandemic of 1918 has been estimated to have caused approximately 40 million deaths [22]. In the United states alone in the 2017-2018 season, an estimated 48.8 million people were infected with Influenza, resulting in an estimated 80,000 deaths [23]. Vaccines are currently the best available measure to control the spread of Influenza, however, the vaccine effectiveness is low

compared to that for other viral infections, and the resulting immunity is narrow and short-lived [24]. The ultimate goal to combat Influenza infection by vaccination, is to design a "Universal" Influenza virus vaccine that induces long-lived protection against drifted seasonal and pandemic influenza infections.

Zika virus (ZIKV) is a flavivirus that sparked global attention in 2015 – with a large number of infections in Brazil followed by outbreaks and transmission throughout the Americas, Africa, and other regions of the world [25]. ZIKV infection during pregnancy has been linked to microcephaly and other congenital neurodevelopment defects [26]. A study showed a 100-fold increase in the incidence of microcephaly incidence from late 2015 to early 2016, mirroring the incidence of ZIKV infection [27]. ZIKV was also found to be associated with the Guillain-Barre syndrome, an inflammatory demyelinating polyneuropathy [28]. Moreover, the risk of disease transmission is exacerbated by the fact that ZIKV can be transmitted sexually. Although, no longer classified as a global emergency, ZIKV continues to spread geographically in areas where the competent vectors (mosquitoes from the *Aedes genus*) are present. To date, there is no approved vaccine, antiviral drug, or other modality to prevent or treat ZIKV – emphasizing the need for a vaccine [29].

Most antibodies bind to the "viral spikes" – which are basically surface proteins that assist the pathogen in infecting the host. These surface proteins, however, are highly variable in sequence. For example, the sequence of hemagglutinin (HA), a surface protein on the influenza virus, changes so rapidly that a different vaccine needs to be manufactured every year. Fig. 1 shows a cartoon of the gp120 surface protein of human-immunodeficiency virus (HIV) and the HA surface protein of influenza, with increasing extents of variability of the amino acids for these surface proteins indicated by increasing shades of purple. For a large

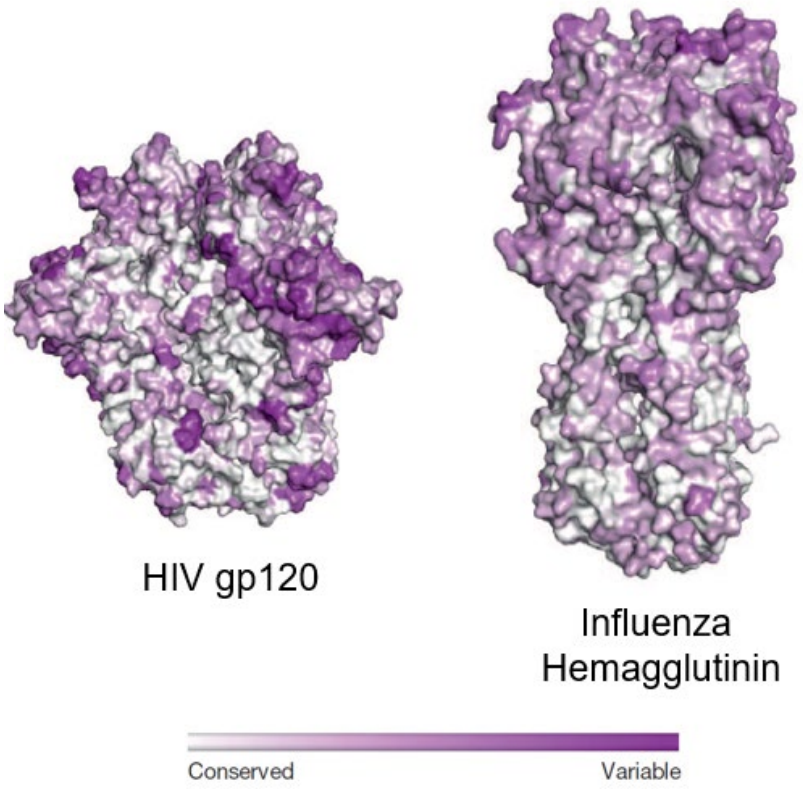

Figure 1. Sequence variability in antigenic surface proteins. Structure of glycoprotein 120 (gp120) of HIV and Hemagglutinin (HA) of Influenza virus shown with the sequence variability of their surface residues highlighted in increasing shades of purple indicating the extent of variability. Figure adapted from Pancera et al., 2014 [16] with permission.

number of pathogens, the host immune response is often focused on the most variable epitopes. In contrast, the conserved regions of these proteins — often receptor binding sites or other essential functional domains – are usually poorly immunogenic and naturally immunosubdominant. As a result, there have been growing efforts to engineer these antigens to refocus the response to their conserved broadly protective regions, using strategies collectively referred to as immunofocusing [30, 31]. Fig. 2 shows the structure of the trimeric ectodomain of influenza hemagglutinin with its globular head and stalk domain marked. The head domain is highly variable (marked by red residues in Fig. 2B) and immunodominant.

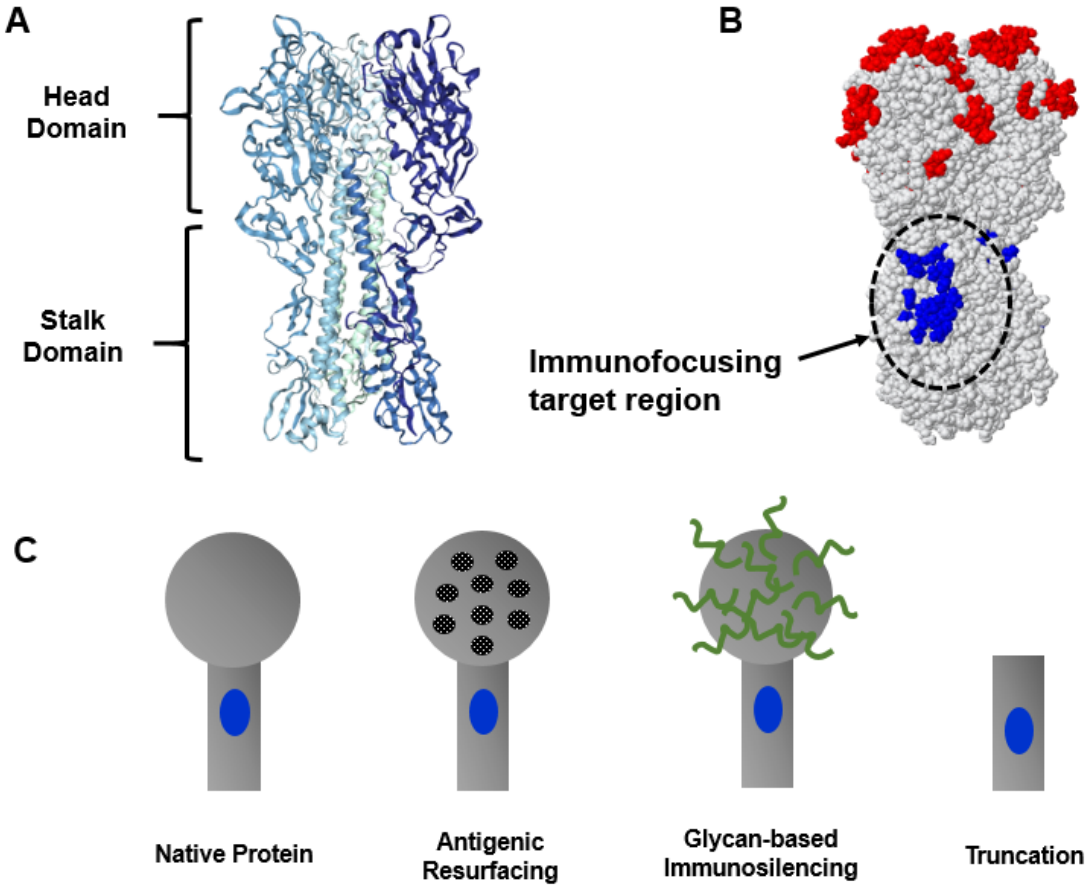

Figure 2. Existing methods of Immunofocusing. (A) Trimeric ectodomain structure of Influenza Hemagglutinin (HA) in a ribbon form. Each protomer of the trimer is highlighted in a different color. HA has a globular head domain and a membrane proximal stem domain. (B) Spacefilled structure of HA with the residues in red showing the variable head epitopes and the residues in blue showing an epitope for a broadly neutralizing stalk antibody. This target region for immunofocusing (stem region) is highlighted by a circle. (C) Schematics for immunofocusing strategies shown with a blue patch indicating the target region.

The stem domain on the other hand is fairly conserved. The epitope for a broadly neutralizing stalk binding antibody is shown in blue in Fig. 2B. As a result, efforts to engineer HA to design a broadly protective vaccine against influenza, involve immunofocusing to the stem domain. Fig. 2 C illustrates various strategies to focus the response to the conserved stem region – indicated by a blue patch [32]. Antigenic resurfacing involves the alteration of all

surfaces other than the desired site where the immune response needs to be focused [33]. However, this approach will still result in an immune response to the resurfaced residues and does not focus the response on the targeted regions. Immunosilencing attempts to reduce the immunogenicity of regions outside of the target epitope through the addition of inert moieties such as N-linked glycans [34, 35]. Glycosylation, however, is a blunt tool allowing limited control over the manipulation of the immune response. Moreover, glycans can themselves become as part of neutralizing epitopes. Truncation cuts out immunologically-irrelevant regions of the antigen leaving behind just regions of interest. This approach has been used successfully to design headless HAs, with a stabilized stalk-only trimer removing interference from head response altogether. Although, truncation is an elegant strategy to focus the immune response to the most relevant parts, this strategy needs significant protein engineering and may need to be reworked for every new antigen. Furthermore, depending on the structure of the antigen and the location of the epitope of interest on this antigen, a truncation strategy may not always be possible.

In this work, we have developed two new strategies to address some of these limitations and to expand the existing toolkit of immunofocusing. First, we have developed a technique referred to as nanopatterning, in which the precise control over the attachment of PEG chains to a protein antigen provides finer control over the modulation of immunogenicity. This approach is in contrast to traditional methods to PEGylate proteins with a high surface density of PEG resulting in global immune suppression [36]. We have demonstrated the success of our approach using green fluorescent protein (GFP) as a model antigen and further extended the idea to an important malarial antigen to focus the response to its broadly protective epitope. This approach has been discussed in Chapter 2. Second, we have

developed another novel approach to immunosilencing that utilizes antibody fragments as shielding agents. Since the binding of an antibody fragment to its antigen is non-covalent in nature, our approach involves engineering these fragments as shields with enhanced binding to the antigen. We have developed two related approaches, one that involves tethering antibody fragments to the antigen and a second approach involving the design of bivalent antibody fragments as shields. We have demonstrated the applicability of antibody fragments as shielding agents in the context of HA (Chapter 3) and a Zika virus surface protein (Chapter 4) to show their ability to suppress the immune response towards "undesirable" epitopes. Methods discussed in this work can be applied to antigens from other infectious diseases to design more effective vaccines.

CHAPTER 2. NANOPATTERNING PROTEIN ANTIGENS TO SELECTIVELY REFOCUS THE IMMUNE RESPONSE

2.1 Introduction

PEGylation of therapeutic proteins has been widely used to improve the physicochemical properties of therapeutic proteins and their biomedical efficacy. Several PEGylated products have been approved for use over the years [36]. This approach, however, has primarily been used to eliminate immunogenicity. Another approach to influence protein immunogenicity involves the modulation of glycosylation [37, 38]. The human immunodeficiency virus (HIV) has a dense glycan network that shields its neutralizing epitopes from the immune system [37, 38]. The removal or addition of glycosylation sites has also been used to modulate the immunogenicity of protein antigens [35, 39-42].

However, there are several limitations to using glycosylation for modulating the immune response to protein antigens. First, this post-translational modification is often vital for the proper folding of proteins. Second, glycans themselves can become part of neutralizing epitopes. For instance, in case of HIV, many broadly neutralizing antibodies directly target glycans or bind to epitopes partially composed of glycans [43]. Finally, glycosylation is a blunt tool that provides limited control over the structure of the glycans.

Similarly, traditionally used PEGylation strategies have several limitations as far as their ability to modulate protein immunogenicity is concerned [44]. Firstly, a succinimide functionalized polyethylene glycol (PEG) moiety reacted non-specifically and randomly to the surface exposed amine groups has limited control over the attachment site. The

cysteine-maleimide chemistry, which involves incorporating a cysteine residues within the protein followed by reaction with a maleimide functionalized PEG, is best suited for proteins lacking internal disulfide bonds [36].

Thus, one needs a technique that is orthogonal to glycosylation, that can be applied even to non-glycosylated proteins, and that allows finer control over shielding of selected regions of a protein antigen. To that end, we have developed an approach, termed as "Nanopatterning", which combines site-specific incorporation of unnatural amino acids [45, 46] with biochemical conjugation to a shielding agent such as PEG.

Fig. 3 shows a schematic of the nanopatterning approach. A model protein is shown in purple with a certain epitope of interest to be shielded shown in cyan. An immune response to this antigen would result in antibodies binding to the epitope of interest (cyan) and those that bind elsewhere on the protein (purple). To nanopattern this protein, with the goal of selectively shielding the cyan epitope, residues around this epitope can be identified to incorporate the unnatural amino acid p-azido-L-phenylalanine (F*). Next, the reactive azide group of F* allows the site-specific functionalization with PEG-DBCO (Dibenzocyclooctyne) via copper-free click cycloaddition [47]. This controlled conjugation of the PEG shield results in the nanopatterned mutant, which selectively suppresses the immune response to the epitope of interest (illustrated by elimination of "cyan" antibodies from the resulting response). Tuning the location of incorporation of F* and the size of the PEG shield provides control over the nanopatterning of the antigen surface.

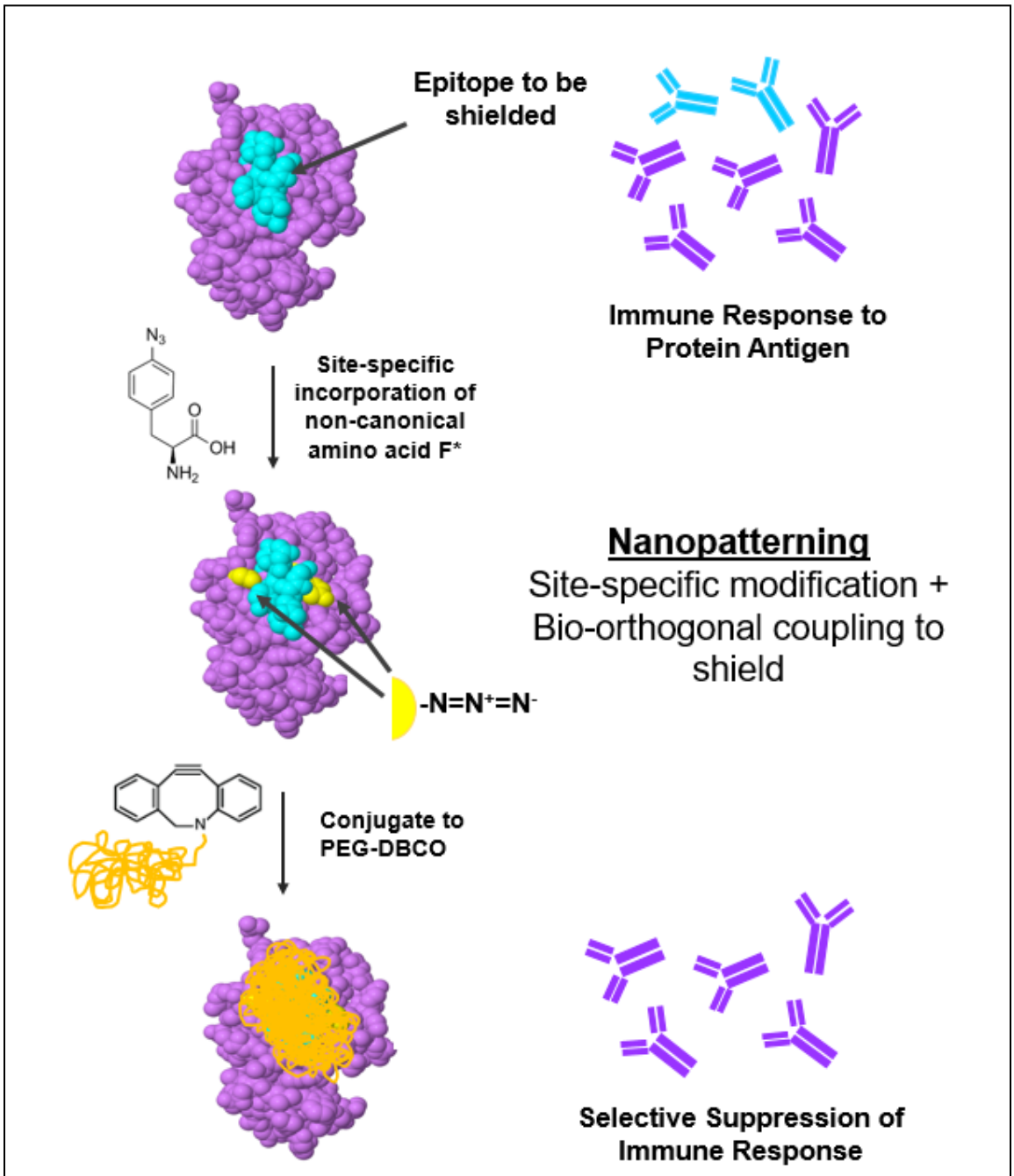

Figure 3. Schematic for the Nanopatterning approach. A model protein shown in purple (top left) with a certain epitope of interest (in cyan) to be shielded. The immune response from this antigen would result in antibodies binding to both the epitope (cyan) and to other regions (purple). Residues in yellow show are sites identified around the epitope of interest, to incorporate the unnatural amino acid F* expressing the reactive azide moiety. On conjugating to PEG-DBCO, the epitope of interest is selectively shielded, resulting in selective suppression of the immune response.

2.2 Materials and Methods

2.2.1 DNA design and Protein Expression and Purification

DNA encoding superfolder green fluorescent protein (PDB ID: 2B3P), SpyCatcher (PDB ID: 4MLI) [48], *Pf*MSP1$_{19}$ (*Wellcome allele*, PDB ID: 1CEJ) [49] and *Py*MSP1$_{19}$ (*P. yoelii yoelii*, isolate *17 xnl*, PDB ID: 2MGP) [50] was optimized for expression in *E. coli* and synthesized by Integrated DNA Technologies, Inc. with C-terminal hexahistidine tags. SpyCatcher had an additional N-terminal Streptag® II. GFP had an additional N-terminal SpyTag [48]. The genes were then cloned in a modified pET28b vector using Gibson cloning (E5520S, New England Biolabs, Ipswich, MA) using primers designed using the NEBuilder tool and following manufacturer's instructions. A version of *Py*MSP1$_{19}$ with a StreptagII replacing the hexahistidine tag was designed by Site-directed mutagenesis (SDM), performed using the Q5-SDM kit (E0554S, New England Biolabs) following manufacturer's instructions. Primers for SDM were designed using the NEBase changer tool. DNA for GFP Nanobody (NB) (PDB: 3OGO) and PyMSP1$_{19}$ (*P. yoelii nigeriensis*, isolate N67) [51] was optimized for expression in *E. coli* and synthesized and cloned in a modified pET28b vector between NdeI/XhoI sites by Gene Universal Inc., Newark, DE. GFP NB had a C-terminal c-myc tag followed by a hexahistidine tag for purification and *Py*MSP1$_{19}$ (*N67* isolate) had a C-terminal Strep-tag® II for purification.

For protein expression, the plasmids encoding GFP, SpyCatcher, and NB were transformed into BL21 (DE3) chemically competent *E. coli* cells (C2527H, New England Biolabs) and all plasmids for MSP1$_{19}$ were transformed into Origami™ 2(DE3) competent *E. coli* cells (71408-3, MilliporeSigma) and grown at 37°C in 2xYT media with 35 µg/mL of

kanamycin overnight. The starter cultures were scaled up to the appropriate culture volume and grown at 37°C. Expression was induced with 1 mM Isopropyl-beta-D-thiogalactoside (IPTG) at OD ~ 0.8-0.9. After induction the temperature was lowered to 16°C and expression continued overnight. For the expression of proteins containing the non-canonical amino acid (ncAA) p-azidophenyl alanine (F*), cells were co-transformed with pEvol-pAcFRS.2.t1 (Addgene plasmid # 73544) to add the machinery to allow incorporation of the unnatural amino acid at the amber codon (TAG). Cell cultures in this case were additionally supplemented with 35 µg/mL of chloramphenicol. At the time of induction at OD ~ 0.8-0.9, 1 mM IPTG 0.02% L-arabinose and 1 mM F* (06162, Chem-Impex International Inc.) were added and expression continued overnight at 16°C.

After expression, for hexahistidine tagged proteins, the cells were pelleted at 6,000-8,000xg for 15 min and gently resuspended in binding buffer buffer [20 mM Tris, 500 mM NaCl, 20 mM imidazole, 5% (v/v) glycerol, pH 8.0] supplemented with a protease inhibitor tablet (S8830, Sigma-Aldrich), lysozyme (0.5 mg/mL; J60701, Alfa Aesar), and benzonase (0.5 µL; E1014, Sigma-Aldrich). The cells were then incubated on ice for 10-15 min with intermittent mixing. Sodium deoxycholate (302-95-4, Alfa Aesar) was added to achieve a final concentration of 0.1% (w/v) before sonication for a total of 6 min (3 s on, 3 s off and 25% amplitude; Sonifier S-450, Branson Ultrasonics). The cell debris was then sedimented at 25,000xg (30 min). The supernatant was filtered (0.45 µm filter; 6869-2504, GE Healthcare) before purification of the hexahistidine-tagged proteins via Immobilized Metal Affinity Chromatography (IMAC) at 4 °C. The supernatant was passed twice over a bed of 2 mL Ni-NTA resin (88222, Thermo Fisher Scientific) in a drip column (786-197, G-Biosciences) that was pre-equilibrated in the binding buffer (20 mM Tris, 500 mM NaCl,

20 mM imidazole, 5% v/v glycerol, pH 8.0). The resin was then washed with 25 column volumes of the binding buffer. For elution, one column volume of elution buffer (20 mM Tris, 500 mM NaCl, 400 mM imidazole, 5% v/v glycerol, pH 8.0) was incubated with the resin for 4-5 min. This elution step was repeated four additional times to obtain five column volumes of the eluted protein. Finally, the protein was concentrated to 1 mL using spin concentrators (Amicon Ultra-15, 10 kDa MWCO, Millipore Sigma) and further purified via size-exclusion chromatography using a Superdex 75 10/300 GL column (GE Healthcare) on an AKTA Pure purification system (29018224, GE Healthcare) with a PBS running buffer (0.5 mL/min).

For purification of proteins with a Strep-tag® II, StrepTrap chromatography was performed. Cells were harvested as described above except the binding buffer used was (100 mM Tris, 150 mM NaCl, 1 mM EDTA, pH 8.0). After harvesting, the clarified lysate was run through a 5 mL StrepTrap HP column (28-9075-47, GE Healthcare) on an AKTA start purification system (29022094, GE Healthcare) at a flow rate of 0.5 mL/min. The column was next washed with the binding buffer (8-10 column volumes) followed by elution with 2-3 column volumes of the elution buffer (100 mM Tris, 150 mM NaCl, 1 mM EDTA, pH 8.0, 2.5 mM desthiobiotin). All proteins were finally purified using size exclusion chromatography (SEC) on a Superdex 75 Increase 10/300 GL column (GE Healthcare, 29-1487-21) in PBS buffer. The SEC refining step removes aggregates if any. The proteins were concentrated and stored at 4°C in the dark until further use.

The DNA for light and heavy chain variable regions (VL and VH resp.) for Fab 12.10 (sequence obtained from [52]) were optimized for mammalian expression and synthesized and cloned in TGEX-LC and TGEX-FH vectors respectively by Gene Universal Inc.

(Newark, DE). A hexa-histidine tag was incorporated at the C-terminus of the heavy Fab chain for purification purposes. Further, a version of *Pf*MSP1$_{19}$ fused to Fab12.10 was also designed. The DNA for *Pf*MSP1$_{19}$ was optimized for mammalian expression, synthesized and cloned upstream of the LC for Fab12.10 in TGEX vector spaced by 3x repeats of flexible GGGGS linker, by Gene Universal Inc. (Newark, DE). Fab12.10 and *Pf*MSP1$_{19}$-3xG4S-12.10Fab were expressed in HEK293F suspension cells using the ExpiFectamine™ 293 transfection kit (A14524, Gibco) using manufacturer's protocol. After expression, the cell culture supernatants were thoroughly dialyzed against PBS and Fabs were purified by IMAC followed by SEC on a Superdex 75 Increase 10/300 GL column (GE Healthcare, 29-1487-21) in PBS buffer. The SEC refining step removes aggregates if any. The purified proteins were concentrated, quantified using the Bicinchoninic acid (BCA) assay, and stored at 4°C until further use.

2.2.2 PEGylation and Purification

The unnatural amino acid F* was incorporated into GFP at residues 175 (S175F*) and 204 (Q204F*) for Mut1-NB* and at residues 111 (E111F*) and 190 (D190F*) for Mut2*. Similarly, F* was incorporated into PfMSP1$_{19}$ at residues 11 (Q11F*) and 84 (Y84F*) for *Pf*MutI*; 36 (Q36F*) and 58 (A58F*) for *Pf*MutB1*; 40 (K40F*) and 71 (G71F*) for *Pf*MutB2*; 36 (Q36F*), 58 (A58F*), 40 (K40F*) and 71 (G71F*) for *Pf*MutB* (quadruple mutant); 13 (N13F*) and 87 (N87F*) for *Py*MutI*; and 38 (K38F*), 43 (T43F*), 61 (P61F*), and 74 (S74F*) for *Py*MutB* (quadruple mutant). The purified mutants incorporating the non-canonical amino acids were then allowed to react with 4-5 fold stoichiometric excess (per F*) of mPEG-DBCO (2k, 5k or 10kDa, Nanocs Inc., Boston, MA). The reaction mixture was left at 4°C in the dark overnight and then run on SDS-

PAGE to determine the extent of PEGylation. The completely PEGylated mutant proteins (doubly or quadruply PEGylated) were purified by SEC using a HiLoad 16/600 Superdex 200 column (GE Healthcare) on an AKTA Pure purification system (GE Healthcare) in PBS. The purified PEGylated proteins were concentrated and quantified using a BCA assay (#23227, Thermo Scientific) and stored at 4°C until further use.

2.2.3 Multivalent display of antigen on a tetrameric scaffold

All GFP antigens were expressed with an N-terminal SpyTag. A SpyCatcher mutant with F* incorporated at residue56 (T56F*) was expressed in BL21 (DE3) *E. coli* cells and purified by IMAC followed by StrepTrap chromatography and then allowed to react with a 4-arm branched polyethylene glycol scaffold (5 kDa PEG arms with terminal DBCO groups) (Creative PEGworks, Chapel Hill, NC). The protein was added at a 4-fold stoichiometric excess (per DBCO group) and the reaction was allowed to proceed at 4°C in the dark overnight. The reaction mixture was characterized by SDS-PAGE to confirm the formation of tetrameric product, which was separated from the incompletely reacted products by SEC using a HiLoad 16/600 Superdex 200 column (GE Healthcare) on an AKTA Pure purification system (GE Healthcare) in PBS. The tetrameric scaffold was concentrated and quantified using the BCA protein assay.

The GFP antigens with an N-terminal SpyTag were then allowed to react with the tetrameric SpyCatcher scaffold overnight at 4°C. The SpyTag-SpyCatcher pair spontaneously forms an isopeptide bond [48], thereby immobilizing the antigens on the tetrameric scaffold, and enabling its multivalent display. The final tetrameric-GFP mutants were purified using SEC and characterized by SDS-PAGE. The amount of GFP in the final

tetrameric form was quantified using a fluorescence-based assay (λ_{ex}=400 nm; λ_{em}=509 nm).

2.2.4 Characterization by ELISA and analytical SEC

Anti-*Pf*MSP1$_{19}$ antibodies 12.8, 12.10, 7.5 and 2.2 were procured from The European Malaria Reagent Repository (University of Edinburgh, Scotland). Anti-His antibody (MA1-21315, Invitrogen), anti-GFP antibody GF28R (MA5-15256, Invitrogen), and anti-c-myc-HRP antibody (A00173, Genscript) were commercially procured. The nanopatterned antigens were characterized by ELISA to confirm the ability to block recognition to desired regions. Briefly, 50 µL of 0.002 mg/mL of the antigen solution was coated per well on ELISA plates (Maxisorp NUNC, Thermo Scientific) overnight at 4°C in PBS. Plates were blocked with 100 µL of 5% Bovine serum albumin (BSA) (12659, EMD Millipore) in PBST (PBS with 0.05% Tween-20) for 1 hr at RT. After 3x washes with PBST, plates were incubated with 50 µL of primary antibody solutions in 1% BSA in PBST for 1 hr at RT. After 3x washes with PBST, plates were incubated with an appropriate HRP-conjugated secondary antibody for 1 hr at RT. After 3x washes with PBST, plates were developed with TMB substrate solution (00-2023, Thermo Fisher) for 5 min and stopped using 160 mM sulphuric acid solution. Plates were read on a Spectramax i3x plate reader (Molecular Devices) at 450 nm. Experiments were performed in triplicates.

Further, an SEC shift assay was performed to confirm the ability of *Pf*MutB*-PEG to bind to the inhibitory Fab 12.10. All SEC chromatograms were run on Superdex 75 Increase 10/300 GL column (GE Healthcare, 29-1487-21) in PBS buffer using 3µg of antigen (on a PfMSP1$_{19}$ basis). A stoichiometric amount of the Fab12.10 was mixed with *Pf*MutB*-PEG

and then run on the SEC. Individual runs for Fab12.10 and *Pf*MutB*-PEG were separately performed. Chromatograms were recorded using UV280 and overlaid for comparison.

2.2.5 Immunizations in mice and rabbits

BALB/c mice were immunized with the nanopatterned GFP mutants or controls adjuvanted with AddaVax (InVivoGen, CA) by ProSci, Inc. (Poway, CA). Samples included tetrameric scaffolds presenting: (i) wtGFP; (ii) Mut1-NB*; (iii) Mut1-NB*-PEG; (iv) Mut2*; (v) Mut2*-PEG as well as (vi) tetrameric scaffolds alone as a control. Five mice were immunized per group. The protein antigens were diluted to 40 μg/mL in PBS (on a GFP basis). Each mouse (groups i-v) was injected subcutaneously with 2 μg of GFP. Mice in the control group (vi) received an equivalent amount of scaffold as mice in the other groups. Mice were injected with antigen on days 0, 21, and 42. On day 70, the mice were terminally bled and serum was stored at -20°C until further analysis. This mouse study was performed under ACUP 2 as approved by the ProSci, Inc. IACUC. The study was performed at ProSci Inc.‘s USDA licensed, registered, and NIH/OLAW assured animal facility.

Groups of five female CB6F1/J (H-2d/b) mice, 6 to 8 weeks of age, were purchased from The Jackson Laboratory. The animals were immunized subcutaneously on days 0, 20, 40 and 88, in the base of the tail and the interscapular area. 7.5 μg of antigens (PyMutI*-PEG, PyMutB*-PEG, PBS control) were emulsified in the adjuvant Montanide ISA 51 VG (Seppic, Fairfield, NJ) prior to injection. All animal protocols were approved by the Emory University’s Institutional animal Care and Use Committee and followed accordingly.

The engineered nanopatterned *Pf*MSP1$_{19}$ mutants were immunized in specific pathogen free rabbits by Covance Research Products, Inc. (Denver, PA). Samples included were: (i) wt *Pf*MSP1$_{19}$, (ii) *Pf*MutI*-PEG, and (iii) *Pf*MutB*-PEG. Three rabbits were immunized per group. 100 µg of antigen was injected subcutaneously (SC) adjuvanted with Freund's complete adjuvant (FCA) on day 0. This prime immunization was followed by 3 boosts with 70 µg of antigen adjuvanted with Freund's incomplete adjuvant (FIA) on days 21, 42, 63. On day 77, the rabbits were terminally bled and serum was stored at -20 °C until further use. This rabbit study was performed under ACUP 2 as approved by the Covance, Inc. IACUC at Covance Inc.'s USDA licensed, registered and NIH/OLAW assured animal facility.

2.2.6 Mice serum analysis and Immunodepletions

The terminal bleed serum was assessed for endpoint titer against wt GFP or *Py*MSP1$_{19}$ (from isolates 17XNL and N67). A version of antigens with a Strep-tag® II were used for ELISAs to avoid signal from anti-His serum antibodies. Briefly, 50 µL of 0.002 mg/mL antigen were added per well to ELISA plates and the protein was allowed to adsorb onto the wells overnight at 4°C in PBS. Plates were blocked with 100 µL of 5% BSA in PBST for 1 hr at RT. After 3x washes with PBST, plates were incubated with 50 µL of sera diluted four-fold starting at 1:100 in 1% BSA in PBST for 1 hr at RT. After 3x washes with PBST, plates were incubated with a secondary HRP-conjugated anti-mouse antibody (115-035-003, Jackson ImmunoResearch) for 1 hr at RT. After 3x washes with PBST, plates were developed with TMB substrate solution (00-2023, Thermo Fisher) for 5 min and stopped using 160 mM sulphuric acid solution. Plates were read on a Spectramax i3x plate reader (Molecular devices) at 450 nm. Titers were expressed as area under the curve (AUC)

determined using GraphPad Prism software. Appropriate positive controls were included: commercially procured antibody GF28R binding to GFP and an anti-Strep-tag® II antibody (600-401-H22, Rockland Immunochemicals Inc.) for the detection of wtGFP and *Py*MSP1$_{19}$.

Immunodepletion assays for the GFP set were carried out with the pooled terminal bleed serum for Mut1-NB*-PEG, Mut2*-PEG, and scaffold alone controls. Briefly, GFP Nanobody was first immobilized on Ni-NTA beads via the hexa-histidine tag on the Nanobody. The beads were thoroughly washed to remove any unbound NB. Next, GFP with the orthogonal Strep-tag® II purification tag was incubated with the NB-coated NTA beads, resulting in a complex of GFP and NB immobilized on NTA beads. After thorough washing to remove any unbound GFP, the GFP-NB-NTA depletant was incubated with serum (at a 1:200 dilution) for 3-4 hrs at 4°C. A total of 4 rounds of depletion were performed for all three serum samples. All incubations, washes, and serum dilutions were carried out in 1% BSA solution in 20 mM Tris, 500 mM NaCl, 20 mM imidazole, 5% (v/v) glycerol, pH 8.0. As a control, NB-negative NTA beads were used as a depletant, and serum samples were similarly depleted 4 times. The depleted and undepleted sera from all 3 groups were characterized by ELISA as described above.

2.2.7 Rabbit serum antibody purification and analysis

*Pf*MSP1$_{19}$ specific antibodies were purified from the pooled rabbit serum for each of the antigen samples. wt *Pf*MSP1$_{19}$ was immobilized on NHS-activated Sepharose™ 4 Fast flow (17-0906-01, GE Healthcare) beads using manufacturer's instructions. Briefly, wt *Pf*MSP1$_{19}$ protein was dialyzed in a coupling buffer (200 mM $NaHCO_3$, 500 mM NaCl pH

8.3). The resin beads were washed with cold 1mM HCl followed by mixing with the protein solution, stirred overnight at 4°C. The unreacted groups on the beads were blocked with 100 mM TRIS-HCl, pH 8.5 for 2-3 hrs. Next the immobilized protein beads were washed alternatively with 100 mM acetate buffer, 500 mM NaCl, pH 4.5 and 100 mM TRIS-HCl, pH 8.5, repeated 3-6 times with each buffer. The resin was then packed in drip columns and washed with PBS buffer. The serum solution was then loaded on the columns, followed by a wash with PBS, finally eluting with 100mM Citric acid, pH 3. The eluted antibodies were immediately neutralized using 1M TRIS-HCl pH 9.0 and dialyzed against PBS, pH 7.4. The entire purification process was carried out at 4°C.

The purified antibodies were characterized by ELISA to confirm binding to wt*Pf*MSP1$_{19}$. SEC shifts were performed for the purified antibodies by complexing with *Pf*MSP1$_{19}$-3xG4S-12.10Fab. All SEC chromatograms were run on Superdex 75 Increase 10/300 GL column (GE Healthcare, 29-1487-21) in PBS buffer using 3ug of *Pf*MSP1$_{19}$-3xG4S-12.10Fab (on a *Pf*MSP1$_{19}$ basis). Purified rabbit antibodies from each group were run with *Pf*MSP1$_{19}$-3xG4S-12.10Fab in a 1:1 stoichiometric ratio. Chromatograms were recorded using UV205 and overlaid for comparison.

2.2.8 Statistical analysis

AUC was calculated using a sigmoidal curve fitting. A minimum of three technical repeats were tested for all ELISAs, and the experiments were repeated at least three times with similar results. One-way ANOVA with post-hoc Tukey's multiple comparison test was applied when indicated in the figure legend. All statistical analysis was performed using GraphPad Prism 8 (GraphPad Software Inc.)

2.3 Results and Discussion

2.3.1 Engineering, Expression and Purification of Nanopatterned GFP

We have developed a bio-inspired approach for nanopatterning protein antigens that combines site-specific mutagenesis with bio-orthogonal coupling to a synthetic shielding molecule or polymer – such as PEG. Our goal was to demonstrate that site-specifically conjugating PEG chains on a protein can suppress immune response locally at selected epitopes as opposed to a global immune suppression. As a proof of principle, we first tested our approach using GFP as a model antigen. GFP is a stable protein that is easy to express and purify; its structure is known; and anti-GFP antibodies are commercially available for characterization. The 'epitope to be shielded' was chosen to be the epitope for a GFP Nanobody that binds to GFP with high affinity (K_d ~ 1.4 nM) [53].

Fig 4A (left) shows a crystal structure complex of GFP (shown in green) bound to the NB (shown in magenta) (PDB ID: 3OGO). A footprint of the NB binding on GFP is marked in pink on GFP in Fig 4A (ii) (right). We identified residues around or within this epitope of interest and mutated them to incorporate the non-canonical amino acid (ncAA) para-azido phenylalanine (F*) using the pEvol-pAcFRS.2.t1 system (Addgene #73544) [45]. Next, these mutant GFP proteins were reacted with PEG-DBCO, to site-specifically conjugate the PEG to the protein. The reaction results in a mixture of completely PEGylated and incompletely PEGylated protein; the former was purified by chromatographic separation using SEC and characterized by SDS-PAGE. The DBCO and azide groups react covalently via the strain promoted alkyne-azide cycloaddition without the need of copper. The copper-free "click chemistry" is biorthogonal, highly specific, highly stable physiologically, and

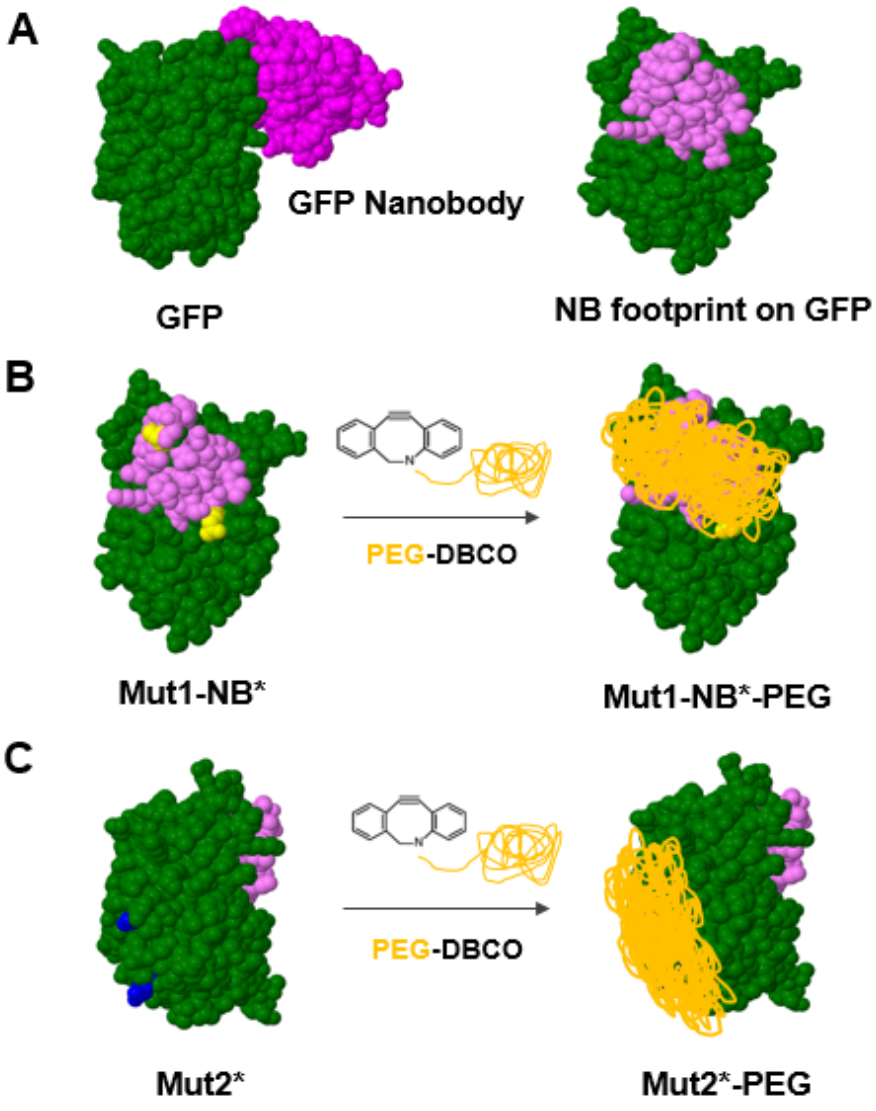

Figure 3. Nanopatterning GFP. (A) Left: The structure of GFP in green bound to the Nanobody (NB) in pink; Right: Structure of GFP in green with the footprint of Nanobody (NB) marked in light pink (B) Mut1-NB*, showing residues in yellow around the NB epitope that were mutated to F*; conjugation to PEG-DBCO generates nanopatterned Mut1-NB*-PEG. (C) Nanopatterned Mut2*-PEG was designed as a control to shield a site distant from the NB epitope.

requires mild reaction conditions suitable for biological molecules such as protein-based antigens [54].

GFP mutants were screened based on their ability to retain protein expression, protein yield, and protein structure (determined by binding to commercial conformational anti-GFP antibodies in ELISAs). The selection of residues was also guided by solvent accessibility (to ensure efficient conjugation to the PEG chain) and their conservation score, (determined by a ConSurf analysis) [55] to estimate the amenability of that residue to mutation to F*. Fig 4B shows design scheme for the mutant of interest (referred to as Mut1-NB*). In yellow are marked the residues (Ser175 and Gln204) where the UAA F* was incorporated using amber stop codons. On reacting with PEG-DBCO and followed by purification, the nanopatterned version of Mut1-NB* (referred to as Mut1-NB*-PEG) was obtained. As a control, another mutant of GFP was designed where the PEG chains were conjugated on a distant face (opposite to the NB epitope). The reaction scheme for this control Mut2* is shown in Fig 4C.

Multivalency has been shown to amplify immune responses by primarily clustering B-cell receptors resulting in robust downstream signaling [3, 56-59]. We next displayed the GFP antigens on a tetrameric polymer-protein based scaffold. The scaffold was designed based on the spontaneous covalent isopeptide bond formation of the protein peptide pair - Spycatcher-Spytag that was engineered from a bacterial adhesion CnaB2 [48]. We first synthesized a tetrameric version of SpyCatcher by conjugating a mutant version of SpyCatcher expressing an azide group to a 4-arm PEG star scaffold with a terminal DBCO group (5000 Da per arm). The azide group on SpyCatcher was inserted replacing residue Thr56 with the ncAA F* using the amber stop codon. The selection of this residues was based on it being on the face opposite to the Spytag binding region on SpyCatcher, its solvent accessibility, and its conservation score (determined by a ConSurf analysis [55]).

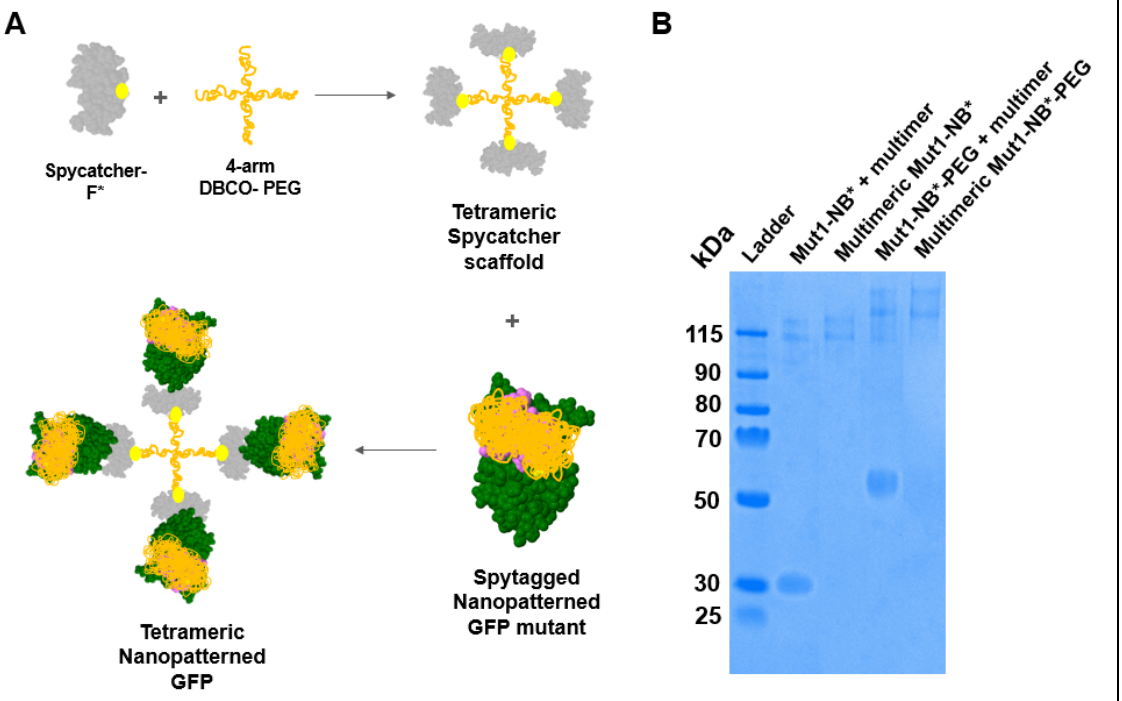

Figure 5. Multivalent display of Nanopatterned GFP. (A) Scheme for synthesizing multivalent GFP conjugates based on SpyCatcher-functionalized branched PEG scaffolds (B) SDS-PAGE gel image showing the multimeric (tetramer-trimer mixture) conjugates for Mut1-NB* and Mut1-NB*-PEG

All GFP mutants were expressed with an N-terminal Spytag, to allow conjugation to the tetrameric SpyCatcher scaffold. The reaction scheme to achieve tetrameric display of GFP mutants is shown in Fig 5A. The multimeric-SpyCatcher (tetramer-trimer mixture) was purified from the incompletely reacted components in the reaction mixture using SEC. Fig. 5B is an SDS-PAGE gel image showing the reaction mixture of Mut1*-NB and Mut1*-NB-PEG with the multimeric scaffold and the two SEC purified antigens on the multimeric scaffold.

2.3.2 Characterization of Nanopatterned GFP mutants by SDS-PAGE and ELISA

The size of PEG to shield the NB epitope was selected based on the estimated root-mean-squared (RMS) end-to-end distance. We initially screened PEG chains of MW 2k, 5k and 10 kDa with our mutant of interest (Mut1-NB*) and tested their ability to block recognition of the NB without an appreciable loss of binding to an orthogonal anti-GFP antibody (GF28R). This test was important because we wanted to make a judicious choice of PEG length that was big enough to shield the region of interest but not excessively large so that it would shield other regions on the protein.

The RMS lengths for a 2k, 5k and 10kDa PEG chain are approximately 3.9 nm, 6 nm and 8.7 nm respectively [60]. Assuming that the PEG conjugated to the protein forms a roughly spherical cloud [61], the corresponding radii of gyration (R_g) for 2k, 5k and 10kDa PEG are approximately 2 nm, 3 nm and 4.5 nm respectively. The NB epitope can be assumed to be circle with a diameter of 2.5-3 nm. The two residues mutated to F* for PEG attachment (to Mut1-NB*) were selected to be on the periphery of the epitope. This site-selection strategy would allow sandwiching the epitope of interest with two PEG clouds shielding the bulk of the NB epitope. Based on this analysis, two 5kDa PEG chains - each forming a PEG cloud of radius ~ 1.5 nm was thought to be appropriate to shield an epitope ~ 3nm in diameter.

To confirm our understanding and to analyze the effect of PEG length on the ability to selectively shield the NB epitope, we synthesized PEGylated versions of Mut1-NB* using PEG chains of length 2k, 5k and 10kDa. Fig. 6A shows cartoons of Mut1-NB* and its PEGylated versions using PEG chains of lengths 2k, 5k and 10kDa. Next, we probed binding of the NB and an orthogonal anti-GFP antibody to these mutants in an ELISA. As we can see in Fig 6B, the binding of the NB to Mut1-NB* is reduced to baseline irrespective

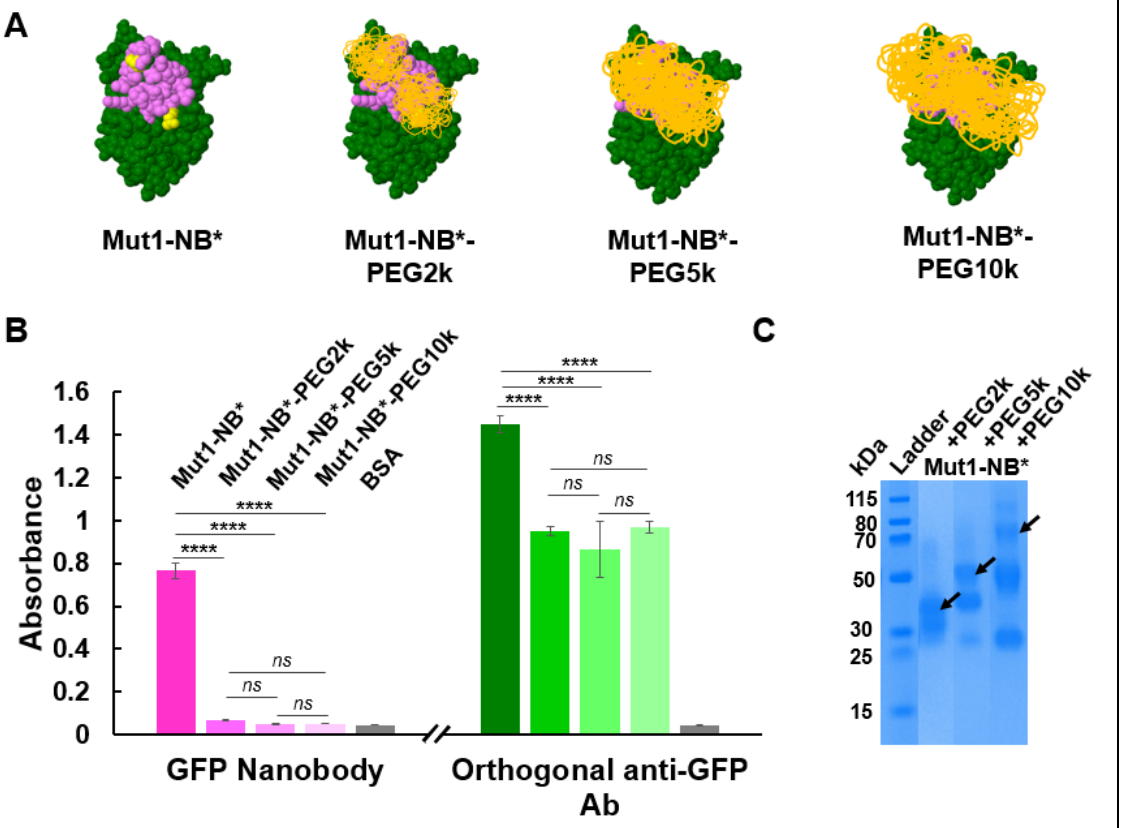

Figure 6. Effect of PEG length on shielding ability of GFP epitopes. (A) Mut1-NB* and its nanopatterned versions using 2k, 5k and 10kDa PEG (B) ELISA result showing binding of the NB and an orthogonal anti-GFP antibody to Mut1-NB* and the nanopatterned mutants with increasing PEG lengths. ELISA binding expressed as absorbance (mean ± SD, n=3). The labelling of the bars for the right cluster follows as labelled on the left. (****p<0.0001, ns – not statistically significant, determined by a one-way ANOVA with post-hoc Tukey's multiple comparison between groups). (C) SDS-PAGE gel image showing reaction mixtures of Mut1-NB* with PEG2k, 5k and 10k, arrows shows desired double PEGylated product.

of the length of PEG chain tested. Similarly, the binding of the orthogonal anti-GFP antibody is unaffected by the length of the PEG chain tested. It is important to note that, although the 2 kDa PEG is successfully able to prevent binding of the NB to the epitope whereas the absence of PEG does not – this is not a conclusive test to say that the 2kDa PEG shields would completely occlude the epitope and prevent elicitation of antibodies to that region. In other words, the 2 kDa PEG shields may successfully shield important

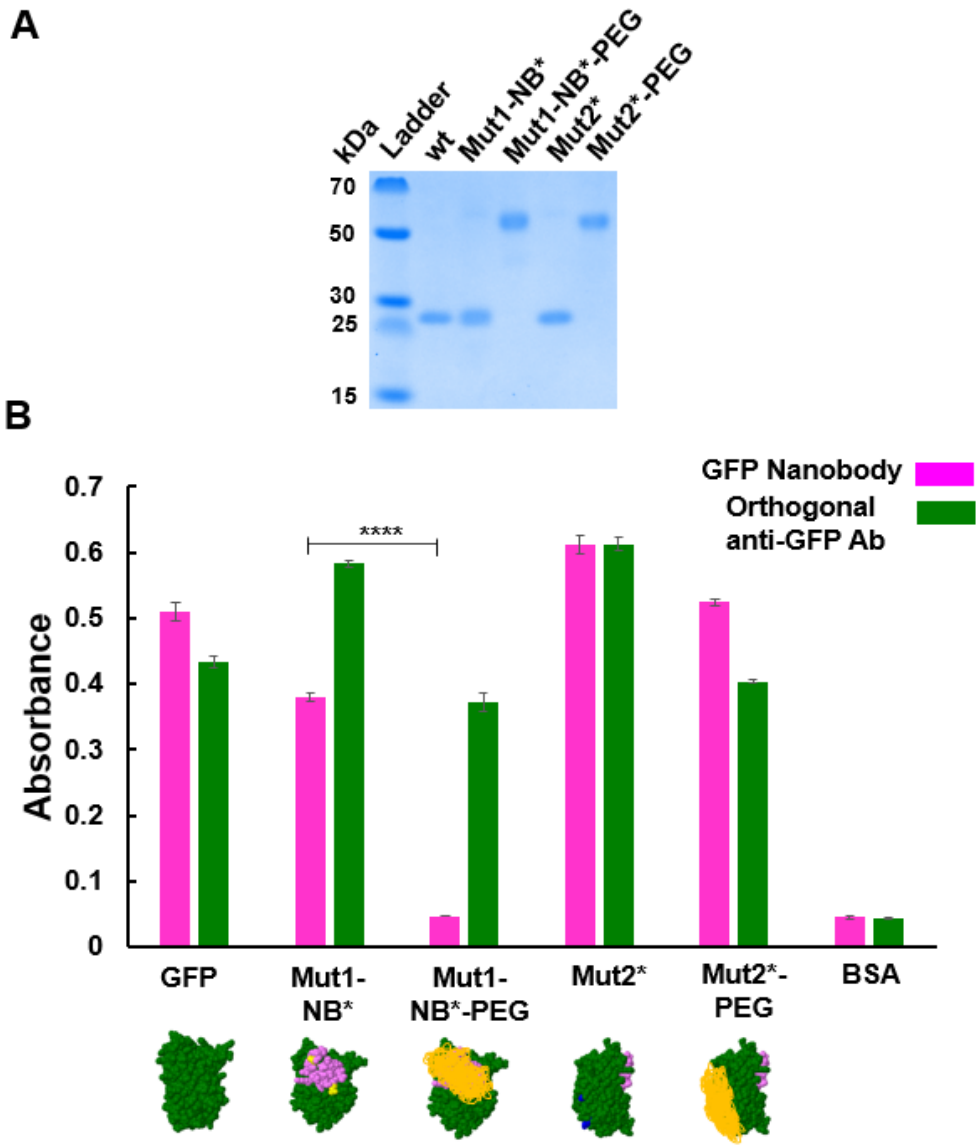

Figure 7. Characterization of Nanopatterned GFP mutants. (A) Characterization of wild-type (wt), mutant, and nanopatterned GFP variants by SDS-PAGE (B) Characterization of binding of NB (pink bars) and an orthogonal anti-GFP antibody (green bars) to multivalent wt, mutant, and nanopatterned GFP variants by ELISA. ELISA binding expressed as absorbance (mean ± SD, n=3). (****p<0.0001, determined by a one-way ANOVA with post-hoc Tukey's multiple comparison between groups).

residues involved in binding to a monoclonal antibody like the NB, but it may or may not shield the epitope entirely. Hence, in this case we relied on the estimates derived from the

analysis of the R_g of PEG shields and chose to proceed with 5kDa PEG chains for our study – as this choice seemed closest to offering an extent of shielding corresponding to the area required to be blocked on GFP.

Fig 7A shows an SDS-PAGE gel image of wtGFP, Mut1-NB*, Mut1-NB*-PEG, Mut2* and Mut2*-PEG (in that order from left to right). The mutants incorporating F* run similar to wtGFP – as expected. The mutants alone run alongside the wtGFP as expected. However, the doubly PEGylated mutants - Mut1-NB*-PEG and Mut2*-PEG run higher because of the additional mass from the two 5kDa PEG chains. All SpyTagged GFP variants were then reacted with the tetrameric-Spycatcher based scaffold and purified using SEC to remove any unreacted excess GFP. The amount of GFP in the final purified samples was determined by fluorescence using a standard curve determined from wt GFP standards.

We further characterized the multivalent conjugates by ELISA. Fig 7B shows the ELISA result showing binding of anti-GFP antibodies – the Nanobody and GF28R (which binds to the N-terminus of GFP) to wt GFP, the unPEGylated mutants Mut1-NB* and Mut2* and their nanopatterned versions. Binding of both antibodies to the unPEGylated mutants is comparable to that with wt GFP, suggesting that the mutations alone do not block binding. However, the relative binding of the NB drops for Mut1-NB*-PEG relative to the orthogonal anti-GFP antibody GF28R binding. Mut2*-PEG, on the other hand behaves as expected, and binds to both antibodies similar to wt GFP. This shows the ability to modulate the recognition of antigens by antibodies by site-specifically conjugating PEG shields to its surface.

2.3.3 Nanopatterning refocuses the immune response of GFP

To understand if this nanopatterning also influenced the specificity of antibodies elicited *in vivo*, we carried an animal study in mice with the engineered GFP mutants. Fig 8A shows the immunization schedule for the study. Serum antibody titers were determined using the area under the curve (AUC) method as it better captures the differences between groups, compared to the end-point titer method (where the true titer may be over-estimated) [62]. Titer results (Fig 8B) showed that all five multivalent GFP conjugates elicited anti-GFP responses, but the scaffold alone control did not, as expected. Furthermore, the titers for the two PEGylated mutants were significantly lower than those for their corresponding non-PEGylated versions (***$p<0.001$, determined by ANOVA comparing all groups). Although the total anti-GFP serum antibody response to the two PEGylated mutants (Mut1-NB*-PEG and Mut2*-PEG) was comparable (statistically not significant – determined by ANOVA comparing all groups), we were interested in determining whether the distribution of the elicited antibodies in terms of their specificity was different. Specifically, we wanted to determine whether nanopatterning has refocused the immune response for Mut1-NB*-PEG away from the Nanobody epitope.

Fig 8C show the hypothesized distribution of antibodies elicited by each of the two mutants. Mut1-NB*-PEG should only elicit *orthogonal* antibodies (shown in green) that bind to GFP on regions other than the NB epitope. Mut2*-PEG on the other hand should elicit antibodies binding to the epitope of interest (shown in pink) as well as *orthogonal* antibodies (shown in green). To test this hypothesis, we performed immunodepletions on the sera from immunized mice to isolate antibodies that bind only to the epitope of interest (pink), while removing all other *orthogonal* antibodies (green). We first immobilized the NB to Ni-NTA beads via the hexahistidine tag on the NB. After washing, the NB bound

beads were then incubated with GFP (fused to an orthogonal Strep-Tag® II as opposed to a hexahistidine tag). Using a Strep-Tag® II version of GFP ensures that it can only bind to

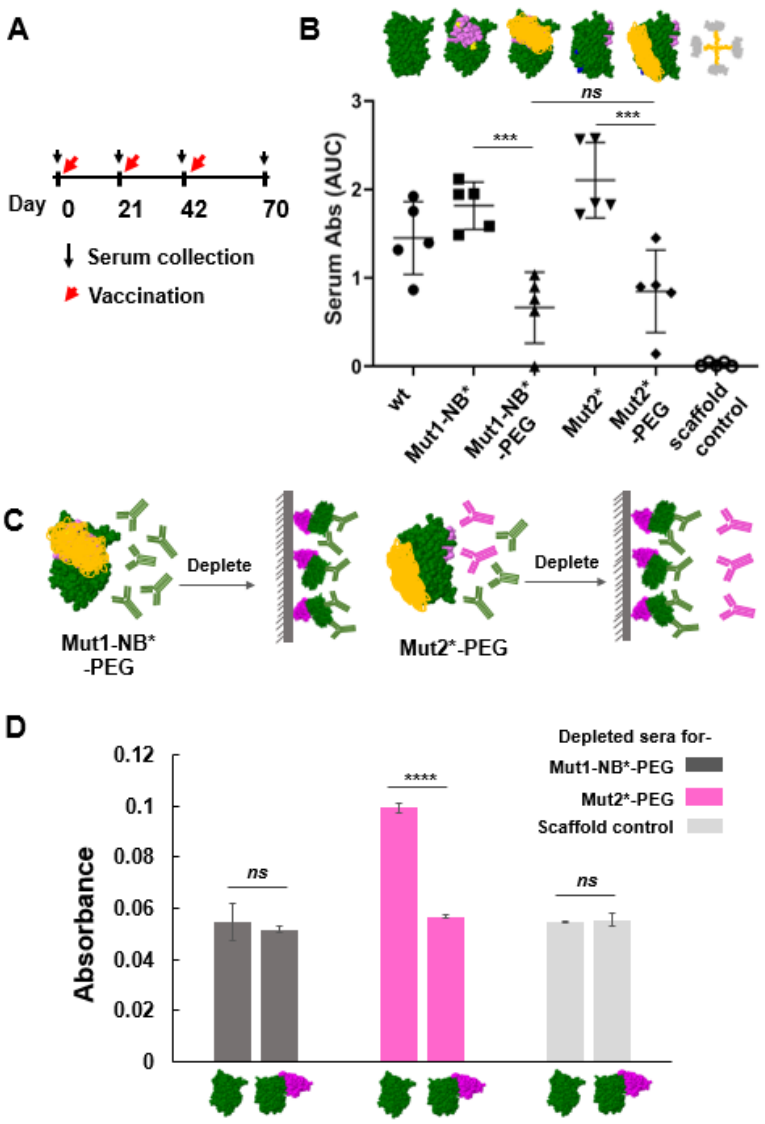

Figure 8. Nanopatterning GFP refocuses the anti-GFP immune response. (A) Vaccination schedule in mice. (B) Serum antibody titers for the multivalent GFP antigens and scaffold alone are expressed as area under the curve (AUC). (C) Scheme illustrating the immunodepletion of anti-nanopatterned-GFP sera to remove antibodies (green) that bind to sites on GFP other than the NB epitope. Antibodies that bind to the NB epitope are shown in pink. (D) Characterization of the binding of immunodepleted sera to wtGFP in the presence and absence of competing NB by ELISA. (****p<0.0001, ns – not statistically significant, determined by a one-way ANOVA with post-hoc Tukey's multiple comparison between groups).

the beads by binding to the NB - and in doing so, the beads now present GFP with its NB epitope occluded (by the NB itself). Fig 8C (left) shows the depletion scheme for Mut1*, which should remove all *orthogonal* antibodies (green) with complete depletion. Fig 8C (right) shows the depletion scheme for Mut2*, which on the other hand should have residual antibodies (pink) post-depletion. The serum from the scaffold alone immunized mice was similarly depleted as a control.

Next, the resulting depleted sera from the 3 samples (Mut1-NB*-PEG, Mut2*-PEG and scaffold control) was tested in ELISA against GFP both in presence (right bar within each group) and absence of competing NB (left bar within each group). As seen in Fig 8D, the depleted control sera (from mice immunized with scaffold control alone) did not show a significant difference in binding to GFP either in present or absence of competing NB. This sets the baseline for the experiment because this serum did not have any anti-GFP antibodies to begin with. Depleted sera from mice immunized with Mut2*-PEG did bind to GFP, but the binding was significantly reduced to baseline in presence of competing NB. This result indicates –as expected -that immunization with Mut2*-PEG elicits antibodies that bind to the NB epitope as hypothesized in Fig 8C. In contrast to that, Mut1-NB*-PEG did not bind significantly to GFP either in presence or absence of competing NB, essentially confirming that nanopatterning had completely refocused the immune response away from the Nanobody epitope.

2.3.4 *Engineering, expression and purification of nanopatterned PfMSP1$_{19}$*

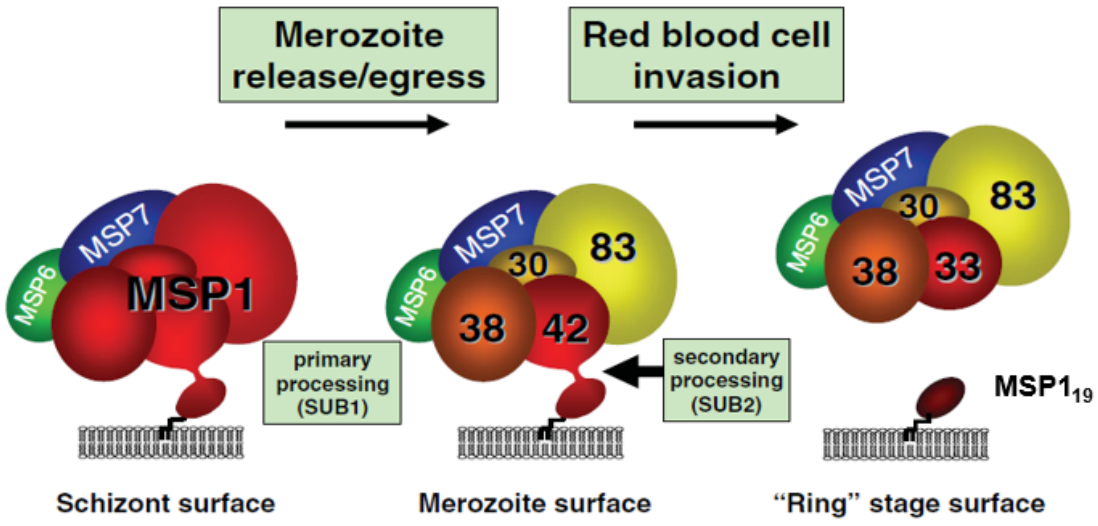

Figure 9. The assembly and processing of the MSP1 complex. Figure adapted from Holder, 2009 [64] with permission.

We next extended the nanopatterning approach to a promising malarial vaccine candidate, Merozoite surface protein 1 (MSP1). Fig. 9 shows the MSP1 complex and its fate just prior to red blood cell invasion. MSP1 undergoes two subsequent proteolytic cleavage steps prior to invading an RBC. Most of its components are shed during this cleavage process, leaving behind a 19-kDa fragment called MSP1$_{19}$ on the parasite surface, that is carried into the invaded RBC [63]. MSP1$_{19}$ is the 19KDa C-terminal fragment of MSP1, shown to be critical to invasion of erythrocytes [63-65]. Inhibitory antibodies elicited against MSP1$_{19}$ inhibit invasion by preventing the proteolytic cleavage of MSP1 [49].

However, a second class of antibodies elicited by MSP1$_{19}$, called "blocking antibodies", interfere with the activity of inhibitory antibodies and constitute a major hurdle in developing an MSP1$_{19}$-based malarial vaccine [66]. To add to this hurdle, the extensive

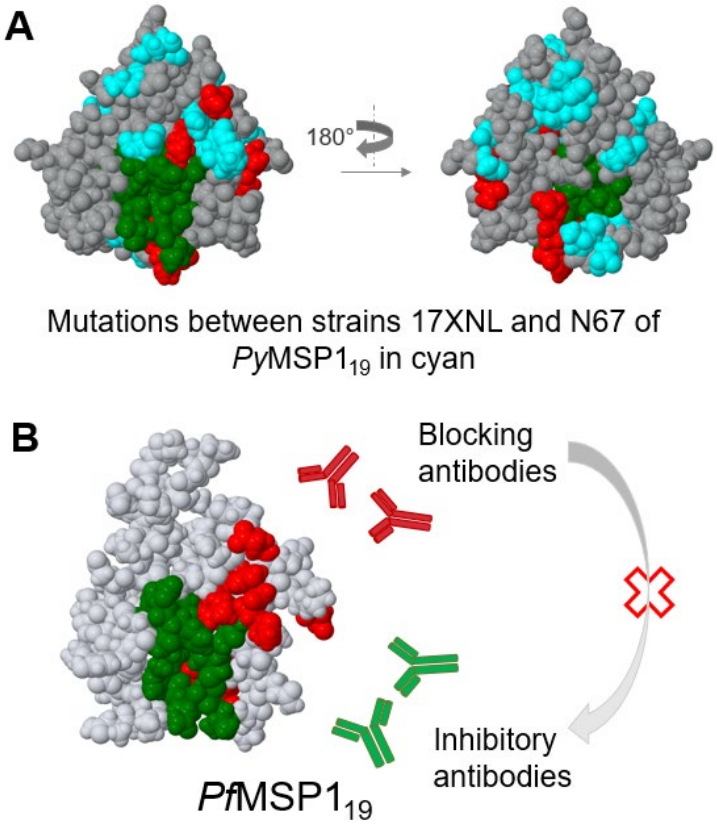

Figure 10. Challenges in vaccine development of MSP1$_{19}$. (A) Structure of *Py*MSP1$_{19}$ (PDB ID: 2MGP) with residues for inhibitory and blocking antibody epitopes marked in green and red respectively. Residues that differ between two strains of PyMSP1$_{19}$ (17XNL and heterologous strain N67) are marked in cyan. (B) Structure of PfMSP1$_{19}$ (PDB ID: 1CEJ) with residues involved in binding to inhibitory and blocking antibodies shown in green and red respectively. Blocking antibodies interfere with the binding of protective inhibitory antibodies.

sequence variability of MSP1$_{19}$ results in a strain-specific immune response [67]. Fig 10A shows the extent of divergence between two strains of *P. yoelii* MSP1$_{19}$ (*Py*MSP1$_{19}$) – 17XNL and N67 by highlighting the divergent residues in cyan (differing at as many as 21 of 96 residues). As a result, immunization with MSP1$_{19}$ offers protection in mice from challenge with a homologous, but not a heterologous strain. Our goal was to test the ability of nanopatterning to selectively suppress the elicitation of "blocking antibodies" (in red in

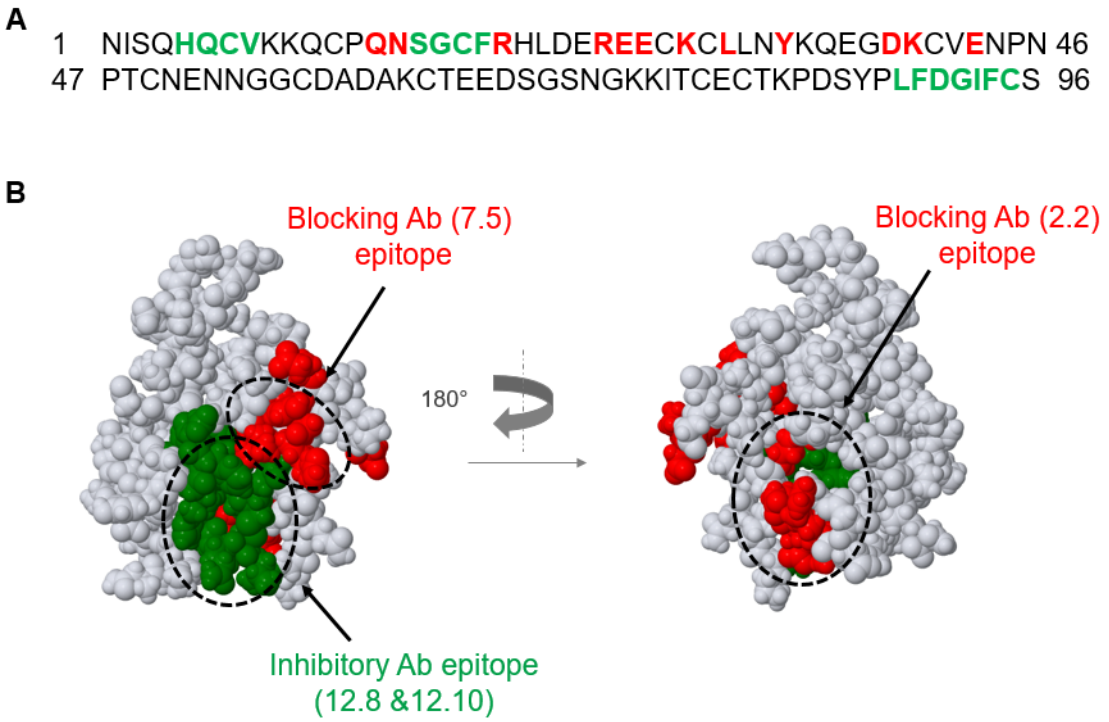

Figure 11. Inhibitory and blocking antibody binding regions on *Pf*MSP1$_{19}$. (A) Protein sequence of *Pf*MSP1$_{19}$ with the residues involved in binding to inhibitory and blocking antibodies marked in green and red respectively. The numbering follows that as in the sequence in PDB ID: 1CEJ. (B) Structure of *Pf*MSP1$_{19}$ (PDB ID: 1CEJ) in gray. The conserved epitope for the inhibitory antibody binding (12.8 and 12.10 Abs) is marked in green. Residues involved in binding to the blocking antibodies 7.5 and 2.2 are marked in red and are spread across both faces of the protein.

Fig 10B) and to refocus the response towards the broadly protective inhibitory epitopes (in green in Fig 10B).

Fig 11A shows the protein sequence of *Pf*MSP1$_{19}$ with the residues highlighted in green marking the conserved epitope for inhibitory antibody binding. These have also been highlighted in green on the crystal structure of the protein as shown in Fig 11B [49, 65]. As for the blocking antibody epitope, Uthaipibull et al. [68] carried out a single residue mutation analysis on PfMSP1$_{19}$ and probed the ability of those mutants to bind to blocking antibodies. They found that there were several residues spread across both faces of the

protein that affected binding of blocking antibodies. These residues have been highlighted in red in the sequence and the protein structure in Fig 11. Interestingly, the blocking antibody epitopes are closely located adjacent to the conserved inhibitory antibody epitope on its either side. It has been speculated that blocking antibodies interfere with the binding of inhibitory antibodies by either sterically blocking them or resulting in conformational changes that prevent inhibitory antibodies from binding [64].

*Pf*MSP1$_{19}$ is a highly cysteine rich protein with 6 disulfide pairs for a ~12kDa protein. To ensure proper protein folding, we expressed the protein in Origami™ *E. coli* cells. These engineered bacterial cells have an oxidizing cytoplasmic environment which allows correct formation of disulfide bonds. Our goal was to shield both of the blocking epitopes (on either side of the protein) using the nanopatterning approach we developed. As a control, we also designed a version of the protein to shield the inhibitory epitope. Guided by the location of inhibitory and blocking antibody epitopes on the protein structure, we identified residues around each of the 3 epitopes to be shielded (1 inhibitory epitope and 2 "blocking" epitopes); the incorporation of the ncAA F* at these residues would allow modification with PEG and shielding.

We screened various residues on either side of each epitope, and ultimately selected a pair of residues sandwiching the epitope of interest. This selection was guided by factors including: the proximity of the residues to the epitope, their solvent accessibility, and their conservation score. We first identified residues on either side of the epitope of interest (the one to be shielded), that were solvent accessible – determined from the crystal structure of the protein. Next, the candidate sites selected, were further narrowed down based on their conservation score as determined by ConSurf Analysis [55]. ConSurf generates a score for

every residue of the protein on a scale of 1 to 9, with 1 being most variable and 9 being most conserved. Residues with a score of lower than or equal to 5 are generally amenable to mutations, in our experience. Further, the ConSurf analysis reports what other amino acids a particular residue of interest is found to mutate to, based on its frequency in other homologous proteins. This information is helpful because one can preferentially pick sites that are compatible with mutations to an amino acid that is closer in structure to the non-canonical amino acid to be incorporated. For example, when attempting to incorporate p-azidophenylalanine (F*), one could pick sites that are compatible with mutations to a phenylalanine (F) or a tyrosine (Y).

Using these guidelines we identified residues Q6, V8, Q11, Q14, and Y84 around the conserved inhibitory epitope, and expressed double mutants Q14Y84, V8Y84, Q6Q14 and Q11Y84 and nanopatterned them. Similarly we identified residues Q36, N50, and A58 around the blocking antibody epitope 1, and expressed double mutants Q36N50 and Q36A58 and nanopatterned them. For the blocking antibody epitope 2, K40, E43, G71, K73, and T75 were identified to generate double mutants K40E43, E43G71, E43K73, E43T75, K40G71 and single mutant E43. An additional important factor for consideration was the protein yield, which can vary considerably among the different variants.

After screening various combinations of double mutants for each of the 3 epitopes based on the binding of conformational anti-*Pf*MSP1$_{19}$ antibodies in ELISA, we selected the best pair of sites for mutation and the subsequent site-selective attachment of PEG shields. This selection was ultimately based on the ability to best shield the epitope of interest without affecting binding to antibodies to other epitopes. MutI* (Q11Y84) is referred to as the mutant incorporating F* around the conserved inhibitory epitope. MutB1* (Q36A58) and

MutB2* (K40G71) were double mutants, each incorporating two F* residues around one of the two blocking antibody epitopes.

2.3.5 Characterization of PfMSP1$_{19}$ by SDS-PAGE, ELISA and analytical SEC

Based on our findings from the GFP system, we found that two 5kDa PEG chains on either side of the 'epitope to be shielded' were optimal to completely suppress the immune response to the epitope. The inhibitory antibody footprint on *Pf*MSP1$_{19}$ (Fig 11B in green) was roughly comparable to that of the GFP NB in terms of epitope area on the antigenic protein. This observation is also in agreement with previous findings from literature about the average area of epitope-paratope contact for an antigen-antibody complex [69]. Similarly, residues marked in red in Fig 11B served as a guide for the location of the blocking antibody epitopes.

We nanopatterned MutI* by conjugating 2kDa and 5kDa PEG attached around the inhibitory epitope to shield binding to inhibitory antibodies 12.8 and 12.10 (Fig 12A top panel). We then probed binding of the inhibitory antibodies to wt*Pf*MSP1$_{19}$ (gray bars), MutI* (dark green), and the 2k (green) and 5k (light green) PEGylated version of MutI*. Fig 12A (bottom panel) shows the result for the ELISA. Interestingly, we see that the 2k PEG shields were insufficient at completely shielding the binding of the inhibitory antibodies 12.8 and 12.10, but the 5k PEG shields resulted in complete shielding with binding dropping down to baseline levels. An anti-His antibody was included as a normalization control. ELISA binding was expressed as absorbance at 450 nm (mean ± SD, n=3). Similarly, we determined the effect of PEG length on the shielding of blocking antibody 2.2 by conjugating 2k and 5k PEG to MutB1*. We again see a similar trend

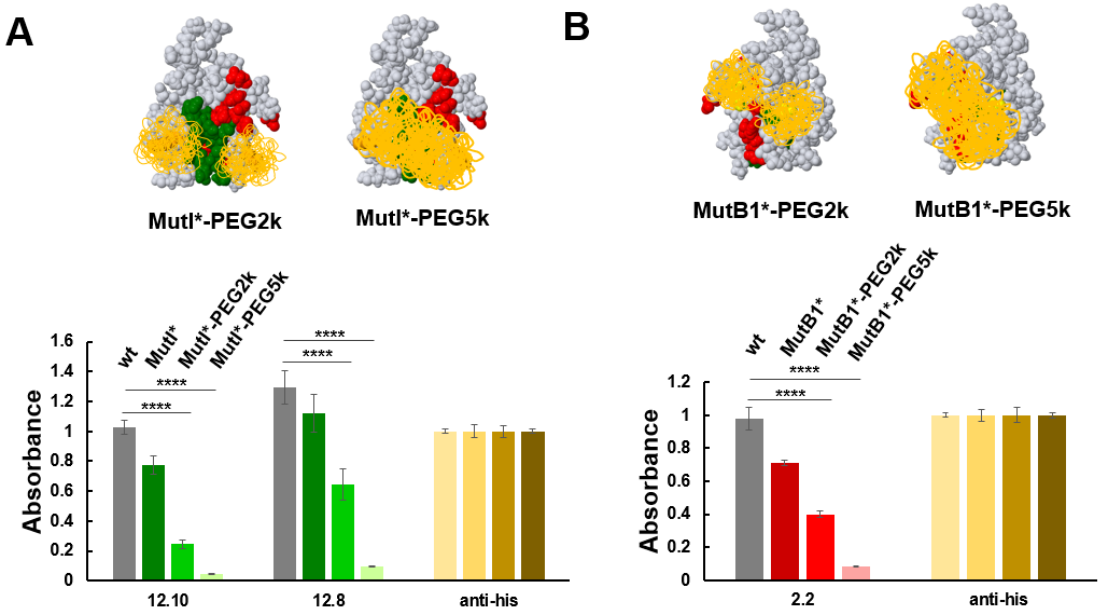

Figure 12. Effect of PEG length on shielding *Pf*MSP1$_{19}$. (A) Top: Cartoons showing MutI* (shielding the conserved inhibitory epitope) PEGylated with 2k and 5kDa PEG. Bottom: ELISA results showing binding of inhibitory antibodies 12.10 and 12.8 to MutI* and the two PEGylated versions. (B) Top: Cartoons showing MutB1* (shielding the blocking epitope for antibody 2.2) PEGylated with 2k and 5kDa PEG. Bottom: ELISA results showing binding of blocking antibody 2.2 to MutB1* and the two PEGylated versions. ELISA binding expressed as absorbance (mean ± SD, n=3). The labelling of the bars follows as labelled for the left cluster in each set. (****p<0.0001, ns – not statistically significant, determined by a one-way ANOVA with post-hoc Tukey's multiple comparison between groups).

suggesting that a 2kDa PEG partially shields the antibody, whereas a 5kDa PEG does so more completely and efficiently (Fig 13B). The effect of PEG length was more pronounced in thecase of MSP1$_{19}$ that for GFP, suggesting that a 5kDa PEG in would be required to shield the epitopes sufficiently. This result was in agreement with our initial calculations for the R_g of a random-coil polymer. Based on this finding, we chose to move forward with using a 5kDa for our nanopatterning attempts with *Pf*MSP1$_{19}$.

Fig 13 shows ELISA results showing the binding of inhibitory antibodies (12.8 and 12.10) and blocking antibodies (7.5 and 2.2) to the 3 nanopatterned mutants using a 5kDa PEG

chain to shield. Fig 13A shows the MutI* with residues highlighted in orange (Gln11 and Tyr84) that were mutated to pAzF to allow conjugation to mPEG5k-DBCO. After reaction with mPEG5k-DBCO, the protein was purified by SEC to remove unreacted PEG and incompletely PEGylated products, to result in MutI*-PEG that was nanopatterned to shield the inhibitory epitope (serving as a control mutant). The ability of MutI*-PEG to prevent binding of inhibitory antibodies (12.8 and 12.10) while retaining binding to blocking antibodies (2.2 and 7.5) was determined by ELISA. The results are shown in the right panel in Fig 13A. Each cluster of 3 bars corresponds to the binding of a particular antibody (12.10, 12.8, 7.5, 2.2 or anti-His) to wt*Pf*MSP1$_{19}$, MutI* and MutI*-PEG. The clusters have been colored to show the inhibitory antibodies in green, blocking antibodies in red and anti-His in gold; with the signal for wt *Pf*MSP1$_{19}$ in each case shown in gray. As expected, MutI*-PEG efficiently blocks the binding of both inhibitory antibodies but does not affect the binding of the two blocking antibodies. Further, MutI* alone does not disrupt binding to any of the conformational antibodies indicating that the shielding is the effect of site-specific functionalization with PEG and not due to the mutations alone. Fig 13B and C similarly show the reaction and design scheme for the blocking mutants MutB1* (to shield blocking antibody 2.2 binding) and MutB2* (to shield blocking antibody 7.5 binding). Residues Gln36 and Ala58 were mutated to F* (shown in yellow) for MutB1* and residues Lys40 and Gly71 mutated to F* for MutB2*. For both blocking mutants, we can see that their nanopatterned versions selectively prevent binding of the antibody of interest, leaving binding to other antibodies only marginally affected.

Having individually characterized the nanopatterning of either blocking epitope (on each of the two faces of the protein), we next attempted to design a quadruply PEGylated mutant

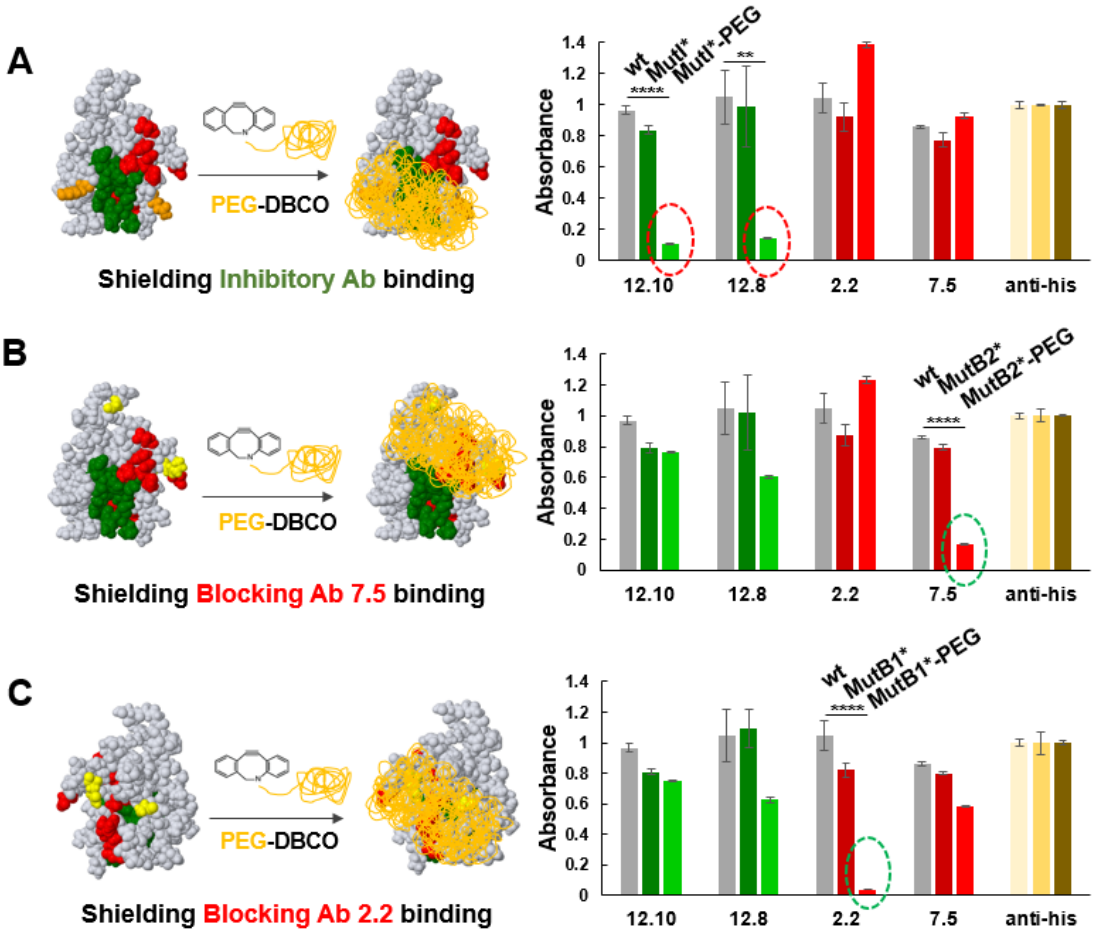

Figure 13. Characterization of nanopatterned PfMSP1$_{19}$ by ELISA. Binding of Inhibitory antibodies 12.8 and 12.10, and blocking antibodies 2.2 and 7.5 to MutI*-PEG (A), MutB1*-PEG (B) and MutB2*-PEG (C) are shown for all four antibodies and an anti-His antibody (as a normalization control). Binding for the correponding unPEGylated mutants (dark green (for inhibitory antibodies) or dark red (for blocking antibodies)) and wtPfMSP1$_{19}$ (gray bars) is also shown in each case for comparison. MutI*-PEG (A) selectively shields binding of inhibtory antibodies 12.8 and 12.10 while retaining binding to the blocking antibodies. Similarly, MutB1*-PEG and MutB2*-PEG selectively shield binding to blocking antibodies 2.2 and 7.5 respectively. ELISA binding expressed as absorbance (mean ± SD, n=3). (**p<0.01, ****p<0.0001, determined by a one-way ANOVA with post-hoc Tukey's multiple comparison between groups).

MutB*-PEG that collectively shields binding to both blocking antibodies on the protein. We expressed, purified and PEGylated the quadruple mutant MutB* with mPEG5k-DBCO and further purified the quadruply PEGylated mutant MutB*-PEG using SEC. We first

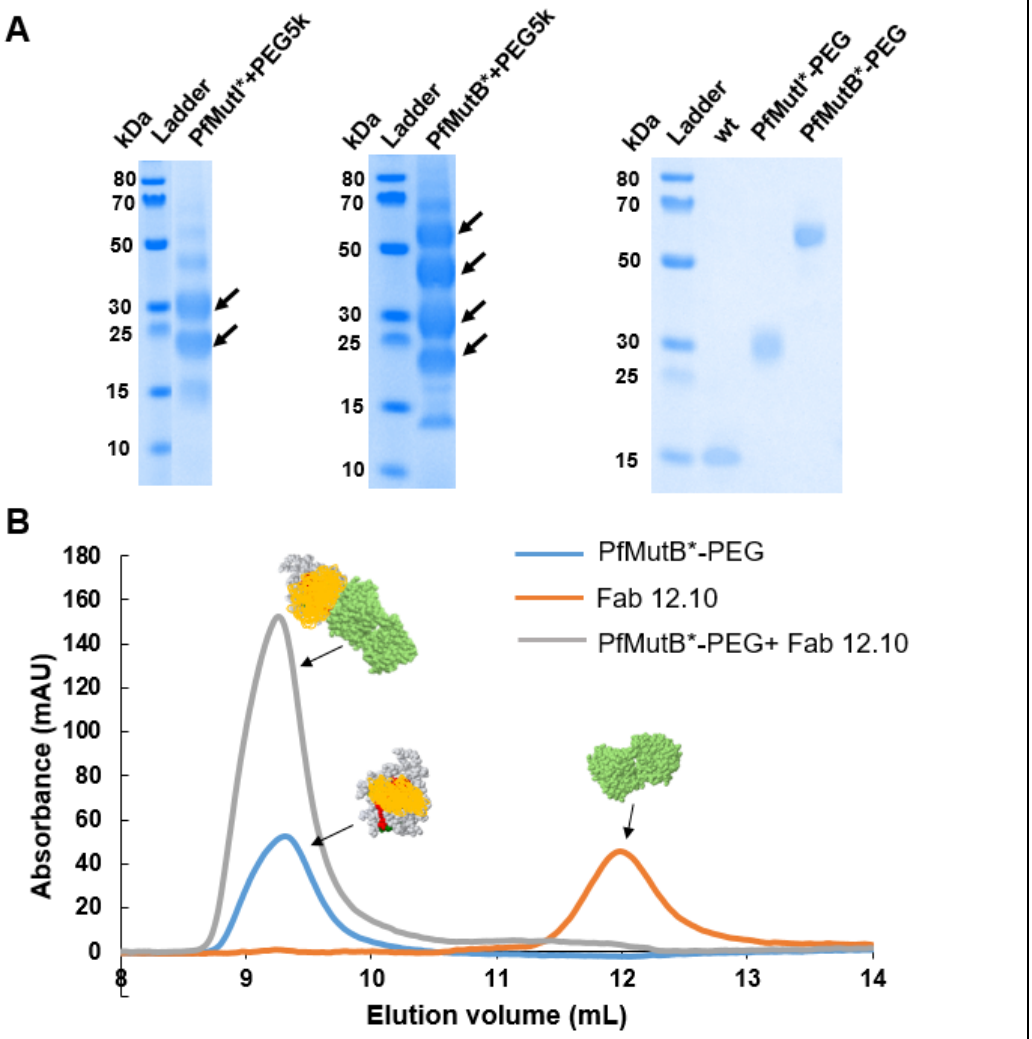

Figure 14. Characterization of Nanopatterned *Pf*MSP1$_{19}$ by SDS-PAGE and analytical SEC. (A) SDS-PAGE images showing – Left: Single and double PEGylated PfMutI* Center: Single, double, triple and quadruple PEGylated PfMutB*, Right: wt *Pf*MSP1$_{19}$, the purified double PEGylated control mutant *Pf*MutI*-PEG, and the purified quadruply PEGylated mutant of interest *Pf*MutB*-PEG (B) Analytical SEC shifts showing the ability of the quadruply PEGylated mutant *Pf*MutB*-PEG to bind to an inhibitory Fab 12.10.

characterized MutB*-PEG by SDS-PAGE. Fig. 14A shows the reaction mixtures of *Pf*MutI* (left gel image) and *Pf*MutB* (center gel image) reacted with PEG5k and run on SDS-PAGE, showing the mutant proteins with one, two, three, or four PEG chains conjugated (marked by arrows). In Fig 14A (far right) we see that the increment from wt

*Pf*MSP1$_{19}$ to *Pf*MutI*-PEG (two 5k-PEGs added) to *Pf*MutB*-PEG (total of four PEG5k conjugated) is characteristic of the behavior of PEG conjugated to a protein run on SDS-PAGE (PEG runs higher than its true molecular weight on SDS-PAGE [70]).

Next, it was important to ensure that the quadruply PEGylated MutB*-PEG binds to the exposed inhibitory epitope (to where it is expected to refocus the immune response to). We first attempted ELISAs by similarly coating this nanopatterned antigen on plates to probe binding to the inhibitory and blocking antibodies. However, because of the presence of four PEG chains on a 12kDa protein it was difficult to coat the quadruple mutant effectively on ELISA wells. As an alternative, we performed an in-solution binding assay using analytical SEC to ensure that the MutB*-PEG binds to the inhibitory antibody. The results from this analytical SEC shift assay are shown in Fig. 15B. We expressed and purified the inhibitory Fab 12.10 from mammalian 293F cells. We then ran MutB*-PEG, Fab 12.10, and a complex of MutB*-PEG on an SEC column and the overlaid chromatograms are shown in Fig 14B. Fab 12.10 exhibits a peak at ~12 mL (orange chromatogram); *Pf*MutB*-PEG peaks at ~9.3 mL (because of an increased hydrodynamic radius from conjugating four PEG chains); and a complex of the same amounts of *Pf*MutB*-PEG and Fab 12.10 exhibits a peak at ~9.2 mL (gray chromatogram). As can be seen for the chromatogram for the mixture of *Pf*MutB*-PEG and Fab 12.10, we do not see a peak for the Fab 12.10 alone and the intensity of the peak at ~9.2 mL is significantly higher than that of the peak for Fab alone – confirming that MutB*-PEG was able to bind to the inhibitory Fab 12.10.

2.3.6 Nanopatterning refocuses the immune response to PfMSP1$_{19}$

Having shown that the nanopatterned *Pf*MSP1$_{19}$ mutants were able to selectively block recognition of either inhibitory (*Pf*MutI*-PEG) or blocking antibodies (*Pf*MutB*-PEG), we next immunized rabbits with these antigens to determine whether this selective recognition of antibodies *in vitro* translates to an altered immune response *in vivo*. The immunization schedule is shown in Fig. 16A. The animals were terminally bled on day 77 and the sera were tested by ELISA to determine titers. Both antigens (*Pf*MutI*-PEG and *Pf*MutB*-PEG) showed an anti-*Pf*MSP1$_{19}$ response (Fig. 15C). The quadruply PEGylated *Pf*MutB*-PEG showed relatively lower titers compared to the doubly PEGylated *Pf*MutI*-PEG – as expected – because of a larger area of the antigen shielded.

Next, it was important to test if the specificity of the elicited antibodies for the two mutants were different. To probe this difference in specificity, we first purified anti-*Pf*MSP1$_{19}$ specific antibodies from the serum by performing antigen-specific affinity column chromatography.

Next we synthesized a version of *Pf*MSP1$_{19}$ fused to the inhibitory Fab 12.10 by co-expressing the antigen and Fab spaced by 3 repeats of GGGGS – termed *Pf*MSP1$_{19}$-12.10Fab (Fig. 15B (far right)). This version of *Pf*MSP1$_{19}$ shields the inhibitory epitope (by the presence of the tethered Fab), in effect, preventing inhibitory antibodies from binding to this antigen. The ability of *Pf*MSP1$_{19}$-12.10Fab to block binding to inhibitory antibodies was confirmed by ELISA and analytical SEC. This version of *Pf*MSP1$_{19}$ thus serves as a reagent to probe the relative presence or absence of inhibitory antibodies in an antibody sample.

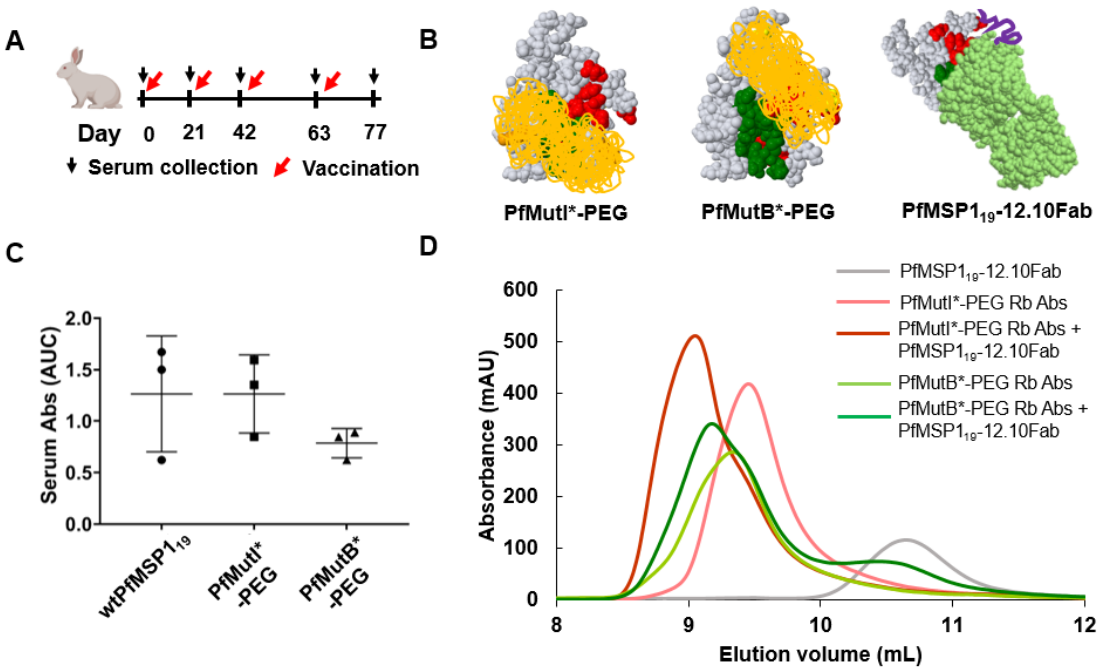

Figure 15. Nanopatterning *Pf*MSP1$_{19}$ refocuses the immune response. (A) Immunization schedule in rabbits (B) Left and center: Nanopatterned *Pf*MSP1$_{19}$ antigens *Pf*MutI*-PEG and *Pf*MutB*-PEG; Right: Cartoon showing *Pf*MSP1$_{19}$ tethered to the inhibitory Fab 12.10 (in light green). (C) Serum antibody titers against wt *Pf*MSP1$_{19}$ from the three immunized groups (D) Overlaid SEC chromatograms for the characterization of purified antibodies from rabbit serum immunized with the nanopatterned antigens.

We next tested the relative binding of purified rabbit serum antibodies resulting from immunization with either *Pf*MutI*-PEG or *Pf*MutB*-PEG to *Pf*MSP1$_{19}$-12.10Fab and analysed the extent of antibody binding using analytical SEC. Fig 15D shows an overlay of chromatogram results from this experiment. The gray chromatogram is for the *Pf*MSP1$_{19}$-12.10Fab fusion protein alone. This fusion protein of *Pf*MSP1$_{19}$ and the 12.10 Fab runs slightly to the left of where a typical Fab runs, as expected. Chromatograms for purified polyclonal antibodies elicited by immunization with *Pf*MutI*-PEG and *Pf*MutB*-PEG are shown in light red and light green respectively. The amount of antibody in each case was stoichiometric to the *Pf*MSP1$_{19}$. Interestingly, when these purified antibodies

were mixed with *Pf*MSP1$_{19}$-12.10Fab (stoichiometrically) and run on the SEC, the extent of peak shifts we see in the two cases were different. The peak for purified antibodies elicited by immunization with *Pf*MutI*-PEG (the control antigen that should elicit fewer inhibitory antibodies and more blocking antibodies) shifts much more to the left when mixed and run on the SEC with a stoichiometric amount of *Pf*MSP1$_{19}$-12.10Fab. Further, the peak also increases in intensity suggesting that most of these antibodies bound to the *Pf*MSP1$_{19}$-12.10Fab fusion protein (dark red chromatogram). In contrast to that, the peak for purified antibodies elicited by immunization with *Pf*MutI*-PEG (the antigen that should elicit fewer blocking antibodies and more inhibitory antibodies) shift to a small extent with only a marginal increase in intensity (shown in dark green). Furthermore, we also see a peak for the *Pf*MSP1$_{19}$-12.10Fab fusion protein alone, suggesting that antibodies elicited by PfMutI*-PEG are primarily specific to the inhibitory epitope. Overall, this data suggests that there was a higher fraction of inhibitory antibodies elicited for *Pf*MutB*-PEG than for *Pf*MutI*-PEG – essentially confirming that nanopatterning refocused the immune response of *Pf*MSP1$_{19}$ towards the conserved inhibitory epitope.

2.3.7 Translating findings to PyMSP1$_{19}$

One important application of nanopatterning protein antigens is to elicit broadly protective antibodies across strains. Although MSP-1 is highly divergent for *P. falciparum*, the 19kDa fragment of MSP-1 is fairly conserved [71]. The rodent parasite plasmodium species – *P. yoelii* - on the other hand, shows significantly greater variability in sequence of *Py*MSP1$_{19}$ between parasite strains (at as many as 21 of 96 residues) than PfMSP1$_{19}$. Hence, we translated findings from the *P. falciparum* system to the *P. yoelii* MSP1$_{19}$ as the latter represented a more challenging test for our approach.

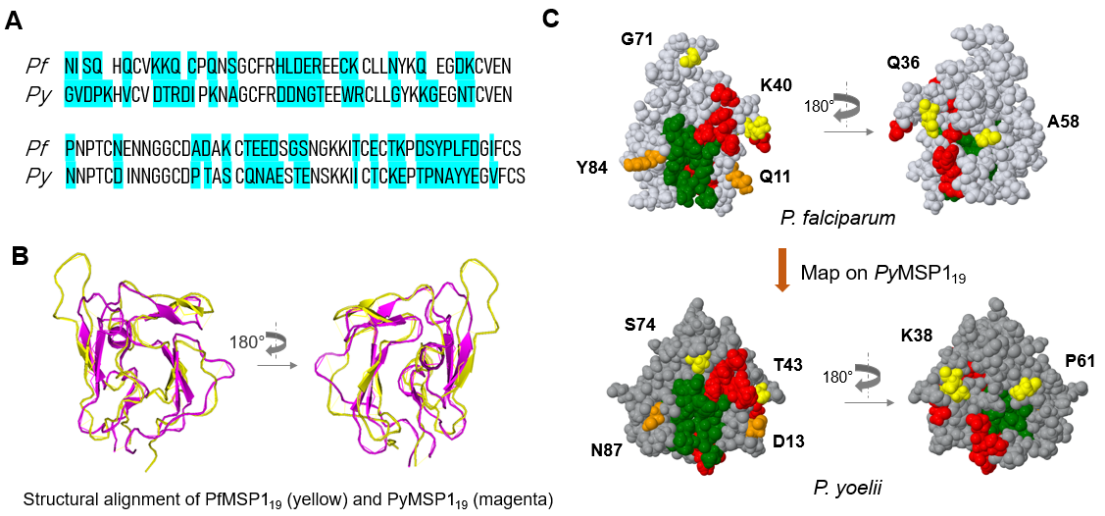

Figure 16. Translating findings from *Pf*MSP1$_{19}$ to *Py*MSP1$_{19}$. (A) Alignment and comparison of the protein sequences for *P. falciparum* (*Pf*) and *P. yoelii* (*Py*) MSP1$_{19}$. Residues that differ between the two sequences are highlighted in cyan. (B) Structural alignment of *Pf* and *Py* MSP1$_{19}$ (C) *Top Panel*: Structure of *Pf*MSP1$_{19}$ (PDB ID: 1CEJ), with residues involved in binding the inhibitory antibodies shown in green and residues involved in the binding of blocking antibodies shown in red. Residues mutated to F* to allow site-specific PEGylation to shield the inhibitory antibody epitope are colored orange. Residues mutated to F* to enable shielding of the blocking antibody epitopes are colored yellow. *Bottom Panel:* Analogous regions (inhibitory epitope, blocking epitopes, and residues mutated to F*) on *Py*MSP1$_{19}$ (PDB ID: 2MGP) based on sequence homology.

*Pf*MSP1$_{19}$ and *Py*MSP1$_{19}$ are highly divergent in sequence, only sharing ~50% homology. This divergence can be seen in Fig 16A where the MSP1$_{19}$ sequences for *Pf*MSP1$_{19}$ and *Py*MSP1$_{19}$ are aligned and divergent residues are highlighted in cyan. Despite being divergent in sequence, MSP1$_{19}$ from these two species shares a high degree of structural similarity as shown in Fig 16B with the PfMSP1$_{19}$ ribbon structure in yellow and that for PyMSP1$_{19}$ in magenta (generated using an academic version of PYMOL). However, the anti-*Py*MSP1$_{19}$ inhibitory and blocking antibody epitopes are not mapped precisely as they are for PfMSP1$_{19}$. Therefore, to guide our nanopatterning efforts, we relied on the structural and functional similarity of Pf and PyMSP1$_{19}$. We first mapped the epitopes for anti-

*Pf*MSP1$_{19}$ antibodies onto the *Py*MSP1$_{19}$ structure using exact analogs based on sequence alignment. Fig 16C shows in the top panel the structure of *Pf*MSP1$_{19}$ (front and back faces) with the epitope for inhibitory antibody binding shown in green and residues involved in binding to blocking antibodies shown in red. The bottom panel shows the structure of *Py*MSP1$_{19}$ with the analogous inhibitory and blocking antibody epitopes mapped. Next, we mapped residues that were mutated to F* to shielding the inhibitory epitope on *Pf*MSP1$_{19}$ (marked in orange) and blocking epitopes (marked in yellow) – onto the *Py*MSP1$_{19}$ structure.

2.3.8 Nanopatterning refocuses the immune response of PyMSP1$_{19}$

Fig. 17A (left) shows the structure of *Py*MSP1$_{19}$ (from strain 17XNL) in dark gray with the residues for inhibitory antibody binding and blocking antibody binding mapped in green and red respectively. Fig. 17A (right) shows the structure of *Py*MSP1$_{19}$ with residues in cyan highlighting the differing residues between highly divergent strains 17XNL and N67. We expressed and purified *Py*MSP1$_{19}$ from strain 17XNL and further generated two mutants: the double PEGylated mutant *Py*MutI*-PEG serving as a control and the quadruply PEGylated mutant *Py*MutB*-PEG, shielding the two "blocking epitopes" – to refocus the immune response to the conserved inhibitory epitope.

We immunized mice with these antigens and analysed anti-*Py*MSP1$_{19}$ serum antibody titers by ELISA against both homologous (17XNL strain) and heterologous (N67 strain) *Py*MSP1$_{19}$. Both antigens were expressed and purified with a Strep-tag® II (as opposed to a hexa-histidine tag for the antigens used for immunizations) to prevent any false positive signal resulting from anti-His serum antibodies. Fig 17D shows the serum antibody titer

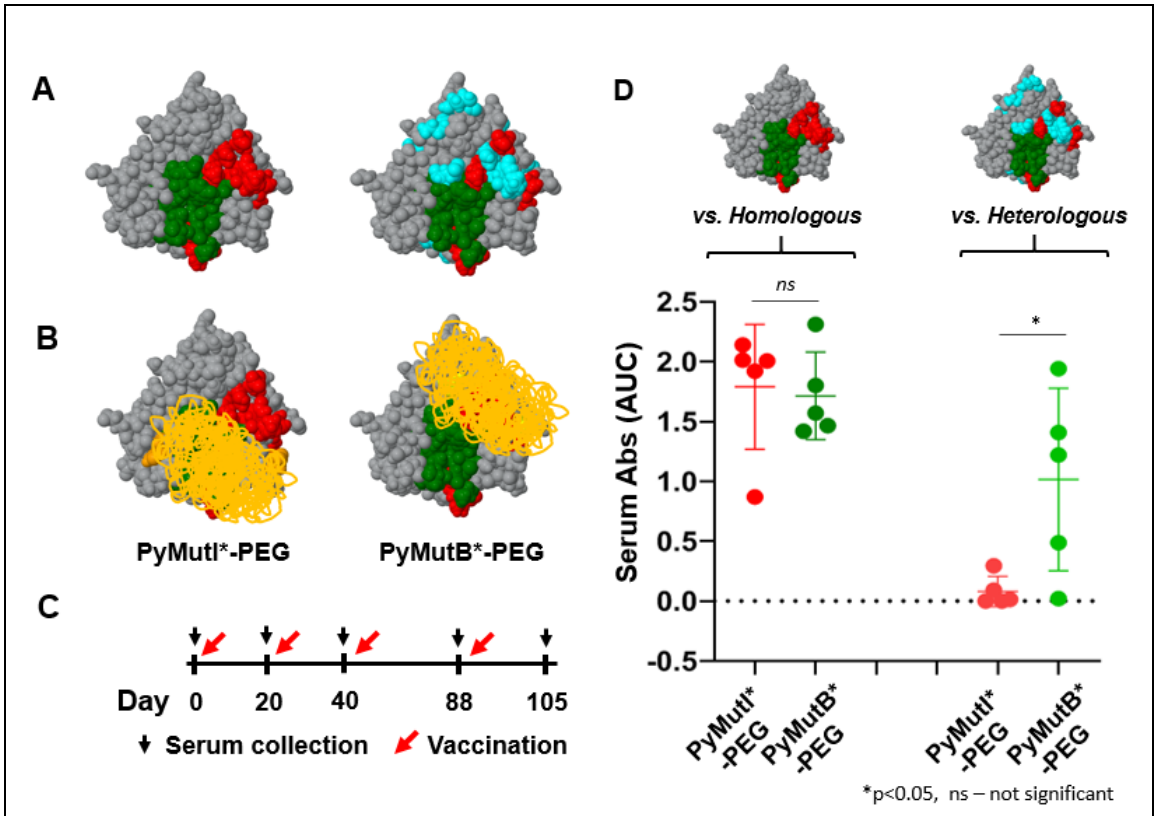

Figure 17. Refocusing the immune response of *Py*MSP1$_{19}$. (A) Structure of *Py*MSP1$_{19}$ (PDB ID: 2MGP) with residues homologous to the *Pf*MSP1$_{19}$ inhibitory and blocking antibody epitopes marked in green and red respectively. *Right Panel*: Residues that differ between two strains of *Py*MSP1$_{19}$ (17XNL and heterologous strain N67) are marked in cyan. (B) Nanopatterned mutants, MutI*-PEG (shielding inhibitory epitope) and MutB*-PEG (shielding blocking epitope). (C) Vaccination schedule in mice. (D) Anti-MSP1$_{19}$ antibody response for the two immunized mutants is comparable against homologous *Py*MSP1$_{19}$ but significantly different against heterologous *Py*MSP1$_{19}$. (*p<0.05, ns – not statistically significant, determined by two-tailed unpaired t-test).

data expressed as area under the curve (AUC) for both mutants – MutI*-PEG and MutB*-PEG against homologous and heterologous *Py*MSP1$_{19}$. The total serum antibody response against homologous PyMSP1$_{19}$ was comparable for mice immunized with MutI*-PEG and MutB*-PEG (Fig. 17D). Importantly, antibodies elicited by immunization with the nanopatterned MutB*-PEG recognized heterologous *Py*MSP1$_{19}$ from strain N67, whereas those elicited using the control MutI*-PEG failed to do so. This result confirms the ability of nanopatterning to refocus the response of *Py*MSP1$_{19}$. This result is in agreement with

the analytical SEC results for *Pf*MSP1$_{19}$ - suggesting that the immune response was focused in both cases (*Pf* and *Py*MSP1$_{19}$) towards the conserved inhibitory epitope.

2.4 Conclusion and Future Directions

We have developed a tool that uses site-specific conjugation of PEG chains to defined regions of a protein antigen, allowing modulation of protein immunogenicity on the nanoscale. A judicious selection of PEG length allows shielding the region of interest, while maintaining recognition to other regions. We have first shown the ability to selectively suppress the immune response to a defined epitope on GFP involved in binding to a Nanobody. We further applied this approach to an important malarial antigen MSP1$_{19}$ that has been shown to be essential to invasion of erythrocytes. Vaccine development of MSP1$_{19}$ suffers from the elicitation of certain "undesirable" blocking antibodies that interfere the protective activity of inhibitory antibody. We nanopatterned MSP1$_{19}$ from two malarial species - *Plasmodium falciparum* and *Plasmodium yoelii* – and have shown that the nanopatterned MSP1$_{19}$ was successful at refocusing the immune response to the conserved inhibitory epitope.

One concern with our proposed approach is the presence of pre-existing or treatment induced anti-PEG antibodies that may interfere with the vaccine efficacy [72, 73]. To avoid complications related to anti-PEG antibodies, the existing approach can be easily extended to other polymers replacing PEG as shields e.g., poly[oligo(ethylene glycol) methyl ether methacrylate] (POEGMA) [74].

Aside from the applications of nanopatterning in immunofocusing, the ability to tune antibody recognition itself is valuable. For example, this strategy can be used as a

diagnostic tool by engineering antigens and using them to screen the presence or absence of antibodies in a serum sample that bind or do not bind to regions of interest. In addition, our group has already started extending the nanopatterning approach to another malarial antigen called *P. falciparum* circumsporozoite protein (*Pf*CSP) – with the goal of suppressing the response to immunodominant regions and refocusing the response to other regions on the antigen that are naturally immunosubdominant yet protective in nature.

While the current work involved the incorporation of a single unnatural amino acid, one can incorporate multiple different unnatural amino acids to conjugate to differently sized PEG chains on different regions of the protein antigen – allowing even finer control over epitope exposure [45]. Our approach can also be extended to antigens expressed in other expression systems such as mammalian cells [75].

CHAPTER 3. DIRECTING THE IMMUNE RESPONSE TO CONSERVED EPITOPES ON INFLUENZA HEMAGGLUTININ USING TETHERED- AND SOLUBLE BI-FAB SHIELDS

3.1 Introduction

Influenza is a serious global health problem. The "Spanish" influenza pandemic of 1918 has been estimated to have caused approximately 40 million deaths [22]. Seasonal influenza epidemics cause an estimated 250,000 to 500,000 deaths annually worldwide [21]. There are two main types of influenza viruses – type A and type B - of which type A is a more virulent human pathogen [76]. Influenza A viruses are further subtyped according to the antigenic properties of their glycoproteins – Hemagglutinin (HA) and Neuraminidase (NA) (Fig. 18A) [76]. The antigenic properties of HA also allow the classification of influenza A viruses into two major groups – group 1 and group 2 [76].

Although commercially available influenza virus vaccines remain the most effective way to prevent influenza virus infection, this approach induces an immune response that is narrow and strain specific and it primarily targets the globular head domain of HA (Fig. 18 B) [77, 78]. This head domain, however, is subject to rapid "antigenic drift", enabling influenza viruses to escape from vaccine-induced immunity. As a result, annual revaccination is required with reformulated vaccines – making the process costly and time consuming [79]. Thus, there have been efforts in recent times to design "Universal Influenza vaccines" that provide protection against a broad range of strains and subtypes.

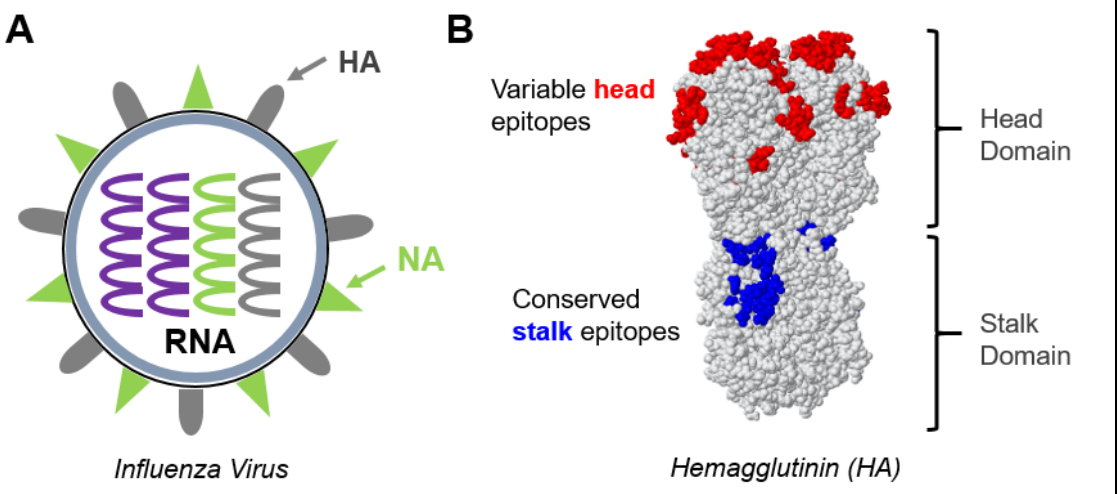

Figure 18. Influenza virus and Hemagglutinin (A) Cartoon showing an influenza virus with its predominant surface proteins Hemagglutinin (HA) and Neuraminidase (NA) shown as spikes. (B) Structure of HA (PDB ID: 1RU7) showing the globular head domain and the stalk domain. The variable antigenic epitopes in the head domain are shown in red. The epitope for a broadly conserved stalk antibody CR6261 is shown in blue.

The antigenic structure of the A/PR/8/34 HA has been previously mapped [80, 81]. There are four immunodominant antigenic sites in the globular head domain, called Sa, Sb, Ca (composed of subsites Ca1 and Ca2), and Cb. Sa, Sb, and Cb are each contained within a single monomer unit of the trimer, with Sa and Sb being close to each other near the tip of the globular head, whereas Cb lies near the bottom of the globular head. Antigenic site Ca spans a cleft between two adjacent monomers.

Despite the elicitation of highly potent neutralizing antibodies directed towards the head domain of HA, extensive amino acid substitutions in this region allow the virus to escape antibody-based immunity. In contrast to the highly variable head domain of HA, the membrane proximal stalk domain is highly conserved because it plays a role in viral membrane fusion to the host cell during infection [79]. Antibodies elicited against this

conserved stalk domain have been shown to provide broad neutralization activity across influenza virus strains and subtypes [82, 83]. However, these antibodies are rare and not effectively induced by seasonal influenza virus vaccines. As a result, there has been a lot of interest in redirecting the immune response of HA towards the stem region. Several groups have worked in this direction by engineering HA to elicit an immune response to the stalk region, as discussed below.

Krammer et al. [84] designed chimeric HA (cHA) structures combining an H1 stalk domain with "exotic" globular head domains derived from other influenza A virus subtypes (Fig. 19A). They next immunized mice sequentially with these chimeric constructs, effectively repeatedly exposing mice to constructs that express the same stalk domain. This approach resulted in the robust elicitation of broadly neutralizing, stalk-specific antibodies. These polyclonal anti-stalk responses were shown to be neutralizing in vitro and protected mice against heterologous and heterosubtypic challenge [84]. However, this approach of immunizing sequentially with chimeric HAs has the disadvantage of eliciting some response to the head domain of HA – by not completely suppressing the anti-head response.

Eggink et al. [35] used a different approach to guide the immune response to the stalk region of HA away from the variable head domain (Fig. 19B). They designed a hyperglycosylated version of HA by introducing seven N-linked glycosylation sites in the head domain to shield the immunodominant antigenic sites. The hyperglycosylated HA was found to enhance the stalk-directed response while dampening the head response on immunization in mice. This enhanced stalk response for the hyperglycosylated HA further translated to better protection upon influenza virus challenge when compared to immunization with wild-type HA [35].

The approach of hyperglycosylating HA requires inserting multiple mutations on the antigen that may interfere with the folding and structural integrity of the protein.

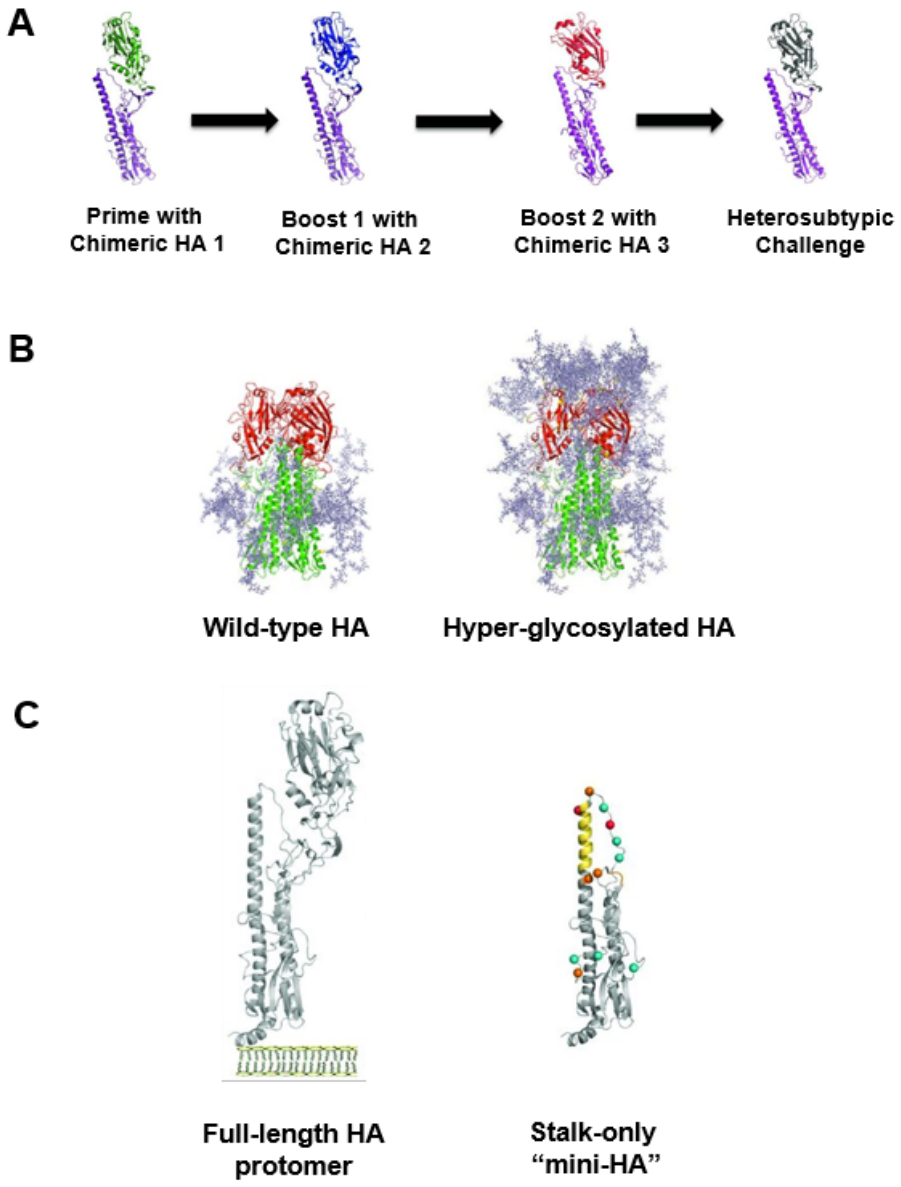

Figure 19. Existing pproaches to direct the immune response of HA to the stalk region. (A) Strategy of sequential immunization with chimeric HAs (B) Hyper-glycosylated HA with additional glycans in the head domain (C) A protomer of full-length HA and its truncated stalk-only "mini-HA" version. Figure adapted from Eggink et al., 2014 [35], Krammer et al., 2013 [84], and Impagliazzo et al., 2015 [85], with permission

Glycosylation is a relatively blunt tool allowing limited ability to vary the structure of the glycan shields. Also, one requires protein expression systems that ensure incorporation of high, complex and dense glycans to achieve sufficient masking – which at the same time may increase the glycan density on other regions of the protein (stalk, in case of HA), and is incompatible with expression of recombinant proteins in hosts such as insect cells.

Impagliazzo et al. [85] and Mallajosyula et al. [86] used rational protein engineering to design stalk-only HA antigens by removing the head domain altogether - referred to as "mini-HAs" or "headless HAs" (Fig. 19C). These stalk-only constructs exhibited binding to broadly neutralizing anti-stalk antibodies similar to that for full-length HA. Further, these immunogens completely protected mice in a lethal heterologous and heterosubtypic challenge model [85, 86]. There have been similar attempts in the past to engineer a stalk-only HA, however, previous attempts exhibited lower affinity of broadly neutralizing stalk antibodies relative to full-length HA, indicating suboptimal conformation [87-89]. Recently, Deng et al. [90] immobilized headless HAs on a core of protein nanoparticles (composed of the influenza matrix protein 2 ectodomain) and observed long-lasting immunity, protecting mice against challenges with divergent influenza A viruses.

Although, the "stalk-only" approach involving truncating the antigen down to only the regions of immunological interest is highly appealing and most promising among other approaches for a "Universal influenza vaccine", a strategy like this involves extensive engineering of the antigen. To extend this tool to antigens from other infectious diseases would be a challenging and an involved task – requiring a unique strategy for each new antigen. Further, depending on the structure of the antigen and the location of the epitope of interest on this antigen, a truncation strategy may not always be possible.

The current work explores an alternative approach to precisely shield regions of a protein antigen from the immune system, in order to refocus the response to the broadly neutralizing regions. This approach involves the use of antibody fragments (Fabs), which are highly specific in their binding to defined regions of an antigen. We have demonstrated the applicability of Fabs as shielding agents to engineer Hemagglutinin by shielding its immunodominant, yet highly variable head domain.

Prior exposure to Influenza antigens has been shown to influence the subsequent response to influenza vaccinations [62, 91-95]. This phenomenon is referred to as Original Antigenic Sin – in which sequential infection with viral variants produces antibodies against older viral strains at the expense of responses to novel or mutated antigenic variants [95]. The schematic in Fig 20A [1] explains this concept better. The left panel in the figure represents a primary infection with a virus with responses to its four epitopes shown in various colors. The right panel shows the case where the same patient is exposed to a mutated version of the virus, later in life. This drifted virus contains two novel epitopes that have mutated from the original version. As can be seen in the corresponding figure, the immune response to the shared epitopes (between the older and drifted strains) are amplified at the expense of the novel epitopes.

A more recent concept that has attracted attention is Original Antigenic Suppression [62], in which *antibodies* to the shared priming epitopes, if present at high titers, can result in immune suppression to this shared epitope. In an interesting experiment, Angeletti et al. [62] vaccinated mice with an inactivated A/PR/8/34 influenza virus mixed with a Fab fragment specific to the Sb antigenic site of the HA head, and observed a selective suppression of the Sb-specific antibody response. Fig. 20B shows a cartoon with the Sb

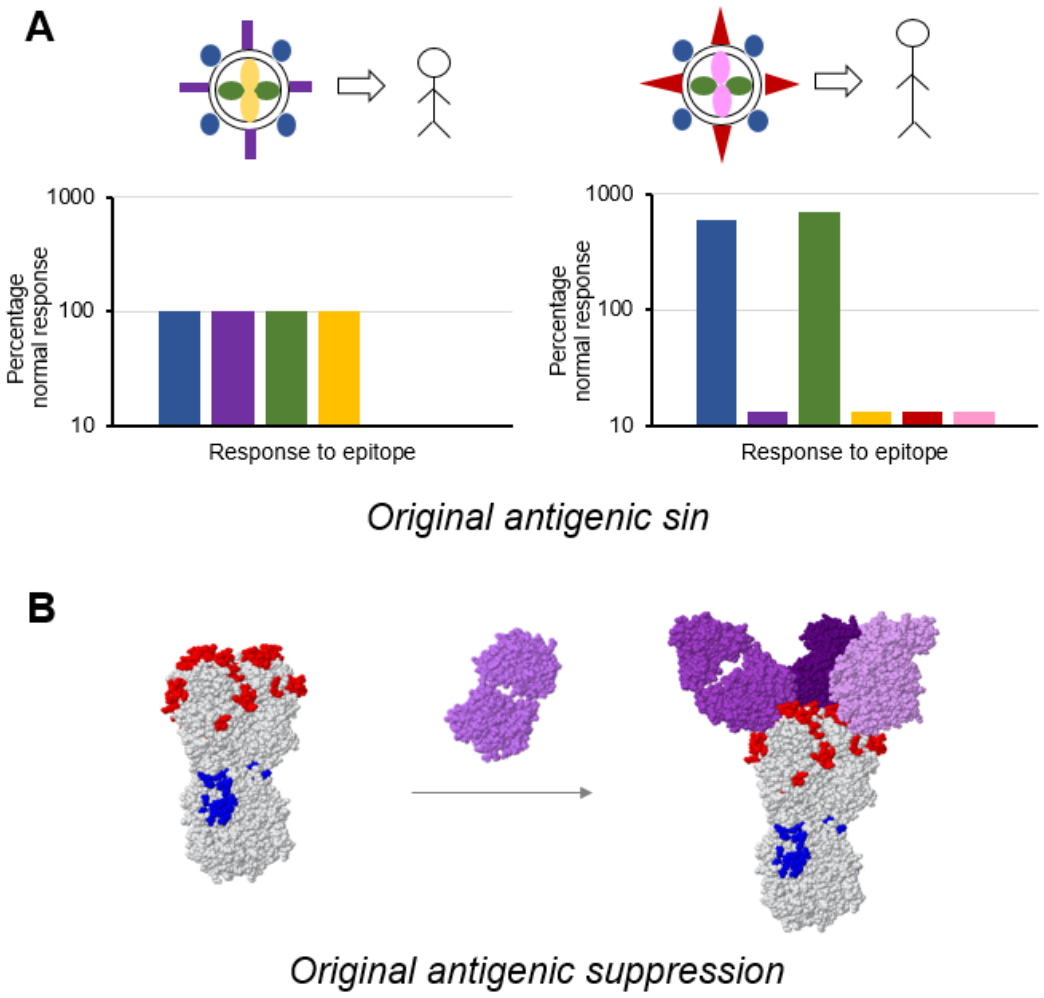

Figure 20. Original antigenic sin and Original antigenic suppression. (A) Schematic illustrating original antigenic sin. (B) Illustration of original antigenic suppression. Figure shows a Fab (in purple) complexed to HA, which on immunizing resulted in selective suppression of the immune response to the cognate antigenic site.

Fab (purple) bound to HA, sterically blocking access to the tip of the HA head. The strength of Original Antigenic Suppression may be governed by the balance of Abs versus their cognate memory B cells. With high levels of antibody, immune response is suppressed (Original Antigenic Suppression); whereas, with low antibody levels, memory B cells dominate naïve B cells (Original Antigenic Sin), resulting in an enhanced response to the shared antigenic epitope.

While this prior work was aimed at a fundamental understanding of immune responses to pathogens, we reasoned that an Ab or an Ab-like molecule might be used to sterically suppress the antibody response to any desired site. Along these lines, we have developed two approaches to utilizing Fabs as shields to suppress the immune response to the head domain of HA. Fabs are highly advantageous as shielding agents because they bind with high specificity to their epitope, effectively shielding it. Moreover, Fabs are considered to be "self-molecules", making them ideal as shields in the context of a vaccine. The most immunogenic region of a Fab is the paratope around its complementary-determining-region (the antigen binding face) [96]. However, when presented to the immune system when bound to its antigen partner, this immunogenic region of the Fab would be occluded, thereby reducing the immunogenicity concerns related to Fabs. Despite all the advantages of Fabs as shielding agents, their binding to the antigen is non-covalent. And so, our approach involves engineering Fab-based shields with enhanced binding to the antigen. We have developed two approaches in this direction: tethered-Fab shields and soluble-Fab shields that are discussed below.

3.2 Shielding the Hemagglutinin head using tethered-Fab shields

Fig. 21 shows a schematic of the proposed tethering approach to shield the head domain of HA. Fig. 21B (top) shows a ligand receptor pair, analogous to a Fab (ligand) with its antigen (receptor) partner. Analysis of the thermodynamics of ligand-receptor binding indicates that tethering a ligand to its receptor increases the effective concentration (C_{eff}) of the ligand by constraining the ligand to the vicinity of the receptor [60, 97-99]. Fig. 21A (top) shows the binding of a monomeric Fab (shown in shades of purple) to the tip of the HA head. This case is similar to the experiment performed by Angeletti et al.[62], where

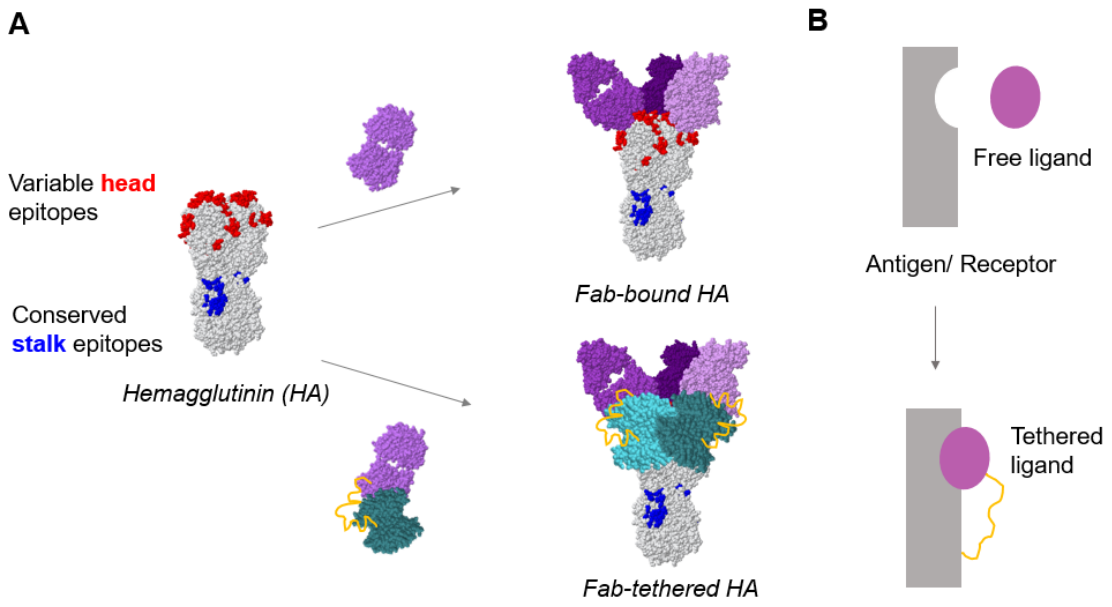

Figure 21. Schematic for tethering a Fab to Hemagglutinin to shield the head domain. (A) Top: HA bound to a Fab (purple) that binds to the tip of the head region; Bottom: Fab tethered to HA via Streptavidin (cyan). (B) Top: Cartoon showing a ligand receptor pair (purple and gray respectively); Bottom: Ligand tethered to the receptor.

on immunizing mice with this complex of an Sb site binding Fab with HA the resulting sera showed selective suppression of an immune response to the Sb antigenic site on HA [62]. However, there was still a response to the head domain of HA as the other antigenic sites were left exposed, as shown by the incompletely shielded red epitopes in Fig. 21A (top).

To build on this model, we proposed to tether the Fab (shown in purple) to HA at a site lower down on the head domain. The "tether" is shown in Fig. 21A (bottom) as a complex of the Fab with another protein (in cyan). On binding to HA, the tether and the Fab collectively should shield the head more completely, as seen in the Fab-tethered HA cartoon in Fig. 21A. In addition, tethering the Fab should also increase the affinity of the

Fab for HA. The stalk region is still accessible in this engineered "head-shielded" HA, which would allow the immune response to be refocused to the conserved stalk epitopes.

3.2.1 Materials and Methods

3.2.1.1 Hemagglutinin engineering, expression and purification

Influenza Hemagglutinin (HA: strain A/Puerto Rico/8/1934 H1N1) was expressed and purified as previously described [100]. The DNA encoding hemagglutinin (PDB ID: 1RU7) was optimized for insect cell expression and synthesized and cloned into pFastBacDual vector by GeneUniversal Inc. (Newark, DE), under the p10 promoter. A C-terminal trimerization domain from T4 phage fibritin followed by a hexa-histidine tag were also included. The DNA encoding the enzyme biotin ligase BirA, which enzymatically adds a biotin to the AviTag (GLNDIFEAQKIEWHE), was also insect optimized, synthesized and cloned under the polyhedrin promoter to allow for *in vivo* biotinylation of HA. Mutants of HA were designed with an AviTag incorporated in the head domain or the stalk domain to allow tethering of the Fab ligand. For the head mutant, the tag was inserted between residues 77 and 78 using site directed mutagenesis. This version of HA is referred to as hb-HA (for head biotinylated HA). For the stalk mutant, the tag was inserted at the C-terminus of the protein before the trimerization domain. This version of HA is referred to as sb-HA (for stalk biotinylated HA).

DNA encoding a chimeric HA – cH5/1 [84] with the head domain from H5N1 and stalk domain from H1N1 was optimized for insect cell expression and synthesized and cloned into pFastBacDual vector by GeneUniversal Inc. (Newark, DE), under the p10 promoter.

A C-terminal trimerization domain from GCN4 followed by a Strep-tag® II were also included.

HA plasmids were transformed into DH10Bac competent cells (10361012, Gibco) as per manufacturer's protocol. The DNA was isolated using PureLink™ HiPure Plasmid Miniprep Kit (K210002, Invitrogen) and transfected in Sf9 insect cells. Baculoviruses were generated to a P3 stock and viral titers were measured using the BacPAK™ Baculovirus Titer kit (631406, Clontech). Protein expression was carried out in HiFive insect cells and the HA protein was purified by IMAC. HA was further purified to complete purity by removing larger aggregates using SEC on Superdex 200 Increase 10/300 GL column (GE Healthcare, 28-9909-44) in PBS buffer. HA was characterized by SDS-PAGE and ELISA against a panel of head and stalk binding antibodies. Gel shift assays with Streptavidin on SDS-PAGE were carried out to confirm biotinylation *in vivo*. The purified trimer of HA was stored at 4°C until further use.

3.2.1.2 Design and synthesis of tethered-Fab shields

The DNA encoding light and heavy chain variable regions (VL and VH resp.) for Fab H28D14 (sequence generously provided by Dr. Jonathan Yewdell, NIH [62]) and Fab CR6261 (PDB ID: 3GBN) were optimized for mammalian expression and synthesized and cloned in TGEX-LC and TGEX-FH vectors respectively by Gene Universal Inc., Newark, DE. A hexa-histidine tag was incorporated at the C-terminus of the heavy Fab chain for purification purposes. Further, versions of the two Fabs were synthesized by incorporating an AviTag at the N-terminus of the VL regions spaced by 5x or 10x repeats of a GGGGS linker.

The Avi-tagged Fabs (H28D14 and CR6261) were expressed in HEK293F suspension cells using the ExpiFectamine™ 293 transfection kit (A14524, Gibco) using the manufacturer's protocol. After expression, the cell culture supernatants were thoroughly dialyzed against PBS and Fabs were purified by IMAC followed by SEC on a Superdex 75 Increase 10/300 GL column (GE Healthcare, 29-1487-21) in PBS buffer. The SEC refining step removes aggregates if any. Next, the Avi-tagged Fabs were biotinylated using the BirA reaction kit (#BirA500, Avidity LLC) using the manufacturer's protocol. Briefly, the Avi-tagged Fabs were buffer exchanged into 20 mM TRIS, 20 mM NaCl, pH 8.0 using spin concentrators. The biotinylation reaction was set up by adding the reaction components provided with the kit that include ATP, biotin, magnesium and biotin ligase BirA. The reaction mixture was incubated at 37°C for 2 hrs and then run on SEC (Superdex 75 10/300 GL) in PBS to separate the biotinylated Fab from the reaction components. The extent of biotinylation was confirmed by gel shift assays with Streptavidin on SDS-PAGE.

Streptavidin was expressed, purified and refolded from bacterial inclusion bodies as previously described [101]. Briefly, the plasmid coding for Streptavidin, which includes a C-terminal hexa-glutamic acid tag, was procured from Addgene (#46367) and transformed in BL21 (DE3) cells. Inclusion bodies were harvested and purified from cells and refolded by rapid dilution. Tetrameric SA was precipitated using ammonium sulfate and further affinity purified to complete purity using Iminobiotin agarose (20221, Thermo Scientific).

Next, to synthesize the complex of a single Fab molecule and SA (SA-monoFab), the biotinylated Fab was mixed with a 6-fold stoichiometric excess of SA. While SA has four biotin binding sites, a maximum of two biotinylated Fabs could bind simultaneously to SA in our experience. Using an excess of SA limits the formation of SA-biFab complexes. To

separate SA-monoFab (desired product) from SA-biFab (undesired) and excess SA, the reaction mixture was run on SEC (HiLoad 16/600 Superdex 200 column, GE Healthcare). The SA-monoFab was further purified to complete purity by using anion exchange chromatography to remove the unbiotinylated Fab that co-elutes in SEC. A MonoQ 5/50 GL column (GE 17-5166-01, GE Healthcare) was used with 20 mM TRIS pH 8.0 as the binding buffer. The protein was eluted using 20 mM TRIS, 1M NaCl, pH 8.0 using a 10%-40% gradient elution over 10 column volumes (CVs). The resulting SA-monoFab complex was characterized by running gel shift assays with biotinylated HA by SDS-PAGE. The SA-Fab complex to shield the head was synthesized by the above procedure by fusing the head binding Fab H28D14 with streptavidin (referred to as SA-H28D14). Similarly to shield the stalk domain, we synthesized a complex of the stalk binding Fab CR6261 with streptavidin (referred to as SA-CR6261).

An alternative strategy to design tethered shields was also developed based on a single fusion of monomeric rhizavidin with the head-binding Fab H28D14. A monomeric enhanced version of rhizavidin (eRA) [102] was used for this purpose. DNA encoding eRA was cloned upstream of the VL region of H28D14 in TGEX-LC, spaced by 5x repeats of GGGGS, synthesized by Gene Univeral Inc., Newark, DE. The eRA-H28D14 Fab fusion was expressed in HEK293F cells and purified as described above.

3.2.1.3 Characterization of Fab-tethered-HA by analytical SEC

Biotinylated HA (hb-HA or sb-HA) was mixed with the appropriate shield (SA-H28D14 or SA-CR6261) in a 1:1.2 stoichiometry with the shield in excess. Analytical SEC was performed to confirm the binding of the tethered shield to HA and further probe the ability

of the Fab-tethered-HAs to shield the head or stalk domain by competing with the head and stalk binding Fabs. Briefly, 5µg hb-HA was run on SEC (i) alone, (ii) complexed with the head shield SA-H28D14, (iii) complexed with the head shield and competed with monomeric head binding Fab H28D14, and (iv) complexed with the head shield and the stalk binding Fab CR6261. The absorbance was recorded by measuring UV205. A similar experiment was performed for sb-HA with the corresponding stalk shielding tether (SA-CR6261) and for the rhizavidin based head shield (eRA-H28D14).

3.2.1.4 Immunizations in mice

BALB/c mice were immunized with the Fab-tethered head-shielded and stalk-shielded HA mutants (referred to as Mut T1 and Mut T2 respectively) at the Rafi Ahmed Lab (Emory University, GA). Samples included were: (i) hb-HA+SA-H28D14 (Mut T1), (ii) sb-HA+SA-CR6261 (Mut T2) and, (iii) PBS control. Four mice were immunized per group. The protein antigens were diluted to 20 µg/mL in PBS (on a HA basis). Two µg of antigen per mouse was injected adjuvanted with Addavax on days 0 and 28. On day 42 the mice were bled for analysis and serum was stored at -20°C until further use.

3.2.1.5 Serum analysis

The day 70 serum from the three groups was assessed for endpoint titer against wild-type HA and against the chimeric cH5/1 HA. Briefly, 50 µL of 0.002 mg/mL HA was coated per well on ELISA plates overnight at 4°C in PBS. Plates were blocked with 100 µL of 5% BSA in PBST for 1 hr at RT. After 3x washes with PBST, plates were incubated with 50 µL of sera diluted four-fold starting at 1:100 in 1% BSA in PBST for 1 hr at RT. After 3x washes with PBST, plates were incubated with a secondary HRP-conjugated anti-mouse

antibody (115-035-003, Jackson ImmunoResearch) for 1 hr at RT. After 3x washes with PBST, plates were developed with TMB substrate solution (00-2023, Thermo Fisher) for 5 min and stopped using 160 mM sulfuric acid solution. Plates were read on a Spectramax i3x plate reader (Molecular devices) at 450 nm. Titers were expressed as area under the curve (AUC) determined using GraphPad Prism software. Appropriate controls were included.

3.2.1.6 Statistical analysis

AUC was calculated using a sigmoidal curve fitting. A minimum of three technical repeats were tested for all ELISAs, and the experiments were repeated at least three times with similar results. One-way ANOVA with post-hoc Tukey's multiple comparison test was applied when indicated in the figure legend. All statistical analysis was performed using GraphPad Prism 8 (GraphPad Software Inc.)

3.2.2 Results and Discussion

3.2.2.1 Expression, purification and synthesis of Fab-tethered HA mutants

Fig. 22 shows the scheme for the design of the tethered HA mutants. We first expressed the head-binding Fab H28D14 with an AviTag fused to the N-terminus of its light chain spaced by a flexible GGGGS linker. The avi-H28D14 Fab was expressed in mammalian cells and purified by IMAC followed by a refining SEC step to remove aggregates. The avi-H28D14 Fab was then biotinylated ex vivo and purified by desalting to remove excess biotin. The extent of biotinylation was determined by performing an SDS-PAGE gel shift assay by complexing with excess streptavidin. Next, the biotinylated Fab was mixed with

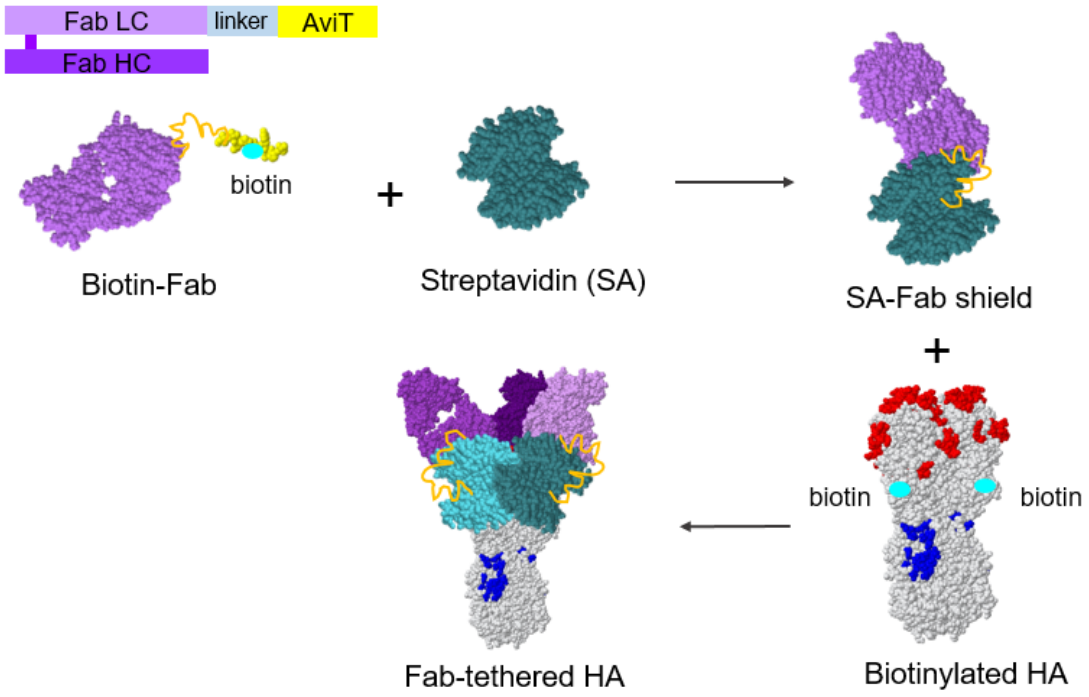

Figure 22. Schematic illustrating the design of Fab-tethered HA

excess streptavidin. The streptavidin (shown in cyan in Fig. 22) was separately expressed and purified from bacterial inclusion bodies.

Streptavidin has four biotin binding sites – with two sites located on each of its diametrically opposite binding interfaces. However, in our experience, when reacting an avi-tagged Fab with streptavidin, a maximum of two Fabs were able to bind (as determined from SDS-PAGE). A possible explanation for this unusual behavior is the steric hindrance from the avitag and the Fab that prevents another biotinylated moiety from binding on the site at the same face once one avi-tagged Fab binds. As we were interested in preferentially synthesizing a complex of Streptavidin with a single Fab bound, this anomaly proved beneficial for our approach.

We next reacted the biotinylated Fab with an excess of streptavidin (6-fold molar excess) to favor the formation of a mono-Fab streptavidin conjugate with a lower proportion of bi-Fab streptavidin conjugate. Despite the excess streptavidin used in the reaction we still saw the presence of up to 50% of the undesirable bi-Fab streptavidin conjugate. We used SEC to separate the mono-Fab streptavidin conjugate from the bi-Fab streptavidin conjugate and the excess streptavidin from the reaction mixture. Further, the unbiotinylated Fab was seen to coelute with the desired mono-Fab streptavidin conjugate post–SEC. An additional anion exchange chromatography step was performed to remove the unbiotinylated Fab fraction.

The SA-Fab complex (shown in Fig. 22 top right) was then mixed with the biotinylated trimeric HA expressed and purified from insect cell cultures. The SA-Fab was added in a 1.2:1 ratio with respect to HA to ensure complete shielding. Fig. 22 shows the final product with the Fab tethered to HA via streptavidin, to completely shield the head domain.

A similar approach was used to design the stalk shielding tether (SA-CR6261) that was mixed with the HA mutant biotinylated near the stalk region (sb-HA). The linker connecting the Fab and the streptavidin was 5x or 10x repeats GGGGS, encoded genetically in the Fab between the avitag and the Fab sequence. In absence of a crystal structure for the H28D14 Fab binding to HA, we relied on the approximate distance between the biotin site on HA (where streptavidin would conjugate to) and the epitope for the H28D14 Fab, to estimate the length of linker.

3.2.2.2 Characterization of Fab-tethered shields by SDS-PAGE and analytical SEC

Fig. 23A shows an SDS-PAGE image for the components used in the synthesis of the Fab-tethered HA. The first lane shows the ladder; the second lane shows the biotinylated HA (which was biotinylated *in situ* during expression); the third lane shows the streptavidin-Fab tether; the fourth lane shows a mixture of HA with the tether. The bands corresponding to HA and the tether alone disappear in the mixture and move higher on the gel indicating the formation of the desired product i.e. HA bound to the SA-Fab shield. The band for HA on SDS-PAGE corresponds to a single protomer as the trimer falls apart in the presence on SDS.

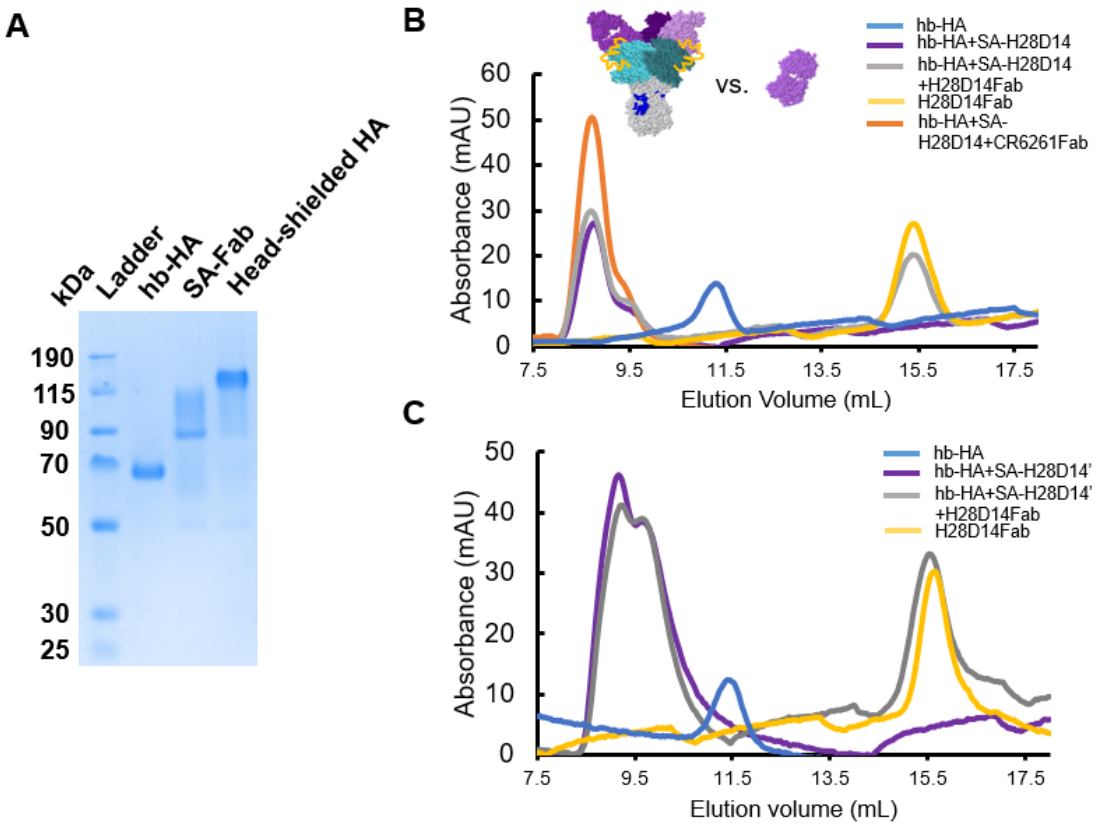

Figure 23. Characterization of Fab-tethered head shielded HA. (A) SDS-PAGE image showing: HA, head-shield, and the mixture. (B) Overlay of chromatograms for Fab-tethered head-shielded HA competed with monomeric Fab with a 5xGGGGS linker. (C) Overlay of chromatograms for constructs with a 10xGGGGS linker

Next we wanted to determine if the Fab-tethered shields were able to shield the antigenic site on the head domain that the Fab shields. Thus, we performed competitive binding assays and analyzed by SEC the ability of the Fab-tethered shield to prevent binding of a competing monomeric Fab. Fig. 23B shows an overlay of chromatograms for the Fab-tethered head-shielded HA, using a 5x GGGGS linker in the Fab-SA conjugate, when competed with monomeric Fab. The blue chromatogram is for the biotinylated HA alone with a peak at ~11.4 mL. When mixed with the SA-H28D14 shield, the peak shifts to the left ~8.2 mL (as shown by the purple chromatogram). When competed with monomeric Fab we see a near-complete blocking of the competing Fab, as suggested by unaffected peak intensity for the HA+SA-H28D14 conjugate (as shown by the gray chromatogram). The yellow chromatogram corresponds to the monomeric competing Fab alone peaking at ~15.5 mL. We also confirmed the ability of the head-shielded sample (HA+SA-H28D14) to bind to a stalk-binding Fab (CR6261), shown by the orange chromatogram. The increase in intensity of the peak ~8-8.5 mL suggests binding of the stalk-binding Fab to the head-shielded sample. Fig. 23C shows a similar overlay of chromatograms for the Fab-tethered head-shielded HA, using a 10x GGGGS linker in the Fab-SA conjugate (SA-H28D14'). Like for the head shield with a 5x GGGGS linker (Fig. 23B), the shield with a 10x GGGGS linker was effective at blocking binding to the competing monomeric H28D14 Fab.

We similarly designed a stalk-shielded version of HA by tethering a stalk-binding Fab (CR6261) to the C-terminus of HA via streptavidin, using a similar strategy. We found comparable results in the analytical SEC characterization for the two linker lengths tested (5x or 10x of GGGGS) for both the head and stalk shields. Hence we proceeded with the shorter 5x GGGGS linker for our animal experiment.

Next, to understand if this shielding effect translates to the suppression of the head or stalk response *in vivo* we proceeded with an animal study with the HA antigens designed by this approach. In parallel, we also designed an alternative strategy to tether the Fab to HA that was less elaborate in synthesis requiring fewer chromatography steps. This alternative strategy involves the expression of the shielding Fab fused to a monomeric Rhizavidin in a single step.

3.2.2.3 Immunization with Fab-tethered HA detects a chimeric HA

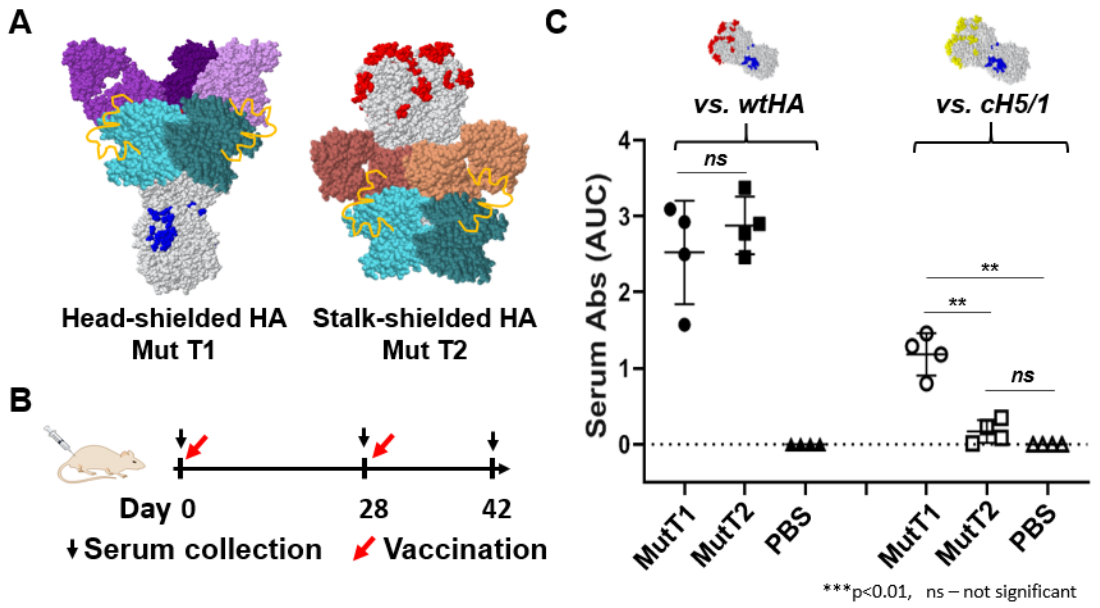

Figure 24. Immunization and antibody titer data for Fab-tethered HA. (A) Cartoon showing the head-shielded and stalk-shielded HA mutants (B) Immunization schedule in mice (C) Day 42 serum antibody titers data for the immunized groups tested against wtHA and cH5/1 HA. (**p<0.01, ns – not statistically significant, determined by a one-way ANOVA with post-hoc Tukey's multiple comparison between groups).

Fig. 24A (left) shows the head-shielded HA obtained by tethering the head specific Fab to HA via streptavidin (referred to as Mut T1). As a control, we similarly designed a stalk-

shielded HA by tethering a stalk-specific Fab CR6261 to HA via streptavidin, as shown in Fig. 24A (right) (referred to as Mut T2). We immunized naïve mice with these two antigens or PBS (control). The immunization schedule is shown in Fig. 24B.

To understand if the immune response had been refocused we expressed and purified a cH5/1 chimeric HA [84] with the head domain sequence from an H5N1 virus and the stalk domain sequence from the H1N1 virus – the one that our HA immunogens were based on. The chimeric cH5/1 recombinant HA protein should selectively bind to stalk antibodies only – allowing us to dissect the specificity of the elicited antibodies for the immunized samples.

Fig. 24C shows the day 42 serum antibody titers when probed against wtHA (left cluster) or against cH5/1 (right cluster). The cartoon for cH5/1 HA is shown in Fig. 24C with the head epitopes highlighted in yellow (as opposed to red for H1) to indicate the head domain from H5. When probing titers against wtHA, both Mut T1 and Mut T2 bind. However, when probing titers against the cH5/1 HA (which should detect binding of stalk antibodies only), the binding of Mut T2 is close to baseline – suggesting that the stalk shielding suppressed the elicitation of stalk antibodies to an appreciable extent. However, the head-shielded mutant Mut T1 was able to detect the chimera suggesting the presence of stalk antibodies upon immunization with Mut T2.

The recombinant wtHA used for the titer experiments was expressed with a T4 foldon trimerization domain and also a hexahistidine tag. The HA samples that were used for immunization were also expressed with the T4 foldon trimerization domain and a hexahistidine tag. Hence, antibodies against the trimerization domain and the hexahistidine

tag would also be present in the serum. In contrast, the cH5/1 (used for titer experiments) was expressed with an alternate trimerization domain (GCN4) and an alternate purification tag (Strep II® tag). One question this result raises is the observed difference in titers for Mut T1 against wtHA and cH5/1. If the head region was successfully shielded, then the titers against wtHA and cH5/1 should be similar. This difference can be explained by the presence of antibodies in Mut T1 serum elicited to the trimerization domain and hexahistidine tag. These antibodies can bind to wtHA (which has the similar trimerization domain and purification tag) but not to cH5/1 HA. In other words, Mut T2 titers against cH5/1 represent binding of antibodies exclusively to the stalk domain whereas those to wtHA include binding to the stalk domain as well as the trimerization domain and the hexahistidine tag.

Based on these promising preliminary results we are working on evaluating the ability of the serum from these immunized samples to inhibit viral infection in a microneutralization assay. This assay should provide more insights into whether the head-shielded group is more effective at neutralizing a heterologous viral strain when compared to the control stalk-shielded group.

3.2.2.4 Alternative approach to tethered shielding using rhizavidin

The approach we described above for tethering a Fab to HA so as to shield its head domain has shown promise in an initial animal study. However, the approach to synthesize the head shields is elaborate involving multiple steps of chromatography. As a result, we parallelly developed a relatively simpler approach to achieve the same shielding effect.

Our alternative strategy involves the use of a monomeric engineered rhizavidin [102] as a substitute for streptavidin in our existing scheme. One advantage of this approach is that because this version of rhizavidin (eRA) is a monomer (as opposed to a tetrameric streptavidin), we could co-express eRA with the Fab, spaced by a linker, in a single step in mammalian cells. Further, eRA is smaller and more compact (15kDa vs. 60kDa for streptavidin), hence the undesirable response to the avidin protein should be significantly lower.

Fig. 25A shows the synthesis scheme for the eRA-based tether. The head-binding Fab was expressed by genetically fusing the eRA DNA sequence spaced by an appropriate linker. For this initial test system we chose 5x repeats of GGGGS as the linker based on our estimates as discussed in the previous section. When mixed with the biotinylated HA, the eRA based tether should allow the Fab to tether to HA, essentially shielding the head domain, as shown in Fig. 25A (far right).

We next tested the ability of the eRA-H28D14 tether to block binding of head antibodies to HA by ELISA. Fig. 25B shows the ELISA results. Each cluster corresponds to the set of antigens tested against a particular antibody as indicated in the bottom. We tested the head specific antibodies for three of the four head antigenic sites (Sa, Sb and Ca) and to the stalk binding antibody CR6261 (shown in blue). The avitag insertion on HA to allow biotin incorporation and further conjugation to the shield was made between residues V77 and R78, which are located in the Cb site. This insertion by itself disrupted binding of the Cb antibody – and so results for that region have not been included in the data set. For each of the antibodies tested, the first bar corresponds to binding to the biotinylated HA; the second bar for binding to the head shielded HA via eRA-based Fab tethering; the third bar

corresponds to a complex of HA and the H28D14 Fab alone (untethered); and the fourth bar is for BSA background. As can be seen, for all three head antibodies the binding drops

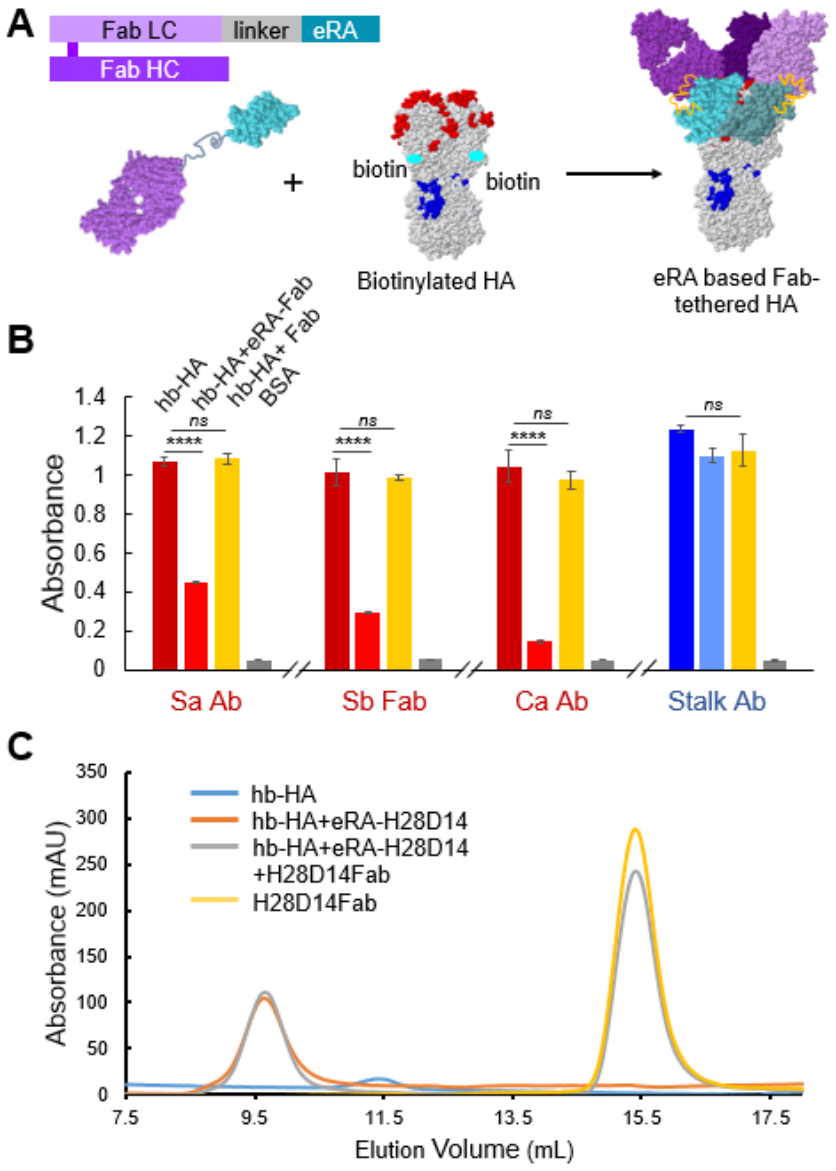

Figure 25. Design and characterization of eRA based head-shields for HA. (A) Synthesis scheme for eRA-H28D14 Fab tether bound to biotinylated HA (B) ELISA result showing binding of head and stalk antibodies to HA and the head shielded HA based on eRA Fab tethering (C) Overlay of SEC chromatograms for a competitive binding assay of monomeric Fab to the HA tethered Fab. (*$p<0.05$, ****$p<0.0001$, ns – not statistically significant, determined by a one-way ANOVA with post-hoc Tukey's multiple comparison between groups).

for the head shielded HA as expected. Further, the binding of the head antibodies to the untethered Fab control is comparable to binding to HA alone – suggesting that the blocking is specifically a result of tethering the Fab to HA. The stalk antibody binds to the head shielded sample as it does to HA alone, as expected.

We next tested the ability of the eRA based Fab tether to block binding to an excess of competing head binding Fab in solution. Fig. 25C shows an overlay of SEC chromatograms run for the eRA-H28D14 tethered head shielded HA when competed with a 10-fold molar excess of monomeric competing H28D14 Fab. The blue chromatogram is for the biotinylated HA alone with a peak at ~11.5 mL. When mixed with the eRA-H28D14 shield, the peak shifts to the left ~9.5 mL (as shown by the orange chromatogram). This peak for the complex is unimodal suggesting the absence of any rosettes. When competed with a 10-fold molar excess of monomeric Fab H28D14 we do not see a shift in the peak at 9.5 mL - suggesting the tethered Fab is strongly bound to HA (gray chromatogram). The yellow chromatogram corresponds to the monomeric competing Fab alone peaking at ~15.5 mL.

These initial results for the alternate tethering strategy are promising. We will in the near future evaluate the ability of these eRA based Fab-tethered head shielded mutants to selectively suppress the immune response to the head domain of HA, by performing an animal study in mice.

3.3 Shielding the Hemagglutinin head using soluble-biFab shields

Fig. 26 shows a schematic of the proposed bivalent-Fab shielding approach to shield the head domain of HA. Fig. 26B (top) shows a cartoon of a ligand-receptor pair where the

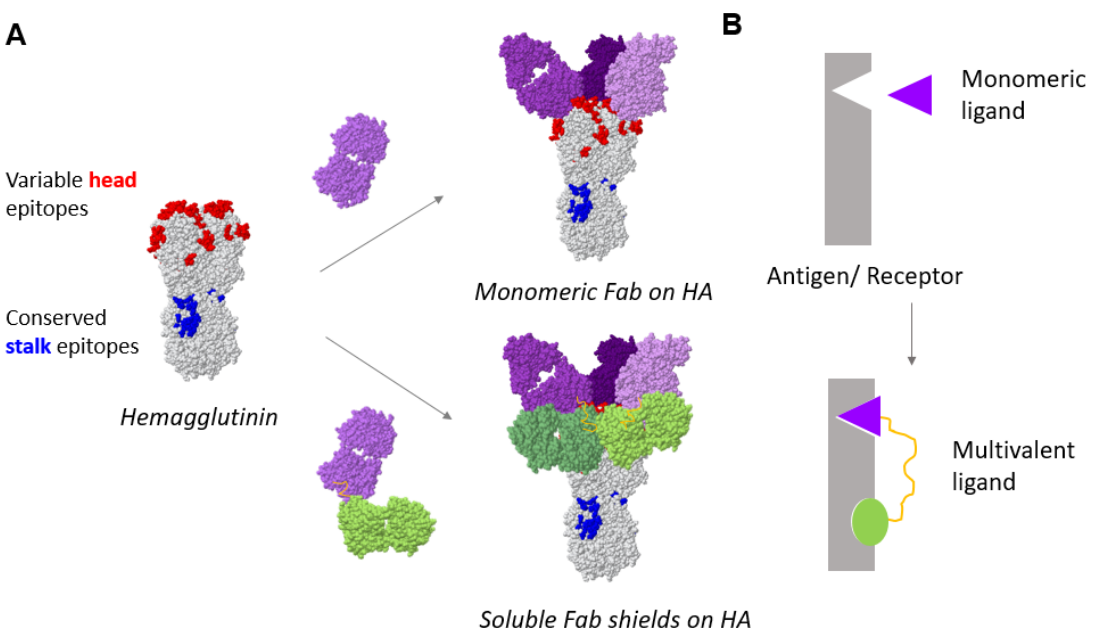

Figure 26. Schematic for a bi-Fab shielding the head domain of HA. (A) Top: HA bound to a Fab (purple) that binds to the tip of the head region; Bottom: A bi-Fab bound to HA (B) Top: Cartoon showing a ligand receptor pair (purple and gray respectively); Bottom: Multivalent ligand binding to the receptor

monomeric ligand is analogous to a Fab binding to its antigen partner. Instead, if the ligand is multivalent - such that multiple copies of the ligand bind to multiple copies of the receptor, the binding avidity can be greater by orders of magnitude [59, 103-106]. The association of one ligand with one receptor increases the local concentration of the other ligand enabling a significant increase in the binding avidity. The cartoon in Fig. 26B (bottom) shows a case where the ligand in purple is dimerized with another ligand in green allowing multivalent binding to the receptor.

Fig. 26A (top) shows the binding of a monomeric Fab (shown in shades of purple) to the tip of the HA head. This case is similar to the experiment performed by Angeletti et al.[62], where on immunizing mice with this complex of an Sb site binding Fab with HA, the

resulting sera showed selective suppression of an immune response to the Sb antigenic site on HA [62]. However, there was still a residual response to the head domain of HA as the other antigenic sites were left exposed, as shown by the incompletely shielded red epitopes in Fig. 26A (top).

To build on this model, we proposed to design a bivalent Fab by dimerizing the Sb specific Fab (shown in purple) to another Fab (shown in green) that binds to the Cb antigenic site at a site lower down on the head domain. The bi-Fab shield would collectively block the head domain more completely as can be seen in the proposed scheme in Fig. 26B (bottom). Moreover, the binding avidity of the bi-Fab for HA should be higher when compared to the affinities of the individual monomeric Fabs, because of the increased binding avidity through multivalency. The stalk region would still be accessible in this engineered "head-shielded" HA, which would allow the immune response to be refocused to the conserved stalk epitopes.

3.3.1 Materials and Methods

3.3.1.1 Hemagglutinin Expression and Purification

Influenza Hemagglutinin (HA: strain A/Puerto Rico/8/1934 H1N1) was expressed and purified as previously described [100]. The DNA for hemagglutinin (PDB ID: 1RU7) was optimized for insect cell expression and synthesized and cloned into pFastBacDual vector by GeneUniversal Inc., Delaware, under the p10 promoter. A c-myc tag (EQKLISEEDL) was inserted at the C-terminus of the HA sequence followed by a trimerization domain from T4 phage fibritin followed by a hexa-histidine tag. The HA protein was expressed and purified from insect cells as described in the previous section.

3.3.1.2 Design and synthesis of soluble-biFab shields

The DNA encoding light and heavy chain variable regions (VL and VH resp.) for HA head specific Fabs H28D14 and H35C12 (sequences generously provided by Dr. Jonathan Yewdell, NIH [62]) were optimized for mammalian expression and synthesized and cloned in TGEX-LC and TGEX-FH vectors respectively by Gene Universal Inc., Delaware. Similarly, the VL and VH regions for a HA stalk specific Fab CR6261 (PDB ID: 3GBN) and the anti-c-myc Fab 9E10 (PDB ID: 2OR9) were cloned in TGEX-LC and TGEX-FH vectors. The SpyCatcher-SpyTag system [48] was used to dimerize the Fabs. We used a truncated version of SpyCatcher (SpyCatcherdN) with the N-terminal region, which has been shown to be redundant, deleted [107]. The DNA encoding SpyCatcherdN was optimized for mammalian expression and cloned upstream of the light chains of Fabs H35C12 and CR6261 spaced by either 5x or 10x repeats of GGGGS. A Spytag was inserted upstream of the light chain of Fab H28D14 and heavy chain of Fab 9E10 by SDM to result in Fabs henceforth termed as spH28D14 and sp9E10. A hexa-histidine tag was incorporated at the C-terminus of the heavy chain of all Fabs for purification purposes.

The SpyCatcher-fused and SpyTagged Fabs were expressed in HEK293F suspension cells using the ExpiFectamine™ 293 transfection kit (A14524, Gibco) using the manufacturer's protocol. After expression, the cell culture supernatants were thoroughly dialyzed against PBS and Fabs were purified by IMAC followed by SEC on a Superdex 75 Increase 10/300 GL column (GE Healthcare, 29-1487-21) in PBS buffer. The SEC refining step removes aggregates if any. Next, the Fabs were quantified by a BCA assay and reacted to allow dimerization of the appropriate Fab pair by isopeptide bond formation between Spycatcher and Spytag. A 50% molar excess of the SpyTagged Fab was reacted to its SpyCatcher fused

Fab partner (H35C12 dimerized with H28D14 and CR6261 with 9E10). The extent of reaction completion was confirmed by SDS-PAGE and the "biFab" was separated from the unreacted monomeric Fabs by SEC (HiLoad 16/600 Superdex 200 column, GE Healthcare) in PBS buffer. The purified biFabs were concentrated, quantified using BCA assay, and stored at 4°C until further use.

The head biFab shield, synthesized by dimerizing Fabs H28-D14 and H35-C12, when mixed with HA results in a head-shielded version of HA - referred to as MutS1. The stalk biFab shield, synthesized by dimerizing Fabs CR6261 and 9E10, when mixed with HA results in a stalk-shielded version of HA – referred to as Mut S2. The shields in both cases were mixed in a 1.2:1 stoichiometric ratio with HA, with the shield in excess.

3.3.1.3 Characterization of biFab shields by ELISA and analytical SEC

Purified antibodies H2-6A1, H28E23, H17-L2, H18-L9 and H18-S48 were generously provided by Dr. Jonathan Yewdell, NIH [62]. The DNA encoding light and heavy chain variable regions (VL and VH resp.) for other HA head specific antibodies - H28-D14 and H35-C12 (sequences generously provided by Dr. Jonathan Yewdell, NIH) and stalk-specific antibodies – C179 (PDB ID: 4HLZ) and CR6261 (PDB ID: 3GBN), were optimized for mammalian expression, synthesized and cloned in TGEX-LC and TGEX-HC vectors by Gene Universal Inc. (Newark, DE). The antibodies were expressed in 293F cells and purified using the HiTrap MabSure Select™ column (29-0491-04, GE Healthcare) on an AKTA Start system following the manufacturer's protocol. These antibodies were further labelled with biotin for ELISA characterization purposes using EZ-Link™ Sulfo-NHS-LC-Biotin (A39257, Thermo Scientific) following manufacturer's

recommendations and purified by desalting. A FLAG tag was inserted at the C-terminus of the heavy chain for Fabs H28-D14, H35-C12 and CR6261via SDM and the FLAG-tagged Fabs were expressed and purified as described in the previous section.

The designed antigens were characterized by ELISA to confirm the ability of the biFab shields to block recognition to desired head epitopes. The biFab shield was mixed with HA in a 1.2:1 stoichiometric ratio with the shield in excess. For the ELISA, 50 µL of 0.002 mg/mL of the antigen solution (on a HA basis) was coated per well on ELISA plates (Maxisorp NUNC, Thermo Scientific) overnight at 4°C in PBS. Plates were blocked with 100 µL of 5% Bovine serum albumin (BSA) (12659, EMD Millipore) in PBST (PBS with 0.05% Tween-20) for 1 hr at RT. After 3x washes with PBST, plates were incubated with 50 µL of primary antibody solutions (biotinylated antibodies or FLAG-tagged Fabs) in 1% BSA in PBST for 1 hr at RT. After 3x washes with PBST, plates were incubated with secondary antibody (either Streptavidin or anti-FLAG Ab conjugated to HRP) for 1 hr at RT. After 3x washes with PBST, plates were developed with TMB substrate solution (00-2023, Thermo Fisher) for 5 min and stopped using 160 mM sulfuric acid solution. Plates were read on a Spectramax i3x plate reader (Molecular devices) at 450 nm. Experiments were performed in triplicates.

SEC shifts were performed with the biFab shielded HA antigens by competing with the corresponding monomeric Fabs or Abs. All SEC chromatograms were run on Superdex 200 Increase 10/300 GL column (GE Healthcare, 28-9909-44) in PBS buffer using 5µg of antigen (on a HA basis). Competing Fabs or Abs were run in a 1.2:1 stoichiometric excess with the biFab shielded antigen. Chromatograms were recorded using UV205 and overlaid for comparison.

3.3.1.4 Immunizations in mice

BALB/c mice were immunized with the engineered HA mutants at the Rafi Ahmed Lab (Emory University, GA). Samples included were: (i) wtHA, (ii) Head-shielded HA (Mut S1) and, (iii) Stalk-shielded HA (Mut S2). 5 mice were immunized per group. The protein antigens were diluted to 1000 µg/mL in PBS (on a DIII basis). 5 µg of antigen per mouse was injected adjuvanted with AddaVax on days 0, 28, 56. On day 56 the mice were bled for analysis and serum was stored at -20°C until further use.

3.3.1.5 Serum analysis

The day 56 serum from the three groups was assessed for endpoint titer against wild-type HA and against the chimeric cH5/1 HA by ELISA, as described before.

3.3.1.6 Statistical analysis

AUC was calculated using sigmoidal curve fitting. A minimum of three technical repeats were tested for all ELISAs, and the experiments were repeated at least three times with similar results. One-way ANOVA with post-hoc Tukey's multiple comparison test was applied when indicated in the figure legend. All statistical analysis was performed using GraphPad Prism 8 (GraphPad Software Inc.)

3.3.2 Results and Discussion

3.3.2.1 Expression, purification and synthesis of shielded HA mutants

Fig. 27 shows the scheme for the design of the bi-Fab shields. We first expressed a version of the Fab H35C12 (Fab1, shown in green) with a SpyCatcher fused to the N-terminus of

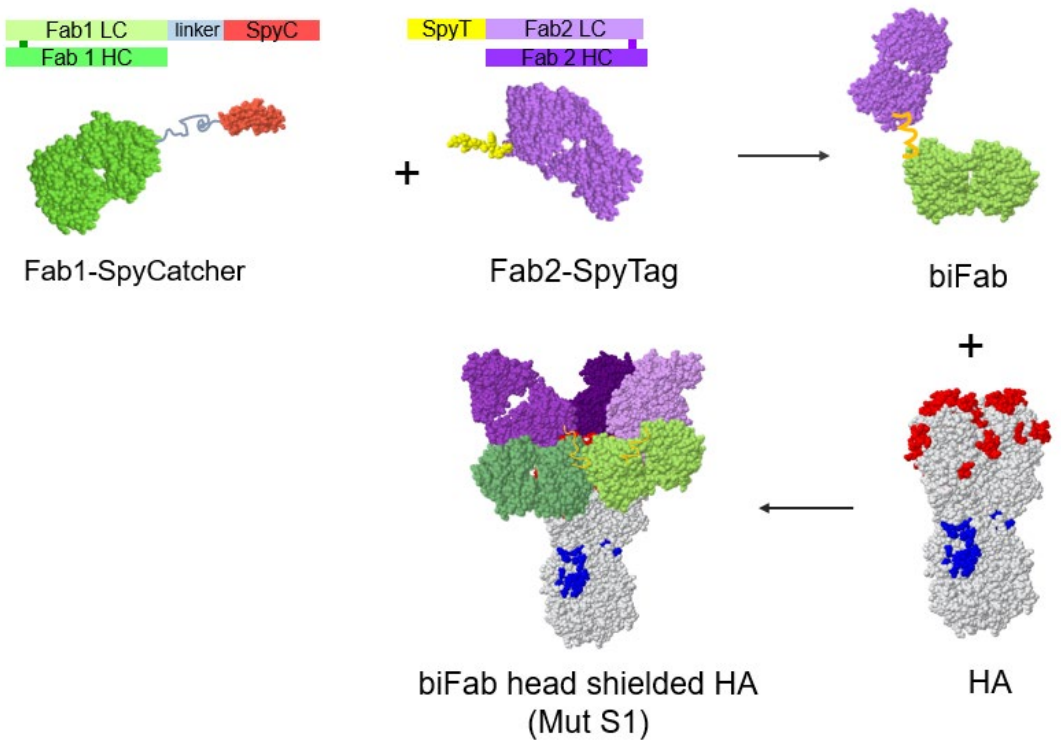

Figure 27. Schematic illustrating the design of bi-Fab shielded HA

its light chain spaced by a linker with either 5x or 10x repeats of GGGGS. The SpyCatcher used here was a version with an N-terminal fragment deleted, which has been shown to be less immunogenic than the full length SpyCatcher, yet retaining the functionality [107]. The SpyCatcher-fused Fab1 was expressed in mammalian cells and purified by IMAC followed by SEC to remove aggregates. We then expressed and purified a version of the Fab H28D14 (Fab2, shown in purple in Fig. 27) with a SpyTag fused to the N-terminus of its light chain. After individual purifying the two Fabs, these were reacted to one another with the Fab2 with a SpyTag (SpyTag-H28D14) in a 1.2:1 ratio wrt to the Fab fused to the SpyCatcher (SpyCatcher-linker-H35C12). The SpyCatcher reacts with the SpyTag spontaneously forming an isopeptide bond and thus conjugating the two Fabs together resulting in a biFab. This biFab shield was then mixed with HA expressed and purified

from insect cells. The resulting complex is the desired product (Mut S1) where the head domain of HA is shielded by the biFab shield.

3.3.2.2 Characterization of bi-Fab head shields by SDS-PAGE, ELISA and analytical SEC

Fig 28A is an SDS-PAGE image showing the various components used for the bi-Fab head shielded HA. The first lane shows the ladder. The second lane shows HA alone, the trimer

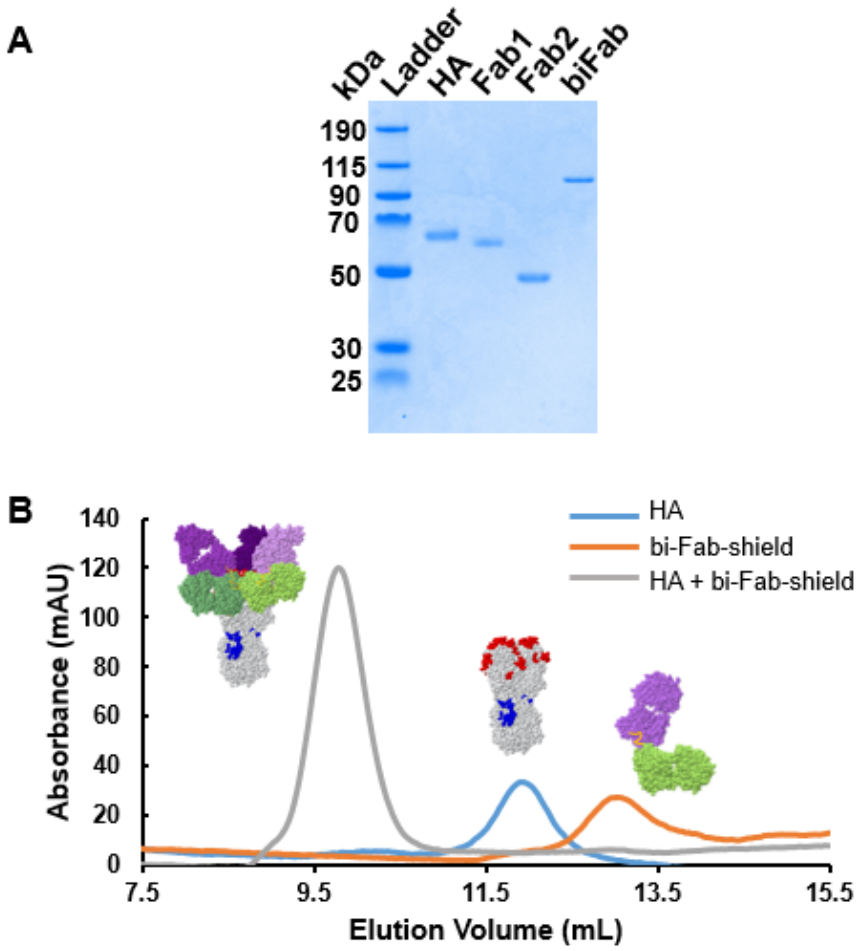

Figure 28. Characterization of bi-Fab HA head shields. (A) SDS-PAGE image showing HA, individual Fabs, Fab1 and Fab2, and the bi-Fab (B) SEC shift showing binding of the bi-Fab shield to HA

of which dissociates in presence of SDS and appears at ~65 kDa corresponding to a single protomer. The third lane shows the Fab1 (H35C12 Fab fused to Spycatcher) and the fourth lane shows the Fab2 (SpyTagged H28D14 Fab). The last lane shows the purified bi-Fab product obtained on reacting the two Fabs followed by purification on SEC.

Next we wanted to confirm that the bi-Fab shield binds to HA as expected. Because this binding is non-covalent, a gel shift on SDS-PAGE is not appropriate. Hence, we performed an analytical SEC shift to confirm the binding of the shield to HA. Fig. 28B shows an overlay of chromatograms run for HA alone (in blue), bi-Fab shield (in orange) and a stoichiometric mixture of HA and the bi-Fab shield (in gray). The peak for HA shifts from ~12 mL to ~10 mL when the bi-Fab shields bind to HA.

Next, it was important to evaluate the ability of the bi-Fab shield bound to HA to block access to the head epitopes. Thus, we performed an ELISA and probed binding of various head antibodies binding to the discrete antigenic sites to wtHA and the head-shielded version of HA. This head shielded mutant of HA will be referred to as Mut S1. Antibodies H2-6A1 (Sa), and H18-L9 (Ca) and Fabs H28-D14 (Sb) and H35-C12 (Cb) were used for the assay [62]. Fig. 29A shows the ELISA results for the binding of head specific antibodies and a stalk binding antibody to wtHA and Mut S1 with either 5x or 10x repeats of GGGGS between the bi-Fab shield. Each cluster of bars corresponds to the antibody used to probe binding. The first bar in each case shows binding of that antibody to wtHA, the second bar shows binding to Mut S1 with 5x linker, the third bar shows binding to MutS1 with 10x linker and the fourth bar in gray is a BSA control. As expected, we see that the binding of all antibodies to HA reduces significantly in the presence of the bi-Fab shields. We did not see a difference in the effect of shielding ability between the 5x and 10x linker lengths

tested. Thus, we chose to proceed with the 5x linker for further experiments. This data suggests that the bi-Fab shield is efficient at blocking access to all antigenic sites of the head domain. Further, we also probed binding of a stalk binding antibody CR6261 [108] to wtHA and the head-shielded Mut S1 (either 5x or 10x linker based) and as shown by the blue bars, the binding of the stalk antibody to the Mut S1 is comparable to its binding to wtHA. This result confirms the ability of bi-Fab shields to selectively block the head domain of HA while retaining binding to the stalk domain.

Furthermore, we were also interested in understanding if the shielding of the head antibodies is dependent on the dose of the bi-Fab shield. To study this we performed ELISA against each of the 4 head-specific antibodies and tested those against wtHA alone and against HA with increasing doses of the bi-Fab shield with the 5x linker. The results for this dose-response ELISA are shown in Fig. 29B. We tested a series of ratios of bi-Fab:HA – 0.1, 0.2, 0.4, 0.8 and 1.2:1. We also tested a sample where the HA was shielded with a mixture of monomeric individual Fabs that were not tethered to each other. This sample is important because it would verify the importance of dimerizing the two Fabs together and emphasize the importance of our strategy. For each of the 4 antibodies tested (H2-6A1 (Sa), H18-L9 (Ca), H28-D14 (Sb) and H35-C12 (Cb)), we saw a dose-response type curve where the extent of blocking increases with an increase in the dose of the bi-Fab (shown as bars in various shades of red). At sub-stoichiometric amounts of the added shield, the blocking is incomplete. A ratio of 1.2:1 was determined to be effective at shielding for most antibodies and we thus chose to proceed with this ratio of bi-Fab:HA for our following experiments. Interestingly, for all four antibodies, the sample that was “shielded” with a monomeric mixture of the two Fabs (yellow bar), we do not see blocking of any of the four

antibodies. The signal for this sample is comparable to the binding to wtHA, suggesting that dimerizing the Fabs together increases the affinity of either Fab to HA.

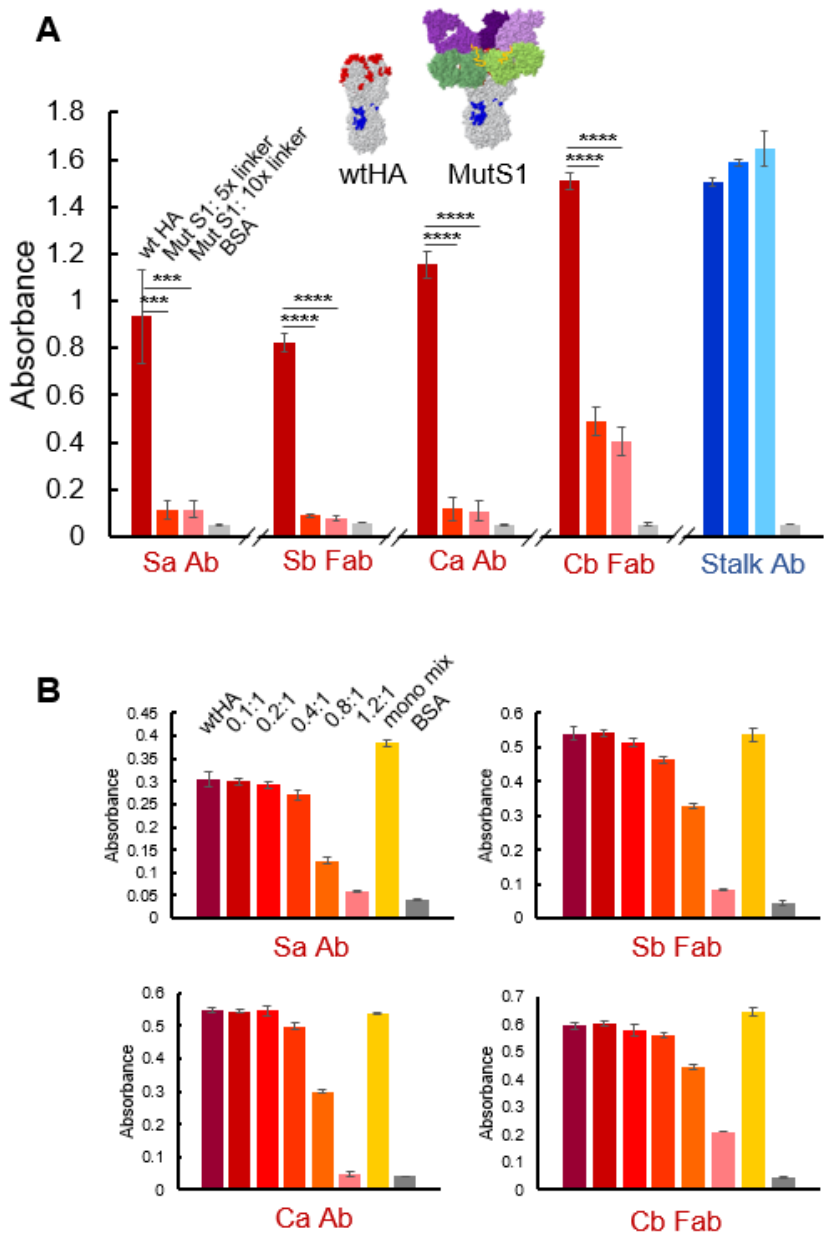

Figure 29. Characterization of bi-Fab head shield by ELISA. (A) Binding of site-specific anti-HA head (in red) and stalk (in blue) antibodies to wtHA and head-shielded HA (Mut S1 with 5x or 10x linker between the bi-Fab shield) (B) Binding of head-specific antibodies to HA shielded with increasing doses of the bi-Fab head shield. (***p<0.001, ****p<0.0001 determined by a one-way ANOVA with post-hoc Tukey's multiple comparison between groups).

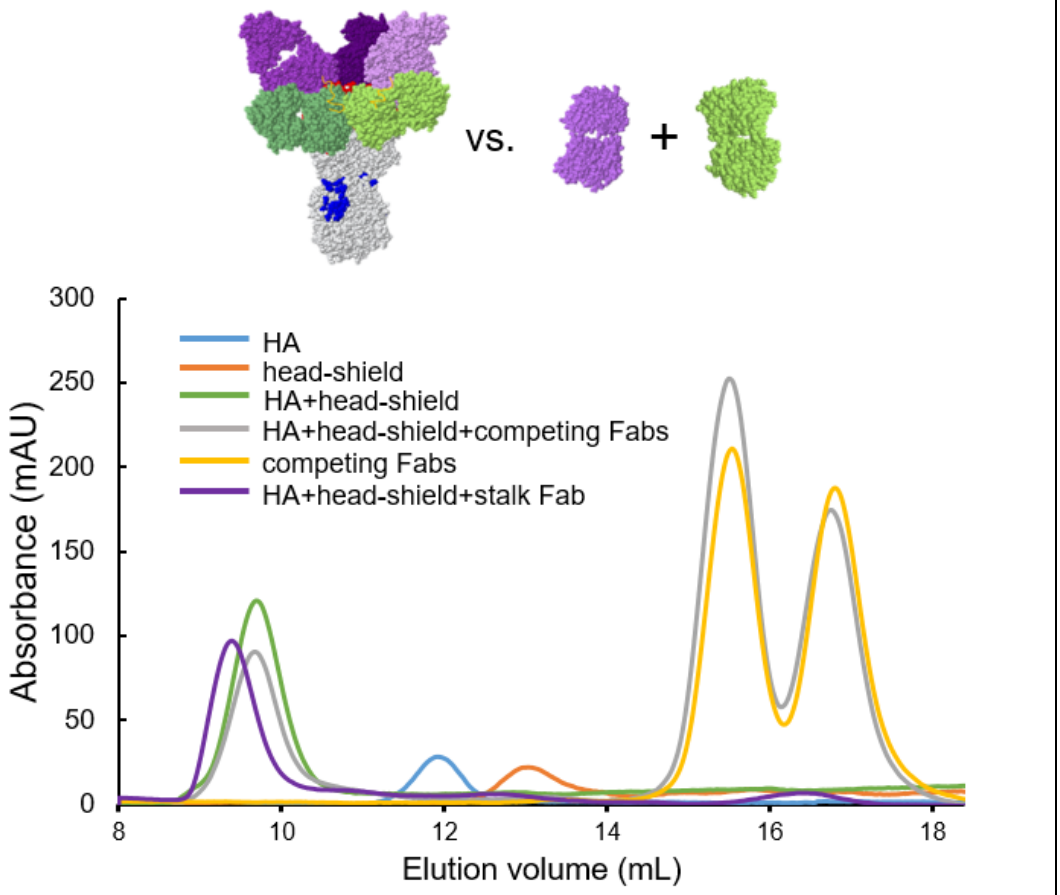

Figure 30. Characterization of bi-Fab head-shielded HA by competitive analytical SEC. Top: Cartoon showing biFab head-shielded HA competed with the monomeric Fabs. Bottom: Overlay of SEC chromatograms for the competitive binding of monomeric Fab to the bi-Fab head-shielded HA.

We next tested the ability of the bi-Fab head shield to block binding to an excess of competing monomeric Fabs in solution. Fig. 30 shows an overlay of SEC chromatograms run for the bi-Fab head shielded HA when competed with a 5-fold molar excess of monomeric competing Fabs H28D14 and H35C12. The blue chromatogram is for wtHA alone with a peak at ~12 mL. The bi-Fab shield alone exhibits a peak at ~13 mL shown by the orange chromatogram. The bi-Fab head-shielded HA is shown by the green chromatogram with a peak at ~9.5 mL. Next, when the bi-Fab head shield mixed with HA

was further competed with a 5-fold molar excess of a mixture of monomeric Fabs H28D14 and H35C12 (shown by the gray chromatogram) we do not see the bi-Fab shield getting displaced as seen by the absence of a peak at 13 mL. The chromatogram in purple shows the bi-Fab head-shielded HA mixed with a stalk binding Fab CR6261, the peak for which shifts further to the left suggesting the ability of a stalk antibody to bind to the head-shielded HA. This result suggests that the bi-Fab shield is bound to HA even in the presence of excess competing Fabs. The yellow chromatogram corresponds to the mixture of the two monomeric competing Fabs with their individual peaks at ~15.5 mL and ~17mL.

We found comparable results in the characterization (by ELISA and analytical SEC) for the two linker lengths tested (5x or 10x of GGGGS) for both the head and stalk bi-Fab shields. Hence we proceeded with the shorter 5x GGGGS linker for our animal experiment. Having characterized the bi-Fab shields for their ability to block the head domain of HA, we next evaluated their ability to suppress the immune response to the head domain upon immunization in naïve mice.

3.3.2.3 Immunization with bi-Fab shielded HA detects chimeric HA

Fig. 31A shows a cartoon for the samples immunized for the animal study. The head-shielded HA with the bi-Fab shielding the head domain is referred to as Mut S1. As a control, we similarly designed a stalk-shielded HA by designing a bi-Fab specific to the stalk domain by dimerizing the stalk specific Fab CR6261 (shown in orange) with an anti-c-myc binding Fab 9E10 (shown in cyan). A c-myc tag introduced at the C-terminus of HA allows binding of the stalk bi-Fab to HA. This stalk-shielded mutant of HA is referred to

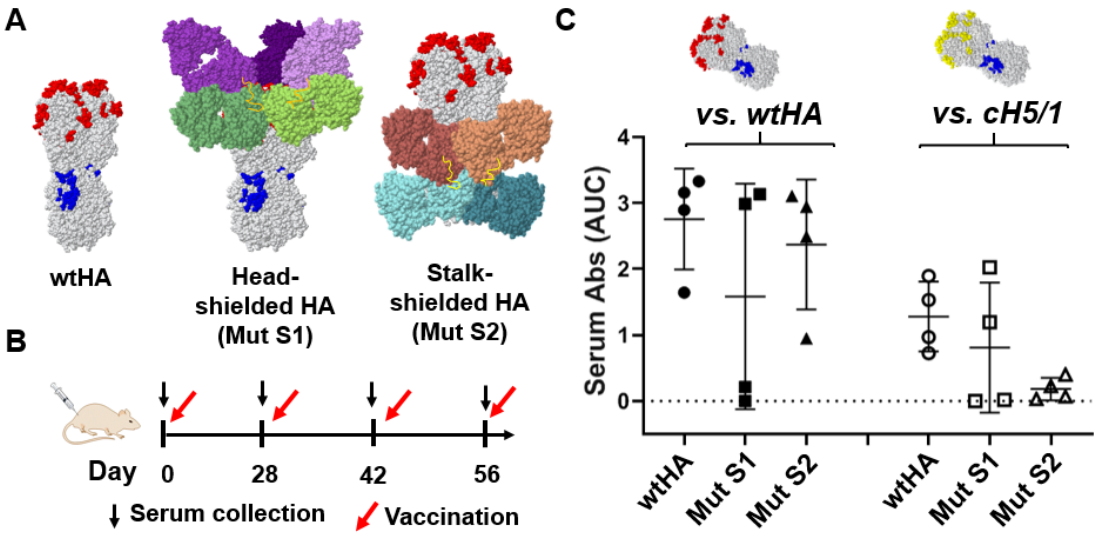

Figure 31. Immunization and antibody titer data for bi-Fab shielded HA. (A) Cartoon showing the head-shielded and stalk-shielded HA mutants (B) Immunization schedule in mice (C) Day 56 serum antibody titers data for the immunized groups tested against wtHA and cH5/1 HA.

as Mut S2. We also included a wtHA control for the experiment. The immunization schedule is shown in Fig. 31B.

To understand if the immune response had been refocused we expressed and purified a cH5/1 chimeric HA [84] with the head domain sequence from an H5N1 virus and the stalk domain sequence from the H1N1 virus – the one that our HA immunogens were based on. The chimeric cH5/1 recombinant HA protein should selectively bind to stalk antibodies only – allowing us to dissect the specificity of the elicited antibodies for the immunized samples.

Fig. 31C shows the day 56 serum antibody titers when probed against wtHA (left cluster) or against cH5/1 (right cluster). The cartoon for cH5/1 HA is shown in Fig. 31C with the head epitopes highlighted in yellow (as opposed to red for H1) to indicate the head domain

from H5. When probing titers against wtHA, all three immunized groups – wtHA, Mut S1 and Mut S2 bind. However, when probing titers against the cH5/1 HA (which should detect binding of stalk antibodies only), the binding of Mut S2 is close to baseline – suggesting that the stalk shielding suppressed the elicitation of stalk antibodies to an appreciable extent. However, the head-shielded mutant Mut S1 was able to detect the chimera suggesting the presence of stalk antibodies upon immunization with Mut S1. Two of the four mice immunized with Mut S1 did not respond to the immunization with HA antigens even after 2 doses. This was unusual, but the trends we see for the two mice that did respond are as expected.

As discussed in the previous section, the difference in titers observed for MutS1 against wtHA and cH5/1 is likely from antibodies elicited against the trimerization domain and the hexahistidine purification tag. The recombinant wtHA used for the titer experiments was expressed with a T4 foldon trimerization domain and also a hexahistidine tag. The HA samples that were used for immunization were also expressed with the T4 foldon trimerization domain and a hexahistidine tag. Hence, antibodies against the trimerization domain and the hexahistidine tag would also be present in the serum. In contrast, the cH5/1 (used for titer experiments) was expressed with an alternate trimerization domain (GCN4) and an alternate purification tag (Strep II® tag).

Based on these promising preliminary results we are working on evaluating the ability of the serum from these immunized samples to inhibit viral infection in a microneutralization assay. This assay should provide more insight into whether the head-shielded group is more effective at neutralizing virus when compared to the control stalk-shielded group. However, it is important to note here that unlike naïve mice that were used for this

immunization experiment, humans are usually exposed to influenza virus, either through vaccination or infection. It has been hypothesized that the low levels of stalk-reactive antibodies could effectively be boosted to protective levels by immunizing with a head-shielded construct as ours [84]. Hence, the efficacy of our engineered head-shielded HA construct can be better evaluated over immunizing with wtHA alone, in the context of preexisting immunity to influenza virus.

In summary, the preliminary results with the bi-Fab shielded mutants suggest refocusing of the immune response and we have shown that the head-shielded mutant of HA (Mut S1) elicits stalk-binding antibodies as shown by binding of serum antibodies to the chimeric cH5/1 HA. As a part of future work, we will evaluate the ability of these serum antibodies to neutralize infection in a microneutralization assay.

3.4 Conclusion and Future Perspectives

We present an approach to selectively suppressing the immune response on an antigen using antibody fragments as shielding agents. Because the binding of the Fab to its antigen partner is non-covalent, we have developed two approaches to enhance the interaction of the Fab-antigen complex. We have explored this immunofocusing approach in the context of shielding the immunodominant yet variable head domain of HA of influenza virus. The first approach involves tethering the Fab to the antigen using avidin-like proteins as the tethering agents. We have shown preliminary animal data that suggests suppression of the immune response towards the desired region of HA. The second approach involves designing bivalent Fabs to shield the head domain of HA more completely than achieved by binding of a single Fab. Further, dimerizing the Fabs together are better at shielding the

head domain than a mixture of the two monomeric Fabs. We have similarly shown preliminary evidence suggesting the ability of these bi-Fab shields in suppressing the immune response towards the desired region of HA.

For future studies, we are interested in evaluating the ability of serum antibodies obtained on immunizing with our Fab-shielded HA constructs to neutralize infection by a microneutralization assay. Further, we are also interested in studying the efficacy of our vaccine constructs in mice with preexisting immunity to influenza – which is a more realistic model for testing.

Strategies developed and discussed in this section can also be extended to engineer antigens from other infectious diseases where focusing the immune response to selected regions of the antigen can result in broad immunity. Our lab is currently exploring to extend this approach to engineer the Fusion protein (F) of respiratory syncytial virus so as to refocus the response towards its broadly protective epitopes.

CHAPTER 4. SUPPRESSING THE ELICITATION OF NON-NEUTRALIZING ANTIBODIES FOR DOMAIN III (DIII) OF ZIKA VIRUS ENVELOPE (E) PROTEIN USING FABS AS SHIELDS

4.1 Introduction

Zika Virus (ZIKV), is a flavivirus that has emerged as a global public health concern because of its ability to cause severe congenital disease [109]. The virus (Fig 32A) contains three structural proteins – capsid (C), pre-membrane (prM) and envelope (E) – of which E

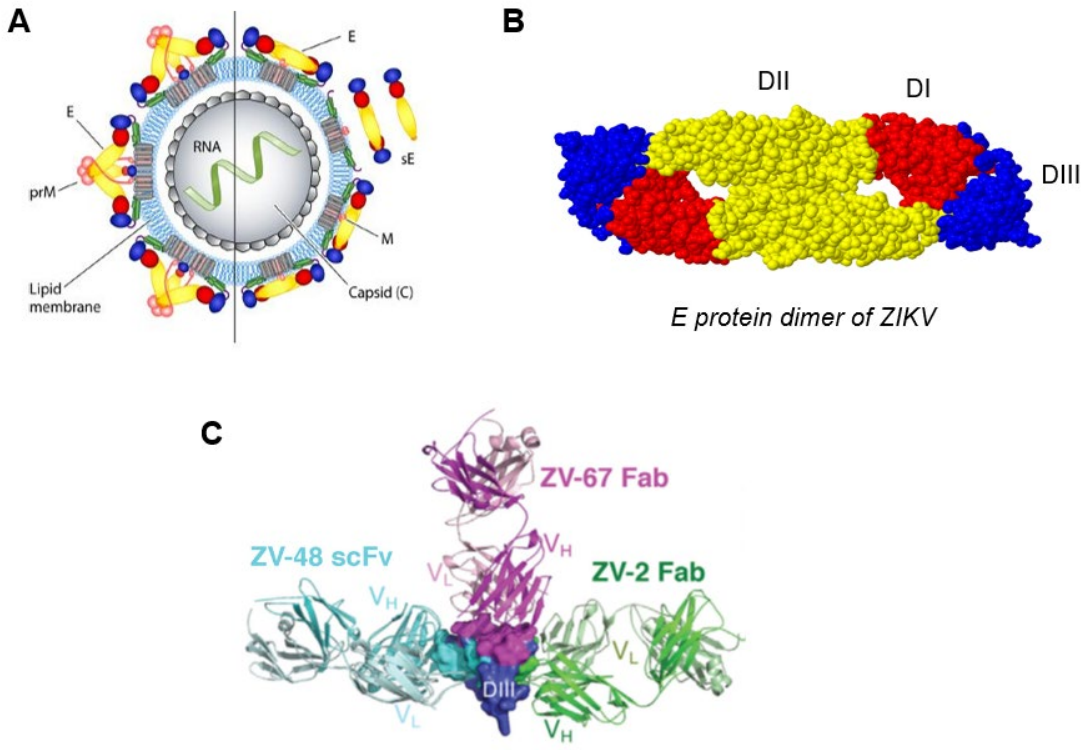

Figure 32. ZIKA virus and its immunogenic surface Envelope protein. (A) ZIKV showing its three structural proteins – Capsid (C), pre-membrane (prM) and envelope (E). (B) Structure of E protein dimer with its three domains shown in different colors. (C) Domain III (DIII) of E protein in blue with three antibodies binding to spatially distinct regions docked on its structure. Figure adapted from Heinz et al., 2017 [111] & Zhao et al., 2017 [115] with permission

mediates viral assembly, attachment, entry and fusion [110, 111]. This E protein is divided into three domains: a central β-barrel domain (domain I (DI)), an extended dimerization domain (DII), and an immunoglobulin-like segment (DIII) [110]. Fig 32B shows a structure of E protein dimers in a herringbone pattern as it lays relatively flat against the lipid envelope on the viral particles. The E protein has been shown to be the primary target of neutralizing antibodies for many flaviviruses. In particular, DIII of E protein is an attractive target for protective immunity because: it has been implicated in the entry of viruses into host cells and has been shown to be a target for protective immunity [112-114].

Zhao et al. [115] generated a panel of antibodies against ZIKV E DIII to gain insights into epitopes that are recognized by neutralizing antibodies. They found that these antibodies recognized three spatially distinct epitopes on DIII. Fig 32C shows the structure of DIII in blue, docked with a representative antibody from each of the three classes. Antibody ZV67 (shown in magenta in Fig 32C) resulted in reduced viremia and complete protection of mice from a lethal ZIKV infection in a passive transfer experiment [115]. ZV67 binds to the "so-called" lateral ridge (LR) epitope on DIII, which is the most accessible in the context of a mature virion as seen in Fig 33 in magenta. Interestingly, DIII-LR-binding mAbs against other flaviviruses e.g., West Nile Virus [113], Dengue Virus serotype-1 [114], or Dengue Virus serotype-2 [116], also protected animals against lethal infection with those viruses.

In contrast to the neutralizing ZV67 antibody, ZV48 and ZV2 (shown in cyan and green respectively in Fig 32C) recognized cryptic epitopes on DIII, which were not predicted to be accessible on the mature virion [117, 118]. ZV48 showed reduced neutralizing activity compared to ZV67, whereas ZV2 was found to be non-neutralizing [115]. The

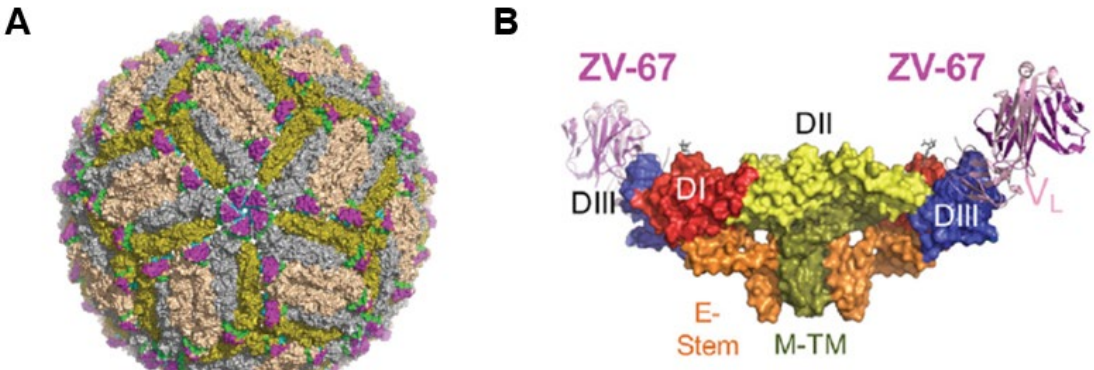

Figure 33. Accessibility of ZIKV DIII epitopes. (A) Mapping of the three distinct ZIKV DIII epitopes on the mature virion; neutralizing lateral-ridge epitopes are highlighted in magenta (B) Docking of ZV67 Fab on E protein dimer. Figure reprinted from Zhao et al., 2017 [115] with permission

neutralization trends correlated with the functional avidities of these antibodies for purified ZIKV subviral particles: ZV67 bound more avidly than ZV2. Even at the highest concentrations tested, ZV2 failed to saturate binding to the ZIKV subviral particles.

Antibody-mediated neutralization of flaviviruses requires engagement of a threshold number of antibody molecules to the virion. For a potently neutralizing West Nile Virus antibody, this threshold has been estimated to be ~30 antibody molecules per virion [119]. In this context, two factors are important for neutralization: antibody affinity for the epitope and epitope accessibility. Non-neutralizing antibodies (e.g., ZV2) elicited on immunization with DIII are undesirable because they bind to poorly accessible (or cryptic) epitopes on the virion, resulting in incomplete coverage of the viral particle. Fig. 33A shows the contrast in accessibility on a mature virion for a non-neutralizing ZV2 antibody epitope (in green) and a neutralizing ZV67 antibody epitope (in pink). The incomplete binding of non-neutralizing antibodies to the virion through these restricted cryptic epitopes, results in

antibody-dependent enhancement (ADE) i.e., increased infection of host cells [120, 121]. ADE occurs following the binding of fewer antibody molecules to virions that is required for neutralizing infection; the bound antibodies then promote viral uptake phagocytic cells, thereby promoting infection [122].

Furthermore, the immunodominance of non-neutralizing regions of DIII may result in lower than expected neutralizing antibody titers [123, 124]. In immunization studies of mice and non-human primates with DIII-based vaccines for Dengue Virus, although a robust antibody response was elicited against DIII, neutralization was modest [125-127], possibly due to the presence of non-neutralizing antibodies [128, 129]. Hence, engineering DIII variants to shield the non-neutralizing epitopes and refocus the immune response on the neutralizing epitopes should result in more effective DIII-based flaviviral vaccines.

One approach to address this shortcoming, has been explored by Frei et al. [130] for Dengue Virus DIII domains. Frei et al. [130] engineered the DIII domain for Dengue Virus (DENV) to suppress the elicitation of undesirable non-neutralizing antibodies. Their strategy involved "resurfacing" DIII (rsDIII) in which epitopes targeted by a broadly neutralizing anti-DENV antibody 4E11 was maintained, but less desirable epitopes (non-neutralizing or serotype-specific) were masked by mutation. Although, one of their designed rsDIII (rsDIII-Ala30) showed decreased binding to non-neutralizing antibodies – upon immunization, the resulting sera failed to protect mice from a lethal DENV-2 challenge [130]. A possible reason for this failure could be the incomplete suppression of the elicitation of undesirable antibodies by the "resurfacing" approach. A single residue mutation may be efficient at disrupting binding of a particular non-neutralizing antibody;

but other regions of the "non-neutralizing" patch would still be left exposed. Hence, strategies that more completely shield the non-neutralizing epitopes are required.

To that end, we have developed an approach that attempts to suppress the elicitation of non-neutralizing antibodies more completely. Our strategy involves the use of antibody fragments to achieve this shielding. When the DIII domain is bound to a non-neutralizing Fab, the non-neutralizing epitope is essentially shielded completely. When this antigen-Fab complex is presented as an immunogen, because of antigenic suppression [62], the antibody response to the cognate antigenic site (non-neutralizing epitope, in this case) should be suppressed. However, the binding of the Fab to the antigen is non-covalent, which may result in the complex falling apart upon immunization. To address this concern, our strategy involves tethering the DIII antigen to the non-neutralizing Fab by expression of the complex as a fusion protein, spaced by an appropriate linker.

4.2 Materials and Methods

4.2.1 Antigen expression and purification

The DNA encoding light and heavy chain variable regions (VL and VH resp.) for ZIKV E DIII specific antibodies – ZV2 (PDB ID: 5KVD), ZV48 (PDB ID: 5KVE), and ZV67 (PDB ID: 5KVG), and a control antibody not specific to ZIKV E DIII – C179 (PDB ID: 4HLZ) – were optimized for mammalian expression and synthesized and cloned in the TGEX-LC, TGEX-FH and TGEX-HC vectors by Gene Universal Inc. (Newark, DE). Further, the DNA encoding DIII (PDB ID: 5KVG Chain E) optimized for mammalian expression was synthesized by Gene Universal Inc. and cloned upstream of the VL regions in TGEX-LC vectors for ZV2, ZV67 and C179 spaced by 3x repeats of GGGGS flexible linkers. A hexa-

histidine tag was incorporated at the C-terminus of the heavy chain of all Fabs for purification purposes.

To express the Fab-tethered DIII antigens, the plasmids for LC (DIII fused to the light chain of the Fab) and its partner FH were transfected in HEK293F suspension cells using the ExpiFectamine™ 293 transfection kit (A14524, Gibco) using manufacturer's protocol. After expression, the cell culture supernatants were thoroughly dialyzed against PBS and Fabs were purified by IMAC followed by SEC on a Superdex 75 Increase 10/300 GL column (GE Healthcare, 29-1487-21) in PBS buffer. The SEC refining step removes aggregates if any. The purified Fab-tethered antigens were concentrated, quantified using BCA assay, and stored at 4°C until further use.

A c-myc tag was inserted at the C-terminus of the heavy chains of Fabs ZV2, ZV48 and ZV67 and the Fabs were similarly expressed in 293F cells and purified via IMAC followed by a refinement SEC step as described above.

Antibodies ZV2, ZV48, and ZV67 were similarly expressed in 293F cells and purified using the HiTrap MabSure Select™ column (29-0491-04, GE Healthcare) on an AKTA Start system following the manufacturer's protocol. The antibodies (ZV2, ZV48, and ZV67) were further labelled with biotin for ELISA characterization purposes using EZ-Link™ Sulfo-NHS-LC-Biotin (A39257, Thermo Scientific) following the manufacturer's recommendations.

4.2.2 Characterization of antigens by ELISA and analytical SEC

The designed antigens were characterized by ELISA to confirm the ability to block recognition to desired regions. Briefly, 50 µL of 0.002 mg/mL antigen solution (on a DIII basis) was coated per well on a 96-well Ni^{+2} coated ELISA plates (15442, Thermo Scientific) overnight at 4°C in PBS. After 3x washes with PBST, plates were incubated with 50 µL of primary antibody solutions (biotinylated antibodies ZV2 and ZV67) in 1% BSA in PBST for 1 hr at RT. After 3x washes with PBST plates were incubated with Streptavidin-HRP conjugated secondary antibody for 1 hr at RT. After 3x washes with PBST plates were developed with TMB substrate solution (00-2023, Thermo Fisher) for 5 min and stopped using 160 mM sulphuric acid solution. Plates were read on a Spectramax i3x plate reader (Molecular devices) at 450 nm. Experiments were performed in triplicates.

SEC shifts were performed with the Fab-tethered antigens by competing with the corresponding monomeric Fabs. All SEC chromatograms were run on Superdex 75 Increase 10/300 GL column (GE Healthcare, 29-1487-21) in PBS buffer using 5ug of antigen (on a DIII basis). Competing and non-competing Fabs were run with the antigen in a 1.2:1 stoichiometric ratio with the monomeric Fab in excess. Chromatograms were recorded using UV280 or UV 205 and overlaid for comparison.

4.2.3 Immunizations in mice

The engineered Fab-tethered DIII mutants were immunized in BALB/c mice at the Florian Krammer Lab (Icahn School of Medicine at Mount Sinai, NY). Samples included were: (i) DIII-linker-ZV2Fab (Mutant 1), (ii) DIII-linker-ZV67Fab (Mutant 2), (iii) DIII-linker-C179Fab (Mutant 3) and, (iv) PBS control. Five mice were immunized per group. The protein antigens were diluted to 40 µg/mL in PBS (on a DIII basis). Two µg of antigen per

mouse was injected adjuvanted with poly I:C on days 0, 27, 54, 99. On day 115 the mice were terminally bled and serum was stored at -20°C until further use.

4.2.4 Serum analysis

The terminal bleed serum from all groups was assessed for endpoint titer against bacterially expressed wtDIII. Briefly, 50 µL of 0.002 mg/mL DIII was coated per well on ELISA plates overnight at 4°C in PBS. Plates were blocked with 100 µL of 5% BSA in PBST for 1 hr at RT. After 3x washes with PBST plates were incubated with 50 µL of sera diluted four-fold starting at 1:100 in 1% BSA in PBST for 1 hr at RT. After 3x washes with PBST plates were incubated with a secondary HRP conjugated anti-mouse antibody (115-035-003, Jackson ImmunoResearch) for 1 hr at RT. After 3x washes with PBST plates were developed with TMB substrate solution (00-2023, Thermo Fisher) for 5 min and stopped using 160 mM sulphuric acid solution. Plates were read on a Spectramax i3x plate reader (Molecular devices) at 450 nm. Titers were expressed as area under the curve (AUC) determined using GraphPad Prism software. Appropriate controls were included.

The DNA encoding DIII was also optimized for bacterial expression, synthesized and cloned in pET28b vector between NdeI/XhoI sites with a C-terminal hexahistidine tag by Gene Universal Inc., Newark, DE. wtDIII protein was expressed in BL21(DE3) *E. coli* and purified from inclusion bodies as previously described [131]

We generated Mut-N*, a variant of DIII with F* introduced at residues 353 (T353F*) and 397 (T397F*). This mutant was further doubly PEGylated using PEG5k-DBCO to generate Mut-N*-PEG. This PEGylated mutant of DIII shields regions on DIII other than

the non-neutralizing ZV2 face using PEG shields (as opposed to a Fab shield). The PEGylation and following separation was carried out as described in Chapter 2.

4.2.5 Statistical analysis

AUC was calculated using sigmoidal curve fitting. A minimum of three technical repeats were tested for all ELISAs, and the experiments were repeated at least three times with similar results. One-way ANOVA with post-hoc Tukey's multiple comparison test was applied when indicated in the figure legend. All statistical analysis was performed using GraphPad Prism 8 (GraphPad Software Inc.)

4.3 Results and Discussion

4.3.1 Design, expression and purification of Fab-tethered DIII antigens

Our approach to engineering DIII, to refocus the immune response towards the neutralizing lateral ridge epitopes (ZV67), involves tethering a Fab to DIII. Depending on the specificity of the Fab tethered to DIII, one can selectively shield an epitope of interest while exposing other regions on DIII. We wanted to suppress the elicitation of non-neutralizing antibodies upon immunizing with DIII. To achieve this, we designed a mutant of DIII tethered to the non-neutralizing Fab ZV2. The non-neutralizing Fab ZV2 when tethered to DIII, would effectively shield the non-neutralizing epitope of DIII, suppressing the elicitation of non-neutralizing anti-DIII antibodies. This would allow refocusing of the immune response to the neutralizing lateral ridge epitopes.

Fig. 34A shows the co-crystal structure of DIII (blue) bound to the non-neutralizing ZV2 Fab (green) (PDB ID: 5KVD). In red are highlighted the C-terminus of DIII and the N-

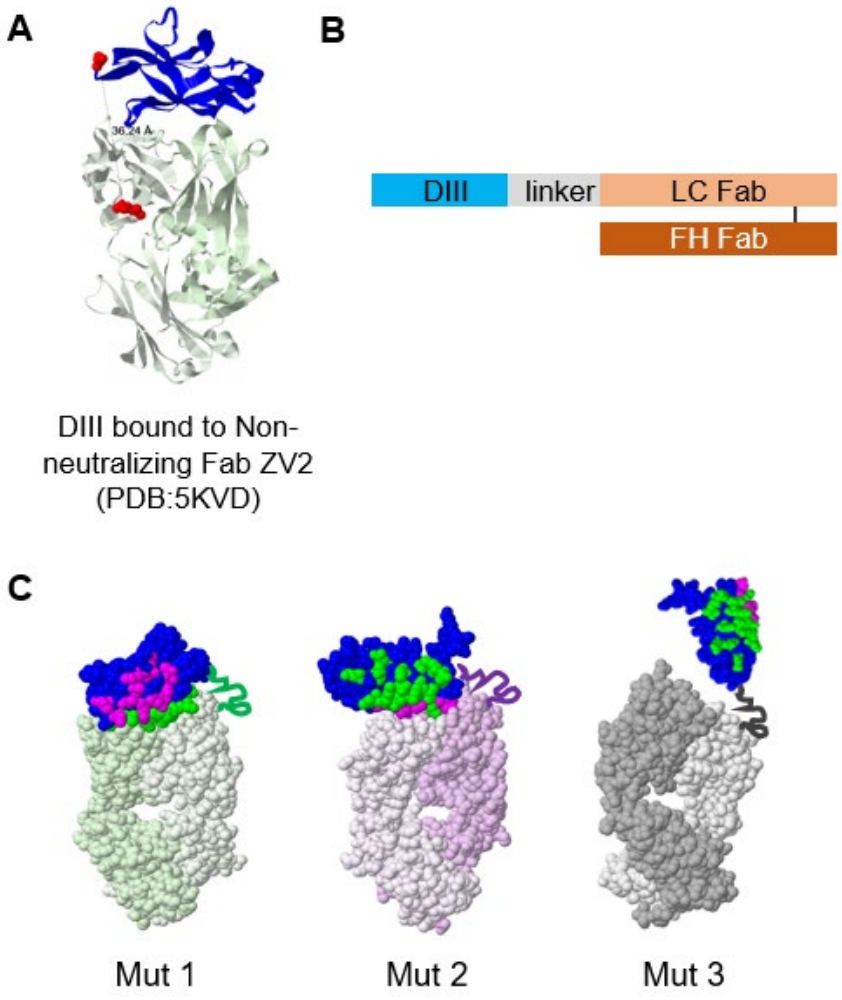

Figure 34. Design of Fab-tethered DIII mutants. (A) Crystal structure of DIII bound to the non-neutralizing Fab ZV2 (PDB ID: 5KVD) with the N-terminus of the light chain of ZV2 Fab and the C-terminus of DIII marked in red. (B) Cloning strategy for the design of Fab-tethered DIII mutants (C) Cartoons showing DIII-tethered Fab mutants – Mut1 (non-neutralizing Fab in green), Mut2 (neutralizing Fab in pink) and Mut3 (non-DIII binding Fab in gray). DIII is shown in blue with the neutralizing epitope in magenta and the non-neutralizing epitope in green.

terminus of the light chain of the Fab. To tether the Fab to DIII, we chose to co-express the two proteins as a fusion protein spaced by repeats of a flexible GGGGS spacer. The crystal structure guided us in determining the appropriate length of the linker required to span the distance between the DIII and Fab (shown by the red residues in Fig 34A). In this case, the

distance to span was ~ 3.5 nm. Coincidentally, this distance is similar to the distance between the VH and VL domain for an scFv – for which 3 repeats of GGGGS is most commonly used [132, 133]. Hence, we chose to use 3x repeats of GGGGS linker to space DIII and the Fab. The light chain of the Fab was more appropriate to fuse to DIII than the heavy chain based on its proximity to the C-terminus of DIII. Fig 34B shows the cloning strategy based on our analysis, where the DNA encoding DIII was fused upstream of the DNA encoding the ZV2 Fab LC spaced by the DNA for the linker. Fig 34C shows the cartoon for the designed DIII mutants. DIII in each case is shown in blue, with the non-neutralizing epitopes marked in green and the neutralizing epitopes marked in magenta [115]. Mut1 is the mutant of interest where the DIII is tethered to the non-neutralizing Fab ZV2 (shown in green). This linker is represented by the squiggly green line. Mut2 is a control mutant that was designed to shield the neutralizing epitope (residues marked in pink), by tethering the neutralizing Fab (ZV67, shown in pink) to DIII. Thirdly, we also designed a Mut3 of DIII, wherein the DIII was tethered to a Fab that is not specific to DIII – effectively serving as a wt-like control. An Influenza Hemagglutinin binding Fab C179 (PDB ID: 4HLZ) [134] was used for this purpose (shown in gray in Fig. 34C).

4.3.2 Characterization of Fab-tethered DIII by SDS-PAGE and ELISA

Fig. 35A shows an SDS-PAGE image of the designed Fab-tethered DIII mutants. All three mutants run on SDS-PAGE at ~65 kDa as expected. The MW for the DIII domain alone is ~15kDa and for a Fab is ~50kDa. This result confirms the successful co-expression of DIII fused to each of the three Fabs.

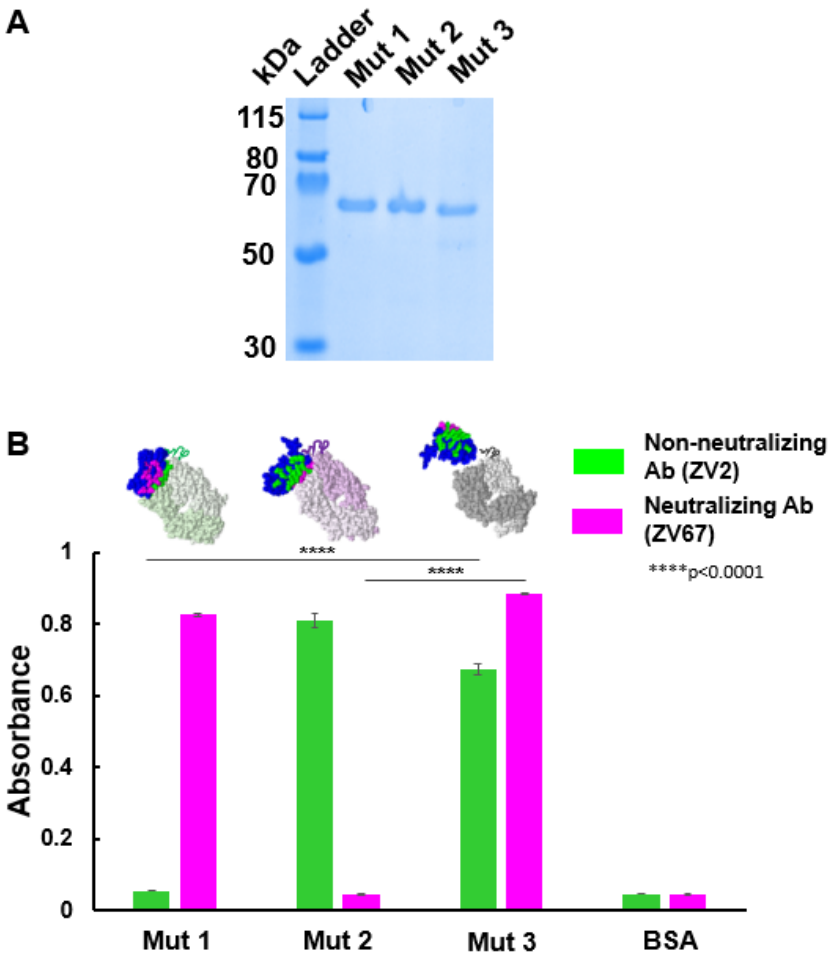

Figure 35. Characterization of Fab-tethered DIII mutants. (A) SDS-PAGE image showing the ladder and the three DIII mutants (B) ELISA result comparing binding of the neutralizing Ab (pink) and non-neutralizing Ab (green) to the DIII mutants. ELISA binding expressed as absorbance (mean ± SD, n=3). (****p<0.0001, determined by a one-way ANOVA with post-hoc Tukey's multiple comparison between groups).

Next we wanted to confirm if the specificity of the Fab tethered to DIII affects the binding of antibodies to DIII. In other words, we wanted to confirm if the non-neutralizing Fab tethered to DIII (Mut1) selectively blocks recognition of the non-neutralizing (ZV2) Ab, while retaining binding to the neutralizing (ZV67) Ab. Fig. 35B shows the ELISA result showing binding of the non-neutralizing Ab (ZV2) in green and of the neutralizing Ab

(ZV67) in pink, to the designed DIII mutants. As expected, Mut1 does not bind to the non-neutralizing Ab (ZV2) but is recognized by the neutralizing Ab (ZV67). In contrast, Mut2 does not bind to the neutralizing Ab (ZV67) but is recognized by the non-neutralizing Ab (ZV2), as expected. Mut3 binds to both antibodies, as expected. This result confirms the ability of a Fab shield tethered to an antigen to selectively block antibody recognition to desired regions.

Next, we wanted to test if this selective suppression of antibody recognition also holds true in solution, which is a more realistic and more stringent test for our approach. We therefore performed competitive analytical SEC shifts. A protein will run on SEC and show a unique peak on the chromatogram corresponding to its size and shape. As a rule of thumb, as the protein or protein complex becomes larger, its peak on the chromatogram will shift to the left. We used this analytical SEC assay to confirm the ability of our engineered DIII mutants to either bind to or not bind to a Fab.

Fig. 36A shows an overlay of chromatograms for SEC runs involving Mut1 competed with a stoichiometric amount of monomeric soluble untethered ZV2 Fab (shown on far right). The blue chromatogram corresponds to the monomeric ZV2 Fab alone. The chromatogram for Mut1, which is DIII fused to the ZV2 Fab, is shown in orange. As expected, the peak shifts to the left because of the added protein mass from DIII when compared to the ZV2 Fab alone. In yellow is the chromatogram for Mut1 complexed with a stoichiometric amount of the neutralizing ZV67 Fab. The peak shifts further to the left when compared to the peak for Mut1 indicating that the Mut1 binds to the neutralizing ZV67 Fab. In addition, this also locates for us what a DIII-tethered mutant would look like if an additional Fab bound to it on the DIII domain. Next, to test if tethering the Fab to DIII prevents binding

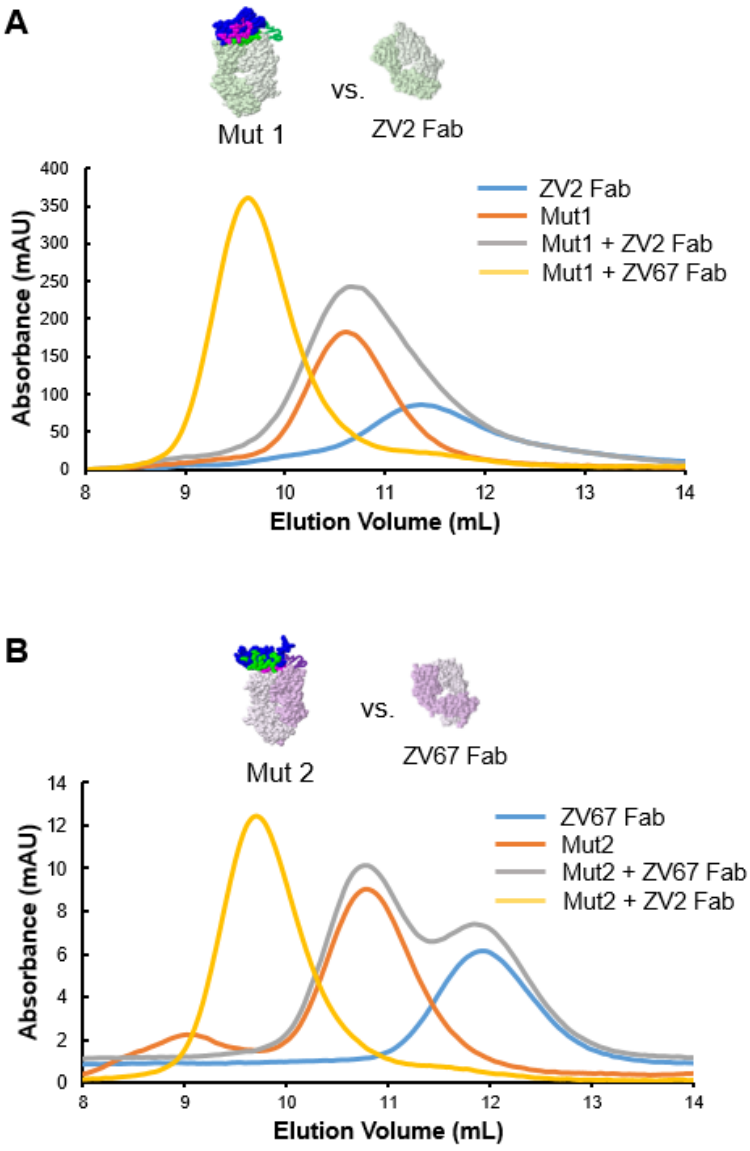

Figure 36. Characterization of Fab-tethered DIII mutants by analytical SEC. (A) Overlaid SEC chromatograms for Mut1 (orange), ZV2 Fab (blue), Mut1 complexed with ZV2 Fab (gray) and Mut1 complexed with ZV67 Fab (yellow) (B) Overlaid SEC chromatograms for Mut2 (orange), ZV67 Fab (blue), Mut2 complexed with ZV67 Fab (gray) and Mut2 complexed with ZV2 Fab (yellow)

of a competing monomeric Fab, we ran a complex of Mut1 with a stoichiometric amount of free ZV2 Fab. This chromatogram is shown in gray. Interestingly, the peak for this sample does not shift to the left (as for the yellow chromatogram), suggesting that the ZV2

Fab tethered to DIII prevents binding of competing ZV2 Fab in solution – and hence confirms the ability of tethering a Fab to an antigen as a way to suppress binding of antibodies to a desired epitope.

Fig. 36B similarly shows the results for Mut2. The blue chromatogram shows the monomeric ZV67 Fab alone. The chromatogram for Mut2 (DIII tethered to ZV67 Fab) is shown in orange. As for Mut1, a mixture of Mut2 and ZV67 Fab does not shift to the left and in fact shows discrete peaks for Mut2 and ZV67 Fab. This result suggests that Mut2 prevents binding of competing ZV67 Fab. As a reference, the yellow chromatogram shows that Mut2 does bind to the non-neutralizing ZV2 Fab as indicated by the leftward shift of the peak from ~10.9 mL to ~9.8 mL.

4.3.3 Fab-tethering refocuses the immune response on DIII

Next, to test the ability of Fab-tethered DIII to refocus the immune response away from undesirable epitopes in vivo, we immunized mice with our engineered DIII antigens (Mut1, Mut2, Mut3) and a PBS alone control. Fig. 37A shows the immunization schedule for the animal study. Fig. 37B shows the serum antibody titers for day 115 terminal bleed sera against wtDIII determined using the area under the curve (AUC) analysis method [62]. The titers for Mut3 were somewhat lower than those for Mut1 or Mut2. This result was not expected and one possible explanation could be the relatively higher protein stability for Mut1 and Mut2 by the binding of the DIII-specific Fabs to DIII when compared to Mut3 which was fused to a non-DIII specific Fab.

Next we wanted to probe if the specificity of the elicited antibodies elicited by the two mutants of interest – Mut1 and Mut 2, was different. In other words, we wanted to

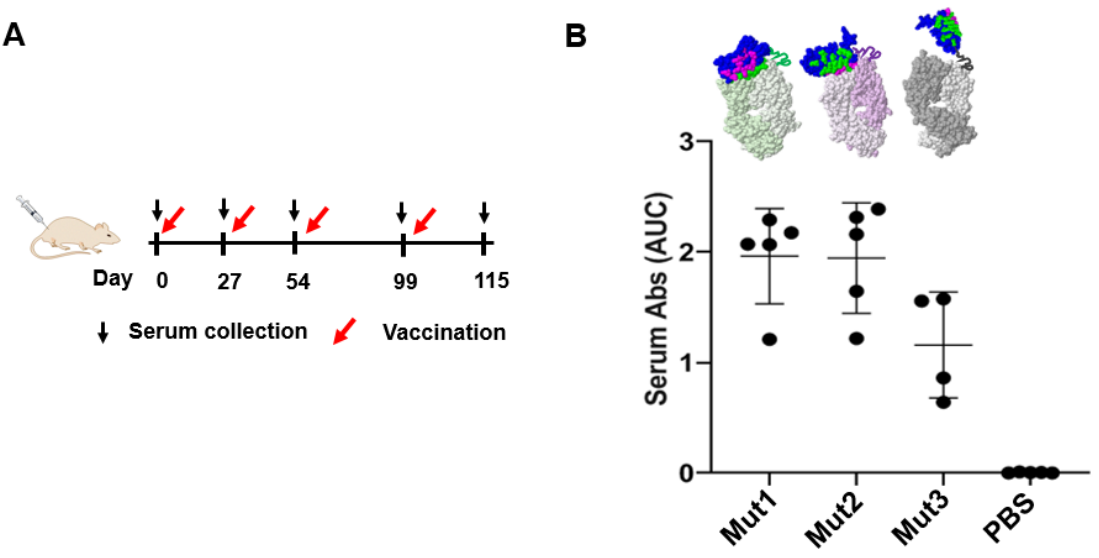

Figure 37. Immunizations of Fab-tethered DIII mutants. (A) Immunization schedule in mice (B) Terminal bleed antibody serum titers for the three mutants and PBS alone control expressed as area under the curve (AUC).

determine if Mut1 elicited fewer antibodies binding to the non-neutralizing regions, when compared to Mut2. Fig. 38A shows a cartoon with the hypothesized immune response resulting from Mut1, Mut2, and Mut3. Mut1 should preferentially elicit neutralizing antibodies (shown in pink), whereas Mut2 should preferentially elicit non-neutralizing antibodies (shown in green). Mut3 (which is essentially a wtDIII equivalent) should elicit both neutralizing and non-neutralizing antibodies. To determine if this is true, we designed a mutant of DIII (using the nanopatterning approach discussed in Chapter 1), referred to as Mut-N*-PEG, the neutralizing (N) epitope of which is shielded by the site-specific conjugation of PEG chains to DIII. We incorporated the non-canonical amino acid F* at sites T353 and T397 and expressed the mutant protein DIII – referred to as Mut-N* (to indicate mutations inserted in the neutralizing epitope regions). We then allowed the mutant protein Mut-N* to react with PEG5k-DBCO and purified the PEGylated protein Mut-N*-PEG.

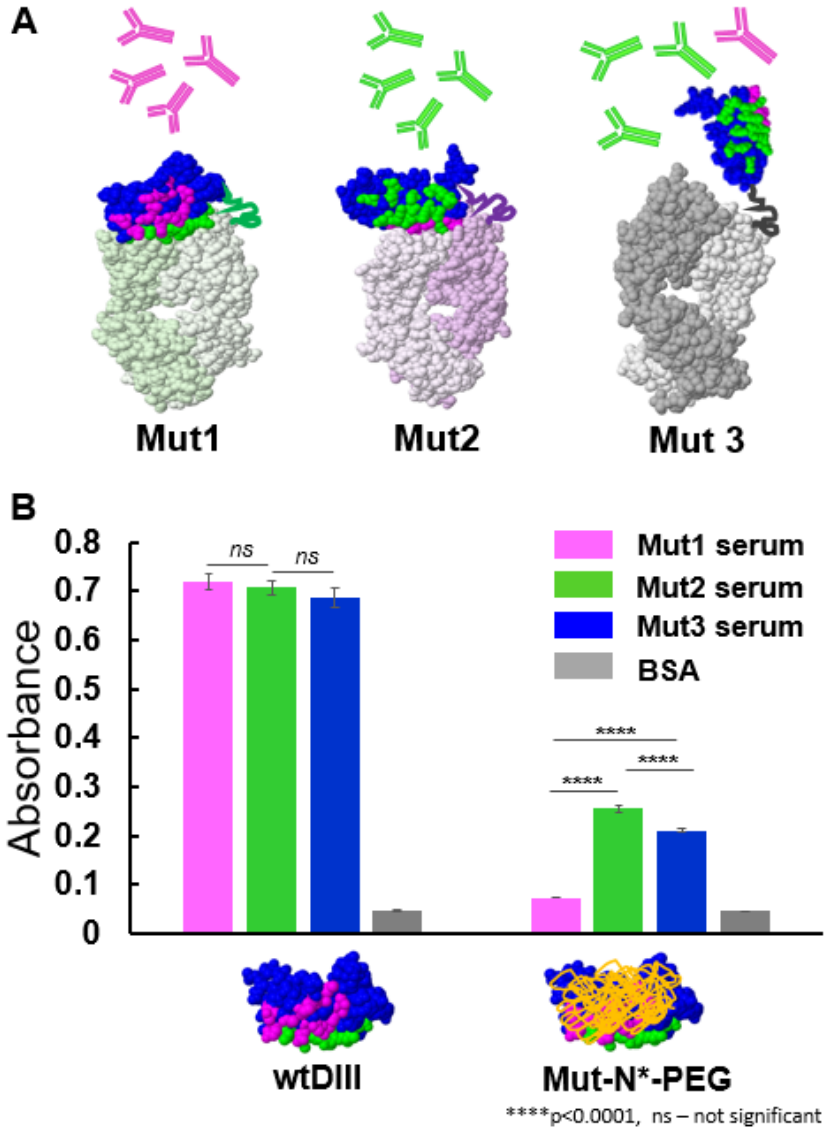

Figure 38. Fab-tethered DIII mutants refocus the immune response. (A) Hypothesized immune response for Mut1 and Mut2. Mut1 should preferentially elicit neutralizing antibodies (pink) whereas Mut2 should preferentially elicit non-neutralizing antibodies (green). (B) ELISA showing binding of terminal bleed serum for Mut1 and Mut2 to either wtDIII or to Mut-N*-PEG (neutralizing epitope of DIII shielded using PEG). ELISA binding expressed as absorbance (mean ± SD, n=3). (****p<0.0001, ns – not statistically significant, determined by a one-way ANOVA with post-hoc Tukey's multiple comparison between groups).

Fig. 38B shows the ELISA results for the binding of the terminal bleed serum for Mut1 (pink bars), Mut2 (green bars), and Mut3 (blue bars) to wt DIII (left cluster) and to Mut-

N*-PEG (right cluster). The gray bars show the background signal. A serum dilution of 1:1000 was used for Mut1 and Mut2 and a dilution of 1:300 was used for Mut3 to normalize for the differences in titers. As can be seen, the binding for Mut1 serum drops to a larger extent when probed against the two antigens (wtDIII or Mut-N*-PEG), when compared to the drop in binding for Mut2 and Mut3 serum to the two antigens. Mut-N*-PEG has the neutralizing epitopes shielded, allowing only the non-neutralizing-like antibodies to bind. The signal for Mut1 serum when probed against Mut-N*-PEG is lower than that for Mut2 serum. This result suggests that there is a smaller proportion of non-neutralizing-like antibodies in Mut1 as compared to that for Mut2 or Mut3. The signal from the binding of Mut3 serum to Mut-N*-PEG is lower than that for Mut2 serum but higher than that for Mut1 serum. In other words, this data suggests that, as expected, the proportion of non-neutralizing-like antibodies in the serum is in the following order: Mut2 (neutralizing epitope shielded) > Mut3 (wild-type equivalent) > Mut1 (non-neutralizing epitope shielded).

This data suggests that tethering antibody fragments to the antigen can selectively suppress the resulting immune response of the cognate antigenic epitope for DIII. Based on promising these preliminary results, as a part of future work, we will perform microneutralization assays to evaluate the functional benefit of selectively suppressing the elicitation of non-neutralizing antibodies for ZIKV E DIII.

4.4 Conclusion and Future work

DIII of E protein is a promising vaccine candidate for a ZIKA virus vaccine. However, the neutralization potential of DIII is limited because of the presence of undesirable non-neutralizing antibodies. Our work presents an approach to selectively suppress the

elicitation of such undesirable antibodies elicited by DIII. We have used antibody fragments as shielding agents to mask the non-neutralizing epitopes from the immune system. We have shown that by tethering the non-neutralizing Fab to DIII, we can suppress the elicitation of non-neutralizing antibodies. As a part of future work, we will further characterize the serum from the engineered DIII mutants discussed in this chapter, by microneutralization assay. This assay will allow us to verify the functional benefit of suppressing the elicitation of non-neutralizing anti-DIII antibodies.

The approach discussed in this section can be also extended to the design of other flaviviral DIII-based vaccines. For example, DIII from Dengue virus similarly elicits non-neutralizing antibodies limiting the broadly neutralizing antibody response and the potential of DIII as an effective immunogen. Non-neutralizing and serotype-specific Fabs have been characterized for DENV DIII [135, 136] allowing our approach to be easily extended to design DENV DIII based vaccines that selectively elicit neutralizing antibodies. Further, the approach of using antibody fragments as shielding agents can be used to design vaccines for other infectious diseases as well, refocusing the response to the broadly conserved regions of their antigens.

CHAPTER 5. CONCLUSION AND FUTURE DIRECTIONS

In the current work we have developed tools to engineer protein antigens to selectively shield regions of the protein to focus the immune response on other regions. Vaccine development suffers from the high antigenic sequence variability on the surface proteins of pathogens. However, there are often conserved regions on pathogenic proteins that are naturally immunosubdominant. Hence, strategies to selectively shield the immunodominant variable regions of these protein antigens to refocus the immune response on the more conserved regions is a useful tool to design broadly protective vaccines.

We have developed two tools to achieve immunofocusing on protein antigens in the current work. The first termed as "Nanopatterning" involves the site-specific conjugation of polymeric chains to targeted regions of the protein antigen with the goal of suppressing the immune response to that defined region. We have used GFP as a model antigen, and nanopatterned a defined epitope for a GFP Nanobody. We have shown the selective suppression of the immune response to the Nanobody epitope by nanopatterning GFP. Next, we extended the nanopatterning idea to an important malarial antigen – $MSP1_{19}$ and showed the ability to refocus the response to a conserved inhibitory epitope. Nanopatterning $MSP1_{19}$ allowed the detection of $MSP1_{19}$ from a highly divergent heterologous strain that differs at as many as 21 of 96 residues.

Nanopatterning allows a much finer control over blocking of selected regions by the site-specific attachment of a defined length of a polymeric chain to a protein. This approach is

in contrast to the traditional multiple and random PEGylation of proteins to suppress the global immune response of therapeutic proteins. This approach can be extended to other antigens to elicit broadly protective antibodies. One can use polymers other than PEG and also use different chemistries by the incorporation of multiple non-canonical amino acids to allow a much finer control over shielding. Further, these nanopatterned proteins could also be used for diagnostics applications to screen for a particular class of antibodies based on where it binds on the antigen.

Having shown the successful refocusing of the immune response of *Py*MSP1$_{19}$ to the conserved epitopes, we are next assessing the functional benefit of the refocusing by evaluating binding of the serum antibodies to a parasite from a heterologous strain by an Immunoflourescence assay (IFA). Similarly for *Pf*MSP1$_{19}$, it would be interesting to evaluate the ability of refocusing the immune response to protect mice in a passive immunoprophylaxis model on challenging with a transgenic *P.berghei* parasite [137]. Further, our lab has already started to work on nanopatterning another important malarial antigen – *Pf* circumsporozoite protein (*Pf*CSP), which the current vaccine candidate RTS,S/A01 is based on. The nanopatterning approach should allow refocusing of the immune response to broadly neutralizing epitopes of *Pf*CSP that are not included in the RTS,S/A01 vaccine.

We have also developed a second approach that uses antibody fragments (Fabs) as shielding agents. We have developed two related approaches using Fabs as shields – one that involves tethering the Fab to the antigen and a second approach that involves designing multivalent Fabs as shielding agents. We have shown that the tethering approach allows refocusing of the immune response to desired regions of an antigen for Hemagglutinin

(HA) from influenza virus and the Domain III (DIII) of the envelope protein of Zika virus. Tethered-Fab shields were explored to refocus the immune response to the broadly conserved stalk domain of HA and to suppress the elicitation of non-neutralizing antibodies for DIII. We have similarly shown an alternative approach to shielding the undesirable head domain of HA by using bivalent Fabs as shields.

As a part of future work, we will test the functional ability of the immune refocusing achieved for these antigens (HA and DIII) in microneutralization assays. It would also be interesting to test these Fab-shielded HA vaccine constructs in a mouse model with pre-existing immunity to influenza virus to better probe the advantage of shielding over wtHA control. We also plan to extend the approach to H3 HA from group II of the influenza virus, as a part of future work. Similarly, we plan to extend our findings from the ZIKV EDIII work to design a Dengue Virus vaccine in the near future. Also, this idea can be extended to other antigens, for example the Fusion protein from RSV, to elicit broadly protective anti-RSV antibodies or to design vaccines against other flaviviruses.

Fabs are advantageous as shielding agents because they selectively bind to a region on an antigen and in effect shield it. Fabs are also considered largely non-foreign by our immune systems – and in using them as shielding agents, their most “immunogenic” regions (CDRs) are shielded by the antigen it binds to. The current work also discusses a strategy to design a bivalent Fab that may be used for applications other than protein shielding or vaccine design. We have already extended the approach discussed in this work to design bivalent Fab-based agonists of the Wnt signalling pathway.

Antigenic sequence variability has stalled vaccine progress for several otherwise highly immunogenic proteins, as the ones discussed in this work. The tools discussed in this work can be applied to immunogens from other infectious diseases. The approach involving Fabs as shielding agents can most easily be translated to a commercial setting. Antibodies and antibody-like molecules have been extensively studied and developed by the pharmaceutical industry, making commercialization of a Fab-shielded antigen a possibility. Similarly, several PEGylated therapeutic proteins are already in the clinic, making the nanopatterning approach adaptable to an industrial setting.

The tools developed in this work have their pros and cons, as for the existing approaches to immunofocusing. It is important to highlight some of the limitations of the approaches discussed. For example, the nanopatterning approach involves the incorporation of non-canonical amino acids which may affect protein folding and stability, and may be expensive to implement. Additionally, the use of this approach is relatively difficult to apply to a protein expressed in insect cell system (e.g. HA), for which the ncAA incorporation machinery is less developed than for bacterial or mammalian protein expression systems.

One important limitation in using Fabs (or other ligands) as shielding agents is the availability of a characterized antibody that binds to the region one wishes to shield. In the absence of any known antibody or ligand that has been structurally characterized to bind to the desired antigen epitope, the Fab-based approach cannot be applied. The tethering approach may require some modification of the antigen (e.g. as in case of HA), that may limit its application. The multivalent-Fab approach requires the availability of Fabs (or

other ligands) that bind to different regions of the antigen; – the absence of suitable ligands would limit the use of this approach.

Despite their limitations, the strategies developed and discussed in this thesis add to the existing, but limited toolkit of immunofocusing. The tools developed in this work can counter immune evasion strategies developed in pathogens and accelerate progress of vaccine research. The development of several potential vaccine candidates is impeded by challenges such as high antigenic sequence variability – which can be addressed by the proposed tools. This work lays the foundation for the design of broadly protective vaccines for Malaria, Influenza, and Zika. We have shown the applicability of our approaches for antigens from these three medically highly relevant diseases. The tools developed in this work can also be applied to designing vaccines for other infectious diseases such as HIV

REFERENCES

1. Murphy, K., Travers, P., Walport, M., & Janeway, C., *Janeway's immunobiology (8th ed.).* New York: Garland Science., 2012.

2. Heesters, B.A., et al., *Antigen Presentation to B Cells.* Trends Immunol, 2016. **37**(12): p. 844-854.

3. Pierce, S.K. and W. Liu, *The tipping points in the initiation of B cell signalling: how small changes make big differences.* Nat Rev Immunol, 2010. **10**(11): p. 767-77.

4. Parker, D.C., *T cell-dependent B cell activation.* Annu Rev Immunol, 1993. **11**: p. 331-60.

5. Minor, P.D., *Live attenuated vaccines: Historical successes and current challenges.* Virology, 2015. **479-480**: p. 379-92.

6. Plotkin, S., *History of vaccination.* Proc Natl Acad Sci U S A, 2014. **111**(34): p. 12283-7.

7. Burton, D.R., *Antibodies, viruses and vaccines.* Nat Rev Immunol, 2002. **2**(9): p. 706-13.

8. Coffman, R.L., A. Sher, and R.A. Seder, *Vaccine adjuvants: putting innate immunity to work.* Immunity, 2010. **33**(4): p. 492-503.

9. Di Pasquale, A., et al., *Vaccine Adjuvants: from 1920 to 2015 and Beyond.* Vaccines (Basel), 2015. **3**(2): p. 320-43.

10. Iwasaki, A. and R. Medzhitov, *Regulation of adaptive immunity by the innate immune system.* Science, 2010. **327**(5963): p. 291-5.

11. Greenwood, B., *The contribution of vaccination to global health: past, present and future.* Philos Trans R Soc Lond B Biol Sci, 2014. **369**(1645): p. 20130433.

12. *WHO. Global Vaccine Action Plan 2011–2020*

13. Finlay, B.B. and G. McFadden, *Anti-immunology: evasion of the host immune system by bacterial and viral pathogens.* Cell, 2006. **124**(4): p. 767-82.

14. Schmid-Hempel, P., *Parasite immune evasion: a momentous molecular war.* Trends Ecol Evol, 2008. **23**(6): p. 318-26.

15. Ploegh, H.L., *Viral strategies of immune evasion.* Science, 1998. **280**(5361): p. 248-53.

16. Pancera, M., et al., *Structure and immune recognition of trimeric pre-fusion HIV-1 Env.* Nature, 2014. **514**(7523): p. 455-61.

17. *WHO. World malaria report 2018. .*

18. Rts, S.C.T.P., *Efficacy and safety of RTS,S/AS01 malaria vaccine with or without a booster dose in infants and children in Africa: final results of a phase 3, individually randomised, controlled trial.* Lancet, 2015.

19. Kester, K.E., et al., *Randomized, double-blind, phase 2a trial of falciparum malaria vaccines RTS,S/AS01B and RTS,S/AS02A in malaria-naive adults: safety, efficacy, and immunologic associates of protection.* J Infect Dis, 2009. **200**(3): p. 337-46.

20. Draper, S.J., et al., *Malaria Vaccines: Recent Advances and New Horizons.* Cell Host Microbe, 2018. **24**(1): p. 43-56.

21. Krammer, F. and P. Palese, *Advances in the development of influenza virus vaccines.* Nat Rev Drug Discov, 2015. **14**(3): p. 167-82.

22. Palese, P., *Influenza: old and new threats.* Nat Med, 2004. **10**(12 Suppl): p. S82-7.

23. *www.cdc.gov/flu/.*

24. Krammer, F., *The human antibody response to influenza A virus infection and vaccination.* Nat Rev Immunol, 2019. **19**(6): p. 383-397.

25. Pierson, T.C. and M.S. Diamond, *The emergence of Zika virus and its new clinical syndromes.* Nature, 2018. **560**(7720): p. 573-581.

26. de Oliveira, W.K., et al., *Infection-related microcephaly after the 2015 and 2016 Zika virus outbreaks in Brazil: a surveillance-based analysis.* Lancet, 2017. **390**(10097): p. 861-870.

27. Franca, G.V., et al., *Congenital Zika virus syndrome in Brazil: a case series of the first 1501 livebirths with complete investigation.* Lancet, 2016. **388**(10047): p. 891-7.

28. Parra, B., et al., *Guillain-Barre Syndrome Associated with Zika Virus Infection in Colombia.* N Engl J Med, 2016. **375**(16): p. 1513-1523.

29. Abbink, P., K.E. Stephenson, and D.H. Barouch, *Zika virus vaccines.* Nat Rev Microbiol, 2018. **16**(10): p. 594-600.

30. Kwong, P.D. and I.A. Wilson, *HIV-1 and influenza antibodies: seeing antigens in new ways.* Nat Immunol, 2009. **10**(6): p. 573-8.

31. Rappuoli, R., *The challenge of developing universal vaccines.* F1000 Med Rep, 2011. **3**: p. 16.

32. Kwong P. D., *Structural Biology and the Design of Effective Vaccines for HIV-1 and Other Viruses.* National Institute of Allergy and Infectious Diseases, NIH. Infectious Disease., 2010.

33. Wu, X., et al., *Rational design of envelope identifies broadly neutralizing human monoclonal antibodies to HIV-1.* Science, 2010. **329**(5993): p. 856-61.

34. Pantophlet, R., I.A. Wilson, and D.R. Burton, *Hyperglycosylated mutants of human immunodeficiency virus (HIV) type 1 monomeric gp120 as novel antigens for HIV vaccine design.* J Virol, 2003. **77**(10): p. 5889-901.

35. Eggink, D., P.H. Goff, and P. Palese, *Guiding the immune response against influenza virus hemagglutinin toward the conserved stalk domain by hyperglycosylation of the globular head domain.* J Virol, 2014. **88**(1): p. 699-704.

36. Jevsevar, S., M. Kunstelj, and V.G. Porekar, *PEGylation of therapeutic proteins.* Biotechnol J, 2010. **5**(1): p. 113-28.

37. Reitter, J.N., R.E. Means, and R.C. Desrosiers, *A role for carbohydrates in immune evasion in AIDS.* Nat Med, 1998. **4**(6): p. 679-84.

38. Wei, X., et al., *Antibody neutralization and escape by HIV-1.* Nature, 2003. **422**(6929): p. 307-12.

39. Sliepen, K., et al., *Immunosilencing a highly immunogenic protein trimerization domain.* J Biol Chem, 2015. **290**(12): p. 7436-42.

40. Du, L., et al., *Introduction of neutralizing immunogenicity index to the rational design of MERS coronavirus subunit vaccines.* Nat Commun, 2016. **7**: p. 13473.

41. Jardine, J., et al., *Rational HIV immunogen design to target specific germline B cell receptors.* Science, 2013. **340**(6133): p. 711-6.

42. Bajic, G., et al., *Influenza Antigen Engineering Focuses Immune Responses to a Subdominant but Broadly Protective Viral Epitope.* Cell Host Microbe, 2019.

43. Moore, P.L., et al., *Evolution of an HIV glycan-dependent broadly neutralizing antibody epitope through immune escape.* Nat Med, 2012. **18**(11): p. 1688-92.

44. Dozier, J.K. and M.D. Distefano, *Site-Specific PEGylation of Therapeutic Proteins.* Int J Mol Sci, 2015. **16**(10): p. 25831-64.

45. Amiram, M., et al., *Evolution of translation machinery in recoded bacteria enables multi-site incorporation of nonstandard amino acids.* Nat Biotechnol, 2015. **33**(12): p. 1272-1279.

46. Link, A.J., M.L. Mock, and D.A. Tirrell, *Non-canonical amino acids in protein engineering.* Curr Opin Biotechnol, 2003. **14**(6): p. 603-9.

47. Jewett, J.C. and C.R. Bertozzi, *Cu-free click cycloaddition reactions in chemical biology.* Chem Soc Rev, 2010. **39**(4): p. 1272-9.

48. Zakeri, B., et al., *Peptide tag forming a rapid covalent bond to a protein, through engineering a bacterial adhesin.* Proc Natl Acad Sci U S A, 2012. **109**(12): p. E690-7.

49. Morgan, W.D., et al., *Solution structure of an EGF module pair from the Plasmodium falciparum merozoite surface protein 1.* J Mol Biol, 1999. **289**(1): p. 113-22.

50. Curd, R.D., et al., *The structure of Plasmodium yoelii merozoite surface protein 119, antibody specificity and implications for malaria vaccine design.* Open Biol, 2014. **4**: p. 130091.

51. Daly, T.M., J.M. Burns, Jr., and C.A. Long, *Comparison of the carboxy-terminal, cysteine-rich domain of the merozoite surface protein-1 from several strains of Plasmodium yoelii.* Mol Biochem Parasitol, 1992. **52**(2): p. 279-82.

52. Lazarou, M., et al., *Inhibition of erythrocyte invasion and Plasmodium falciparum merozoite surface protein 1 processing by human immunoglobulin G1 (IgG1) and IgG3 antibodies.* Infect Immun, 2009. **77**(12): p. 5659-67.

53. Kubala, M.H., et al., *Structural and thermodynamic analysis of the GFP:GFP-nanobody complex.* Protein Sci, 2010. **19**(12): p. 2389-401.

54. Baskin, J.M., et al., *Copper-free click chemistry for dynamic in vivo imaging.* Proc Natl Acad Sci U S A, 2007. **104**(43): p. 16793-7.

55. Ashkenazy, H., et al., *ConSurf 2016: an improved methodology to estimate and visualize evolutionary conservation in macromolecules.* Nucleic Acids Res, 2016. **44**(W1): p. W344-50.

56. Puffer, E.B., et al., *Activating B cell signaling with defined multivalent ligands.* ACS Chem Biol, 2007. **2**(4): p. 252-62.

57. Mukherjee, S., et al., *Monovalent and multivalent ligation of the B cell receptor exhibit differential dependence upon Syk and Src family kinases.* Sci Signal, 2013. **6**(256): p. ra1.

58. Bennett, N.R., et al., *Multivalent Antigens for Promoting B and T Cell Activation.* ACS Chem Biol, 2015. **10**(8): p. 1817-24.

59. Arsiwala, A., et al., *Designing Multivalent Ligands to Control Biological Interactions: From Vaccines and Cellular Effectors to Targeted Drug Delivery.* Chem Asian J, 2019. **14**(2): p. 244-255.

60. Krishnamurthy, V.M., Estroff, L. A., and Whitesides, G. M., *Multivalency in Ligand Design*, in *Wiley-VCH Verlag GmbH & Co.: Weinheim, Germany*. 2006

p. 11− 54.

61. Cattani, G., L. Vogeley, and P.B. Crowley, *Structure of a PEGylated protein reveals a highly porous double-helical assembly.* Nat Chem, 2015. **7**(10): p. 823-8.

62. Angeletti, D., et al., *Defining B cell immunodominance to viruses.* Nat Immunol, 2017. **18**(4): p. 456-463.

63. Blackman, M.J., et al., *A single fragment of a malaria merozoite surface protein remains on the parasite during red cell invasion and is the target of invasion-inhibiting antibodies.* J Exp Med, 1990. **172**(1): p. 379-82.

64. Holder, A.A., *The carboxy-terminus of merozoite surface protein 1: structure, specific antibodies and immunity to malaria.* Parasitology, 2009. **136**(12): p. 1445-56.

65. Morgan, W.D., et al., *Precise epitope mapping of malaria parasite inhibitory antibodies by TROSY NMR cross-saturation.* Biochemistry, 2005. **44**(2): p. 518-23.

66. Guevara Patino, J.A., et al., *Antibodies that inhibit malaria merozoite surface protein-1 processing and erythrocyte invasion are blocked by naturally acquired human antibodies.* J Exp Med, 1997. **186**(10): p. 1689-99.

67. Benjamin, P.A., et al., *Antigenic and sequence diversity at the C-terminus of the merozoite surface protein-1 from rodent malaria isolates, and the binding of protective monoclonal antibodies.* Mol Biochem Parasitol, 1999. **104**(2): p. 147-56.

68. Uthaipibull, C., et al., *Inhibitory and blocking monoclonal antibody epitopes on merozoite surface protein 1 of the malaria parasite Plasmodium falciparum.* J Mol Biol, 2001. **307**(5): p. 1381-94.

69. Ramaraj, T., et al., *Antigen-antibody interface properties: composition, residue interactions, and features of 53 non-redundant structures.* Biochim Biophys Acta, 2012. **1824**(3): p. 520-32.

70. Zheng, C., G. Ma, and Z. Su, *Native PAGE eliminates the problem of PEG-SDS interaction in SDS-PAGE and provides an alternative to HPLC in characterization of protein PEGylation.* Electrophoresis, 2007. **28**(16): p. 2801-7.

71. Miller, L.H., et al., *Analysis of sequence diversity in the Plasmodium falciparum merozoite surface protein-1 (MSP-1).* Mol Biochem Parasitol, 1993. **59**(1): p. 1-14.

72. Zhang, P., et al., *Anti-PEG antibodies in the clinic: Current issues and beyond PEGylation.* J Control Release, 2016. **244**(Pt B): p. 184-193.

73. Amr S.Abu Lila, T., Tatsuhiro Ishida, *PEGylation and anti-PEG antibodies.* Engineering of Biomaterials for Drug Delivery Systems, 2018: p. 51-68.

74. Qi, Y., et al., *A brush-polymer conjugate of exendin-4 reduces blood glucose for up to five days and eliminates poly(ethylene glycol) antigenicity.* Nat Biomed Eng, 2016. **1**.

75. Liu, W., et al., *Genetic incorporation of unnatural amino acids into proteins in mammalian cells.* Nat Methods, 2007. **4**(3): p. 239-44.

76. Medina, R.A. and A. Garcia-Sastre, *Influenza A viruses: new research developments.* Nat Rev Microbiol, 2011. **9**(8): p. 590-603.

77. Wrammert, J., et al., *Rapid cloning of high-affinity human monoclonal antibodies against influenza virus.* Nature, 2008. **453**(7195): p. 667-71.

78. Margine, I., et al., *H3N2 influenza virus infection induces broadly reactive hemagglutinin stalk antibodies in humans and mice.* J Virol, 2013. **87**(8): p. 4728-37.

79. Krammer, F. and P. Palese, *Universal influenza virus vaccines: need for clinical trials.* Nat Immunol, 2014. **15**(1): p. 3-5.

80. Brownlee, G.G. and E. Fodor, *The predicted antigenicity of the haemagglutinin of the 1918 Spanish influenza pandemic suggests an avian origin.* Philos Trans R Soc Lond B Biol Sci, 2001. **356**(1416): p. 1871-6.

81. Caton, A.J., et al., *The antigenic structure of the influenza virus A/PR/8/34 hemagglutinin (H1 subtype).* Cell, 1982. **31**(2 Pt 1): p. 417-27.

82. Ekiert, D.C. and I.A. Wilson, *Broadly neutralizing antibodies against influenza virus and prospects for universal therapies.* Curr Opin Virol, 2012. **2**(2): p. 134-41.

83. Tan, G.S., et al., *A pan-H1 anti-hemagglutinin monoclonal antibody with potent broad-spectrum efficacy in vivo.* J Virol, 2012. **86**(11): p. 6179-88.

84. Krammer, F., et al., *Chimeric hemagglutinin influenza virus vaccine constructs elicit broadly protective stalk-specific antibodies.* J Virol, 2013. **87**(12): p. 6542-50.

85. Impagliazzo, A., et al., *A stable trimeric influenza hemagglutinin stem as a broadly protective immunogen.* Science, 2015. **349**(6254): p. 1301-6.

86. Mallajosyula, V.V., et al., *Influenza hemagglutinin stem-fragment immunogen elicits broadly neutralizing antibodies and confers heterologous protection.* Proc Natl Acad Sci U S A, 2014. **111**(25): p. E2514-23.

87. Bommakanti, G., et al., *Design of an HA2-based Escherichia coli expressed influenza immunogen that protects mice from pathogenic challenge.* Proc Natl Acad Sci U S A, 2010. **107**(31): p. 13701-6.

88. Bommakanti, G., et al., *Design of Escherichia coli-expressed stalk domain immunogens of H1N1 hemagglutinin that protect mice from lethal challenge.* J Virol, 2012. **86**(24): p. 13434-44.

89. Lu, Y., J.P. Welsh, and J.R. Swartz, *Production and stabilization of the trimeric influenza hemagglutinin stem domain for potentially broadly protective influenza vaccines.* Proc Natl Acad Sci U S A, 2014. **111**(1): p. 125-30.

90. Deng, L., et al., *Double-layered protein nanoparticles induce broad protection against divergent influenza A viruses.* Nat Commun, 2018. **9**(1): p. 359.

91. Davenport, F.M., A.V. Hennessy, and T. Francis, Jr., *Epidemiologic and immunologic significance of age distribution of antibody to antigenic variants of influenza virus.* J Exp Med, 1953. **98**(6): p. 641-56.

92. Fazekas de St, G. and R.G. Webster, *Disquisitions on Original Antigenic Sin. II. Proof in lower creatures.* J Exp Med, 1966. **124**(3): p. 347-61.

93. Fazekas de St, G. and R.G. Webster, *Disquisitions of Original Antigenic Sin. I. Evidence in man.* J Exp Med, 1966. **124**(3): p. 331-45.

94. Kim, J.H., et al., *Strategies to alleviate original antigenic sin responses to influenza viruses.* Proc Natl Acad Sci U S A, 2012. **109**(34): p. 13751-6.

95. Kim, J.H., et al., *Original antigenic sin responses to influenza viruses.* J Immunol, 2009. **183**(5): p. 3294-301.

96. Harding, F.A., et al., *The immunogenicity of humanized and fully human antibodies: residual immunogenicity resides in the CDR regions.* MAbs, 2010. **2**(3): p. 256-65.

97. Krishnamurthy, V.M., et al., *Dependence of effective molarity on linker length for an intramolecular protein-ligand system.* J Am Chem Soc, 2007. **129**(5): p. 1312-20.

98. Kane, R.S., *Thermodynamics of multivalent interactions: influence of the linker.* Langmuir, 2010. **26**(11): p. 8636-40.

99. Wong, J.Y., et al., *Direct measurement of a tethered ligand-receptor interaction potential.* Science, 1997. **275**(5301): p. 820-2.

100. Margine, I., P. Palese, and F. Krammer, *Expression of functional recombinant hemagglutinin and neuraminidase proteins from the novel H7N9 influenza virus using the baculovirus expression system.* J Vis Exp, 2013(81): p. e51112.

101. Fairhead, M., et al., *Plug-and-play pairing via defined divalent streptavidins.* J Mol Biol, 2014. **426**(1): p. 199-214.

102. Lee, J.M., et al., *A Rhizavidin Monomer with Nearly Multimeric Avidin-Like Binding Stability Against Biotin Conjugates.* Angew Chem Int Ed Engl, 2016. **55**(10): p. 3393-7.

103. Mammen, M., S.K. Choi, and G.M. Whitesides, *Polyvalent Interactions in Biological Systems: Implications for Design and Use of Multivalent Ligands and Inhibitors.* Angew Chem Int Ed Engl, 1998. **37**(20): p. 2754-2794.

104. Huskens, J., et al., *A model for describing the thermodynamics of multivalent host-guest interactions at interfaces.* J Am Chem Soc, 2004. **126**(21): p. 6784-97.

105. Joshi, A., et al., *Structure-based design of a heptavalent anthrax toxin inhibitor.* Biomacromolecules, 2011. **12**(3): p. 791-6.

106. Joshi, A., et al., *The design of polyvalent therapeutics.* Chemistry, 2008. **14**(26): p. 7738-47.

107. Liu, Z., et al., *A novel method for synthetic vaccine construction based on protein assembly.* Sci Rep, 2014. **4**: p. 7266.

108. Ekiert, D.C., et al., *Antibody recognition of a highly conserved influenza virus epitope.* Science, 2009. **324**(5924): p. 246-51.

109. Brasil, P., et al., *Zika Virus Infection in Pregnant Women in Rio de Janeiro.* N Engl J Med, 2016. **375**(24): p. 2321-2334.

110. Dai, L., et al., *Structures of the Zika Virus Envelope Protein and Its Complex with a Flavivirus Broadly Protective Antibody.* Cell Host Microbe, 2016. **19**(5): p. 696-704.

111. Heinz, F.X. and K. Stiasny, *The Antigenic Structure of Zika Virus and Its Relation to Other Flaviviruses: Implications for Infection and Immunoprophylaxis.* Microbiol Mol Biol Rev, 2017. **81**(1).

112. Beasley, D.W. and A.D. Barrett, *Identification of neutralizing epitopes within structural domain III of the West Nile virus envelope protein.* J Virol, 2002. **76**(24): p. 13097-100.

113. Oliphant, T., et al., *Development of a humanized monoclonal antibody with therapeutic potential against West Nile virus.* Nat Med, 2005. **11**(5): p. 522-30.

114. Shrestha, B., et al., *The development of therapeutic antibodies that neutralize homologous and heterologous genotypes of dengue virus type 1.* PLoS Pathog, 2010. **6**(4): p. e1000823.

115. Zhao, H., et al., *Structural Basis of Zika Virus-Specific Antibody Protection.* Cell, 2016. **166**(4): p. 1016-1027.

116. Sukupolvi-Petty, S., et al., *Structure and function analysis of therapeutic monoclonal antibodies against dengue virus type 2.* J Virol, 2010. **84**(18): p. 9227-39.

117. Kostyuchenko, V.A., et al., *Structure of the thermally stable Zika virus.* Nature, 2016. **533**(7603): p. 425-8.

118. Sirohi, D., et al., *The 3.8 A resolution cryo-EM structure of Zika virus.* Science, 2016. **352**(6284): p. 467-70.

119. Pierson, T.C., et al., *The stoichiometry of antibody-mediated neutralization and enhancement of West Nile virus infection.* Cell Host Microbe, 2007. **1**(2): p. 135-45.

120. Katzelnick, L.C., et al., *Antibody-dependent enhancement of severe dengue disease in humans.* Science, 2017. **358**(6365): p. 929-932.

121. Flipse, J., et al., *Antibody-Dependent Enhancement of Dengue Virus Infection in Primary Human Macrophages; Balancing Higher Fusion against Antiviral Responses.* Sci Rep, 2016. **6**: p. 29201.

122. Dejnirattisai, W., et al., *Cross-reacting antibodies enhance dengue virus infection in humans.* Science, 2010. **328**(5979): p. 745-8.

123. Martina, B.E., et al., *Immunization with West Nile virus envelope domain III protects mice against lethal infection with homologous and heterologous virus.* Vaccine, 2008. **26**(2): p. 153-7.

124. Schneeweiss, A., et al., *A DNA vaccine encoding the E protein of West Nile virus is protective and can be boosted by recombinant domain DIII.* Vaccine, 2011. **29**(37): p. 6352-7.

125. Hermida, L., et al., *A recombinant fusion protein containing the domain III of the dengue-2 envelope protein is immunogenic and protective in nonhuman primates.* Vaccine, 2006. **24**(16): p. 3165-71.

126. Simmons, M., et al., *Characterization of antibody responses to combinations of a dengue virus type 2 DNA vaccine and two dengue virus type 2 protein vaccines in rhesus macaques.* J Virol, 2006. **80**(19): p. 9577-85.

127. Bernardo, L., et al., *Immunogenicity and protective efficacy of a recombinant fusion protein containing the domain III of the dengue 1 envelope protein in non-human primates.* Antiviral Res, 2008. **80**(2): p. 194-9.

128. Li, X.Q., et al., *Dengue virus envelope domain III immunization elicits predominantly cross-reactive, poorly neutralizing antibodies localized to the AB loop: implications for dengue vaccine design.* J Gen Virol, 2013. **94**(Pt 10): p. 2191-201.

129. Sukupolvi-Petty, S., et al., *Type- and subcomplex-specific neutralizing antibodies against domain III of dengue virus type 2 envelope protein recognize adjacent epitopes.* J Virol, 2007. **81**(23): p. 12816-26.

130. Frei, J.C., et al., *Engineered Dengue Virus Domain III Proteins Elicit Cross-Neutralizing Antibody Responses in Mice.* J Virol, 2018. **92**(18).

131. Nelson, C.A., C.A. Lee, and D.H. Fremont, *Oxidative refolding from inclusion bodies.* Methods Mol Biol, 2014. **1140**: p. 145-57.

132. Chen, X., J.L. Zaro, and W.C. Shen, *Fusion protein linkers: property, design and functionality.* Adv Drug Deliv Rev, 2013. **65**(10): p. 1357-69.

133. Huston, J.S., et al., *Protein engineering of antibody binding sites: recovery of specific activity in an anti-digoxin single-chain Fv analogue produced in Escherichia coli.* Proc Natl Acad Sci U S A, 1988. **85**(16): p. 5879-83.

134. Dreyfus, C., D.C. Ekiert, and I.A. Wilson, *Structure of a classical broadly neutralizing stem antibody in complex with a pandemic H2 influenza virus hemagglutinin.* J Virol, 2013. **87**(12): p. 7149-54.

135. Midgley, C.M., et al., *Structural analysis of a dengue cross-reactive antibody complexed with envelope domain III reveals the molecular basis of cross-reactivity.* J Immunol, 2012. **188**(10): p. 4971-9.

136. Austin, S.K., et al., *Structural basis of differential neutralization of DENV-1 genotypes by an antibody that recognizes a cryptic epitope.* PLoS Pathog, 2012. **8**(10): p. e1002930.

137. de Koning-Ward, T.F., et al., *A new rodent model to assess blood stage immunity to the Plasmodium falciparum antigen merozoite surface protein 119 reveals a protective role for invasion inhibitory antibodies.* J Exp Med, 2003. **198**(6): p. 869-75.